STRESSES IN A MULTIFERROIC THIN FILM - MULTI-LAYER COATING SYSTEM

A THESIS SUBMITTED TO
THE GRADUATE SCHOOL OF NATURAL AND APPLIED SCIENCES
OF
MIDDLE EAST TECHNICAL UNIVERSITY

BY

EREN ŞAHİN

IN PARTIAL FULFILLMENT OF THE REQUIREMENTS
FOR
THE DEGREE OF MASTER OF SCIENCE
IN
MECHANICAL ENGINEERING

APRIL 2025

Approval of the thesis:

STRESSES IN A MULTIFERROIC THIN FILM - MULTI-LAYER COATING SYSTEM

submitted by **EREN ŞAHİN** in partial fulfillment of the requirements for the degree of **Master of Science** i**n Mechanical Engineering, Middle East Technical University** by,

Prof. Dr. Naci Emre Altun
Dean, **Graduate School of Natural and Applied Sciences** _____

Prof. Dr. Serkan Dağ
Head of the Department, **Mechanical Engineering** _____

Prof. Dr. Serkan Dağ
Supervisor, **Mechanical Engineering, METU** _____

Examining Committee Members:

Prof. Dr. Fevzi Suat Kadıoğlu
Mechanical Engineering, METU _____

Prof. Dr. Serkan Dağ
Mechanical Engineering, METU _____

Prof. Dr. Hüsnü Dal
Mechanical Engineering, METU _____

Assoc. Prof. Dr. Ulaş Yaman
Mechanical Engineering, METU _____

Prof. Dr. Erdem Acar
Mechanical Engineering, TOBB ETU _____

Date: 10.04.2025

I hereby declare that all information in this document has been obtained and presented in accordance with academic rules and ethical conduct. I also declare that, as required by these rules and conduct, I have fully cited and referenced all material and results that are not original to this work.

Name Last name : Eren Şahin

Signature :

ABSTRACT

STRESSES IN A MULTIFERROIC THIN FILM - MULTI-LAYER COATING SYSTEM

Şahin, Eren
Master of Science, Mechanical Engineering
Supervisor : Prof. Dr. Serkan Dağ

April 2025, 115 pages

Multiferroic or magneto-electro-elastic (MEE) materials, consisting of Piezoelectric (PE) and Piezo-magnetic (PM) phases, has coupling effects of mechanical deformation, electric and magnetic fields. The studies in this area increase in the recent years due to its wide and important applications in the general smart structures. The problem for a multiferroic thin film which is bonded to transversely isotropic multi-layer coatings on an isotropic homogenous substrate is solved by performing analytical approach in this study. All the layers are assumed to be bonded perfectly without an adhesive layer. The thin film is assumed to behave as "membrane", and the coupling effects of the magnetic and electrical fields are considered. In the analytical approach the governing Navier equations are obtained for the plane elasticity problem. These partial differential equations are solved to find the displacement fields that satisfy the boundary conditions by using Fourier transformation techniques. The numerical solutions for the singular integral equations (SIE) which are derived from the displacement fields are obtained by using collocation-expansion method and the contact stresses and stress intensity factors are

determined. The results obtained from analytical method are compared with the studies from literature to evaluate the accuracy of this study.

Keywords: Multiferroic, Thin Film, Multilayer Coating, Contact Stresses, Transversely Isotropic.

ÖZ

BİR MULTİFERROİK İNCE FİLM - ÇOK KATMANLI KAPLAMA SİSTEMİNDE GERİLMELER

Şahin, Eren
Yüksek Lisans, Makina Mühendisliği
Tez Yöneticisi: Prof. Dr. Serkan Dağ

Nisan 2025, 115 sayfa

Piezoelektrik (PE) ve Piezo-manyetik (PM) fazlardan oluşan multiferroik veya manyeto-elektro-elastik (MEE) malzemeler; mekanik deformasyon, elektrik ve manyetik alanların bağlaşım etkilerine sahiptir. Genel akıllı yapılardaki yaygın ve önemli uygulamaları nedeniyle bu alandaki çalışmalar son yıllarda artmaktadır. Bu çalışmada izotropik homojen bir substrat üzerinde enine izotropik çok katmanlı kaplamalara bağlanmış olan multiferroik ince bir filmin temas problemi, analitik bir yaklaşım kullanılarak çözülmüştür. Tüm katmanların yapıştırıcı bir katman olmadan mükemmel bir şekilde yapıştırıldığı varsayılmaktadır. İnce filmin "membran" gibi davrandığı varsayılmış olup, manyetik ve elektrik alanların bağlaşım etkileri göz önünde bulundurulmuştur. Analitik yaklaşımda, düzlem elastisitesi problemi için geçerli Navier denklemleri elde edilmiştir. Bu kısmi diferansiyel denklemler, Fourier dönüşüm teknikleri kullanılarak sınır koşullarını sağlayan deplasman alanlarını bulmak için çözülmüştür. Deplasman alanlarından türetilen tekil integral denklemlerinin (SIE) sayısal çözümleri, açılım-düzenleme yöntemi kullanılarak elde edilmiştir ve bunun sonucunda temas gerilmeleri ve gerilim yoğunluğu faktörleri

belirlenmiştir. Analitik yöntemden elde edilen sonuçlar literatürdeki çalışmalarla karşılaştırılarak bu çalışmanın doğruluğu değerlendirilmiştir.

Anahtar Kelimeler: Multiferroik, İnce film, Çok katmanlı kaplama, Temas Gerilimleri, Enine İzotropik.

To my grandfather Zülfü Demirel and to the lonely children of my lost country…

ACKNOWLEDGMENTS

Firstly, the author wishes to express his gratitude to his supervisor, Professor Dr. Serkan Dağ, for his assistance, guidance and mentorship throughout the dissertation process.

The technical assistance of Dr. Selim Ercihan Toktaş and the moral support of Mr. Fırat Cem Yücel are gratefully acknowledged.

Last and foremost, the author wishes to thank his wife Ms. Hilal Gürses Şahin, his mother Ms. Nacide Şahin, his father Mr. Ferit Şahin and his sister Ms. Deniz Şahin for their lifelong support and endless love.

TABLE OF CONTENTS

LIST OF TABLES

TABLES

LIST OF FIGURES

FIGURES

LIST OF ABBREVIATIONS

ABBREVIATIONS

SIF	:	Stress Intensity Factor
SIE	:	Singular Integral Equation
FGM	:	Functionally Graded Material
MEE	:	Magneto-Electro-Elastic

LIST OF SYMBOLS

SYMBOLS

$C_{11}^f, C_{12}^f, C_{22}^f$	:	The elastic stiffness coefficients for the thin film
e_{11}^f, e_{12}^f	:	The piezoelectric stiffness coefficients for the thin film
h_{11}^f, h_{12}^f	:	The magnetic stiffness coefficients for the thin film
E_x^f	:	The electric field in x-direction
H_x^f	:	The magnetic field in x-direction
$\sigma_{xx}^f, \sigma_{xy}^f, \sigma_{yy}^f$	:	The stresses of the thin film
$\sigma_{(i)xx}, \sigma_{(i)xy}, \sigma_{(i)yy}$	:	The stresses of the i-th layer coating
$\sigma_{xx}^s, \sigma_{xy}^s, \sigma_{yy}^s$	:	The stresses of the substrate
P_a, P_b	:	Edge loading on the thin film
ε_0	:	Far-field loading on multilayer coating-substrate
$k_1(t,y), k_2(t,y)$	:	Fredholm Kernels
$K_1(s,r), K_2(s,r)$	:	Normalized Fredholm Kernels
$k_{II,a}, k_{II,b}$	:	Stress Intensity Factors
ω	:	Fourier Transform Variable
$s_{(i)j}$	:	Roots of the characteristic equation
a, b	:	End points of the thin film

CHAPTER 1

INTRODUCTION

The objective of this study is to propose a method to study the stresses in a single layer multiferroic thin film and the transversely isotropic multilayer coating system on its underside. The investigation, which assumes plane elasticity and perfect bonding between the layers, is performed for both edge loading in the thin film and uniform strain conditions in the rest of the system. This chapter presents a survey of the literature on multiferroic materials and related problems. It then describes the scope of this study.

1.1 Literature Survey

In the context of the ongoing development of artificial intelligence and machine learning, the pursuit of smaller, more energy-efficient consumer electronic and data storage devices have intensified the search for new multifunctional materials that could potentially supplant the current semiconductor technologies. Among the advanced materials that have seen a surge in research activities, multiferroics have emerged as a particularly prominent area of interest due to their intriguing physical properties and the unique technological applications they offer (Ramesh and Spaldin [1]).

A crystal is provisionally designated as "ferroic" when it exhibits two or more distinct orientation states in the absence of external magnetic, electric, and mechanical stimuli, and is capable of transitioning between these states through the application of a magnetic field, electric field, mechanical stress, or a combination thereof (Aizu [2]). Multiferroic materials are a sub-class of ferroics that

simultaneously show multiple ferroic orders. These orders include ferroelectricity, ferromagnetism, and ferro elasticity. In essence, these materials elicit properties that are characteristic of both magnetic and dielectric substances, thereby enabling them to respond to both electric and magnetic fields. When the multiferroic term is introduced by Schmid [3], it is employed to describe the materials that display a coexistence of two or more primary ferroic orders within the same phase. However, the term has since been expanded to encompass the coexistence of ferroelectric and ferro-, ferri-, or antiferromagnetic order in single- or multiphase materials. The single-phase materials can be classified into two distinct categories, designated as Type I and Type II, as illustrated in **Figure 1-1**. (Fiebig et al. [4]). Type-I multiferroics demonstrate favorable ferroelectric properties, with the critical temperatures of the magnetic and ferroelectric transitions often exceeding that of the ambient temperature. However, it is undesirable to note that the coupling between magnetism and ferroelectricity in these materials is usually relatively weak (Khomskii [5]). The ferroelectricity observed in type I multiferroics may be resulted by several different mechanisms, including the influence of electronic lone pairs, geometric effects, and charge order (Singh et al. [6]). Type-II single-phase multiferroics are materials in which the ferroelectric order is induced by magnetism, thereby implying the presence of a markedly strong magnetoelectric coupling (Vopson [7]). Cr_2O_3 (McGuire [8]), $BiFeO_3$ (Wang et al. [9]), $PbFeTiO_3$ (Palkar and Malik [10]), YIG (Krichevtsov et al. [11]) and $TbMn_2O_5$ (Hur et al. [12]) are some examples of single phase multiferroics. Obtaining multiferroicity in a single phase is a challenging endeavor due to the inherent chemical incompatibility between ferroelectricity and magnetism (Spaldin [13]). Furthermore, single-phase multiferroic materials have yet to yield any characteristic that can simultaneously exhibit large and robust electric and magnetic polarizations at room temperature (Ma et al. [14]).

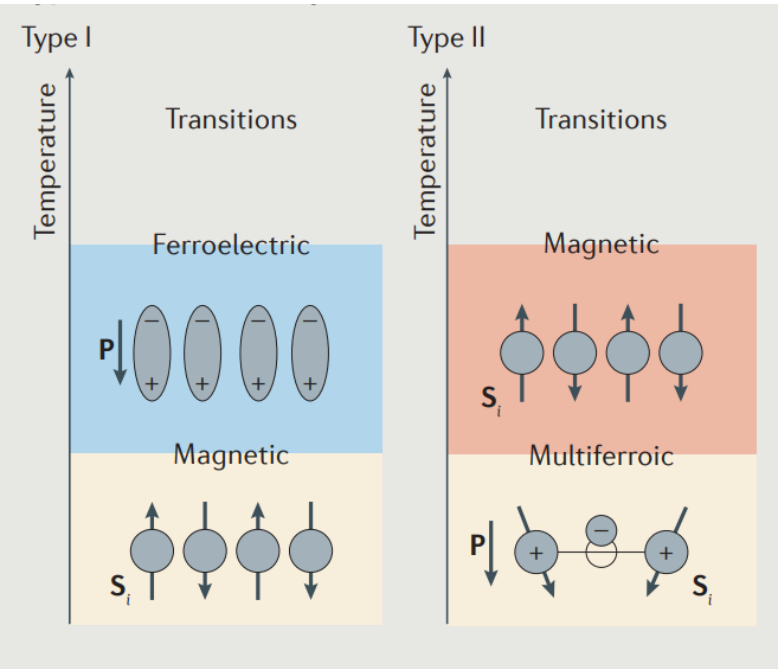

Figure 1-1. Types of single phase multiferroicity [4]

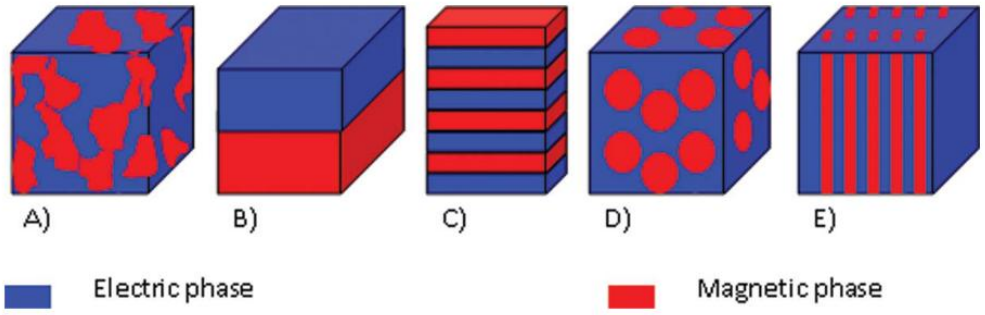

Figure 1-2. A structural diagrammatic representation for multiferroic composite structures. (A) homogeneous mixture of electric and magnetic phases; (B) laminated bi-layer structure; (C) laminated multi-layer structure; (D) composite made of particles mixed in a matrix; and (E) fiber multiferroic composite. [7]

To address the limitation of low ME coupling coefficients in single-phase multiferroics, composite-type multiferroics, which primarily comprise both ferroelectric and magnetic phases in the form of thin/thick films and nano/heterostructures, have been developed to enhance their performance (Gupta and Kotnala [15]). The concept of fabricating multiferroic composites presents a promising avenue for advancing materials science, offering substantial advantages

including greater flexibility in designing materials for specific applications and optimization of magneto-electric coupling. $BaTiO_3$/Fe laminated layers (Srinivasan et al. [16]), FeBSiC/PZT laminated layers (Ma et al. [17]) and AlN/FeCoSiB bilayers (Jahns et al. [18]) can be demonstrated as representative examples of multiphase multiferroics. **Figure 1-2** illustrates several potential multiferroic composite structures.

As previously stated, multiferroic structures have significant potential for incorporation into innovative devices, including those utilized in smart structures (See **Figure 1-3**). These applications can be demonstrated through a variety of devices, including random access memorys (Spaldin and Ramesh [20], Barman and Kaur [22]), resonators (Fetisov and Srinivasan [21], Corso et al. [27]), energy harvesters (Ryu et al. [23]), Naifar et al. [26]), sensors (Yarar et al. [25], Ribeiro et al. [32]), gyrators (Zhuang et al. [24], Bhuktare et al. [34]), transducers (Muralt et al. [28], Rupp et al. [33]), quantum wells (Ortmann et al. [29]), spintronic devices (Chang et al. [30]), antennas (Nikitin et al. [31]), and so forth.

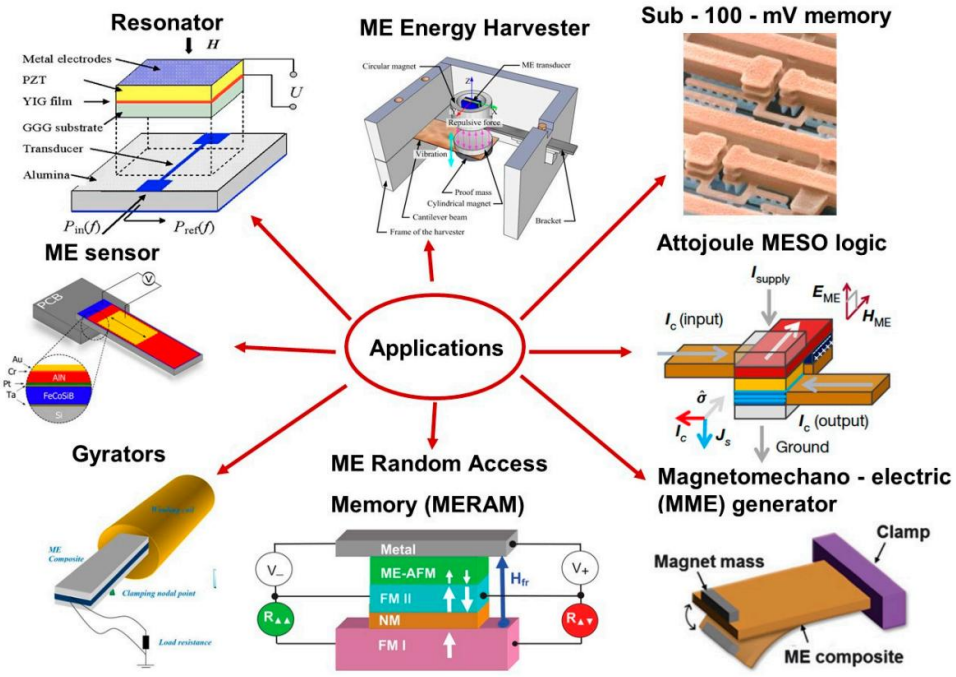

Figure 1-3. Some applications of multiferroic materials. (Dhiren et al. [19])

Contact mechanics plays an important role in the field of solid mechanics. The objective of the studies in this area is primarily to analyze the stress and displacement fields that result from contact loading, as this type of loading has the potential to cause failure of the components in the system. Hertz's study represents the inaugural study in this field [35]. Muskhelishvili shares important studies about punch problems and the solution techniques about the singularities faced in this problem in his book [36]. The punch problems are typically associated with substrate and/or coating(s) for varying material properties and a moving or stable punch, which determines whether the problem is elasto-statics or elasto-dynamic. The singular integral equations are derived in these problems by using stress-displacement relations and these equations are solved by using different techniques. The following doctoral dissertations exemplify studies of this type of problem. Dağ put forth a solution to the contact-crack coupling problem of a FGM substrate for different punch profiles [37]. Balcı investigated a contact problem involving the movement of a punch on both the FGM and the homogeneous coatings. [38]. Toktaş examined a contact issue pertaining to the motion of a punch on both the FGM and the multiferroic-homogenous multilayer coatings [39].

Erdoğan and Gupta studied on an elastic stiffener bonded to a substrate [40]. In point of fact, this was not a problem of punching; nevertheless, the relationship between the thin film and the substrate created an analogy to punching loads, from which the singular integral equations could be derived. It is also assumed that the peek stresses in the thin film are zero in this study. Erdoğan and Joseph conducted a study on the properties of multilayered films on a substrate, the results of which were published in two papers [41], [42]. In this study, stress relations for multiple films were also investigated. Thin films were modelled as orthotropic membranes with either shear interfaces or perfect bonding. In a study conducted by Guler et al., the stress in a thin film bonded to a FGM substrate was examined [43]. In his master's thesis, Gulver devised solutions for thin film bonded to FGM coating with edge loading and far-field loading conditions. The issue of a piezoelectric thin film bonded to a graded substrate through a bonding layer is investigated by Chen et al. (2018) using the

membrane assumption [44]. Chen et al. (2016) studied thin film bonded to FGM coating with far-field loading [45].

A review of the published literature reveals no studies that address the problem between a single layer multiferroic thin film and transversely isotropic multilayer coating. This is attributable to the inherent challenges associated with the synthesis of a single layer multiferroic thin film. The thin film model is selected for use with multiferroic materials, but it has the capacity to address the piezoelectric and ferromagnetic models by eliminating unnecessary parameters inherent to the nature of the problem.

1.2 Scope of the Study

In this study an analytical method is conducted for the contact stresses in a single layer multiferroic thin film and the transversely isotropic multilayer coating system on its underside. The issue of contact mechanics has been addressed in the context of thin film and multiferroic materials. However, a problem between a single layer multiferroic thin film and transversely isotropic multilayer coating has not been yet overseen. Section 1.1 gives brief information about multiferroic materials, and the problems related to multiferroics or thin films. Section 1.2 describes the scope of this study.

In Chapter 2, the formulation commences with the introduction of equilibrium equations in partial differential equation forms, utilizing the stress-displacement relations for multilayer coatings and substrate. Subsequently, the Fourier transform is employed to transform these equations into ordinary differential equations. The unknowns are eliminated through the application of continuity relations among the layers. Finally, these unknowns are defined with respect to a shear stress between the thin layer and uppermost layer through the utilization of boundary conditions between the uppermost layer and the thin film. Singular integral equation of the second kind with Cauchy singularity and Fredholm kernel is obtained at this step. In

consideration of the assumption that the normal stress within the contact surface in a thin film is zero, a single Fredholm kernel is obtained, thereby simplifying the problem and reducing the necessary solution time.

Chapter 3 covers the solution of singular integral equation and the derivation of stress in thin films. The singular integral equation is solved for both single end loading and far-field loading conditions. In order to facilitate the application of collocation methods, the aforementioned equations are subjected to a process of normalization. The Fredholm kernel is simplified by Gauss-Legendre quadrature. Thereafter, the singular integral equations are transformed into a linear equation system by Chebyshev polynomials. Stress intensity factors for mode-II at singularity points a,b are also derived at this step.

The numerical results are presented in Chapter 4. The results of two studies from the literature are used for verification. The parametric studies on two different models are derived for different geometric and material properties.

In Chapter 5, the results of parametric studies and possible future works are presented.

CHAPTER 2

PROBLEM STATEMENT AND FORMULATION

2.1 Problem Definition

In this study, it is assumed that a single layer multiferroic thin film is bonded to transversely isotropic multi-layer coating system. This coating system is placed onto an isotropic homogenous semi-infinite substrate. All the layers are considered perfectly bonded to each other without any defect. An elastic membrane model [37] is used for the thin film which implies that the normal stresses and the bending for it is negligible. The edge loads defined as P_a and P_b are applied on the thin film. The other loadings on the multi-layer coating and substrate system are also represented by an uniform strain ε_0. The thickness of the thin film is described as h_f. The end points of the thin film in y-coordinate are presented as a and b. The coating layers are numbered as from 1 to n in the negative x-direction. The layer number is shown in the parenthesis part of the subscript for the coatings. The features of the thin film and substrate are displayed by using f and s letters in the superscript, respectively. Whereas the continuity conditions are declared from substrate to n-th layer, the boundary conditions are only defined at $x=0$. All structures are modeled under the plane elasticity assumptions. The relations for each structure are analyzed under the sub-titles.

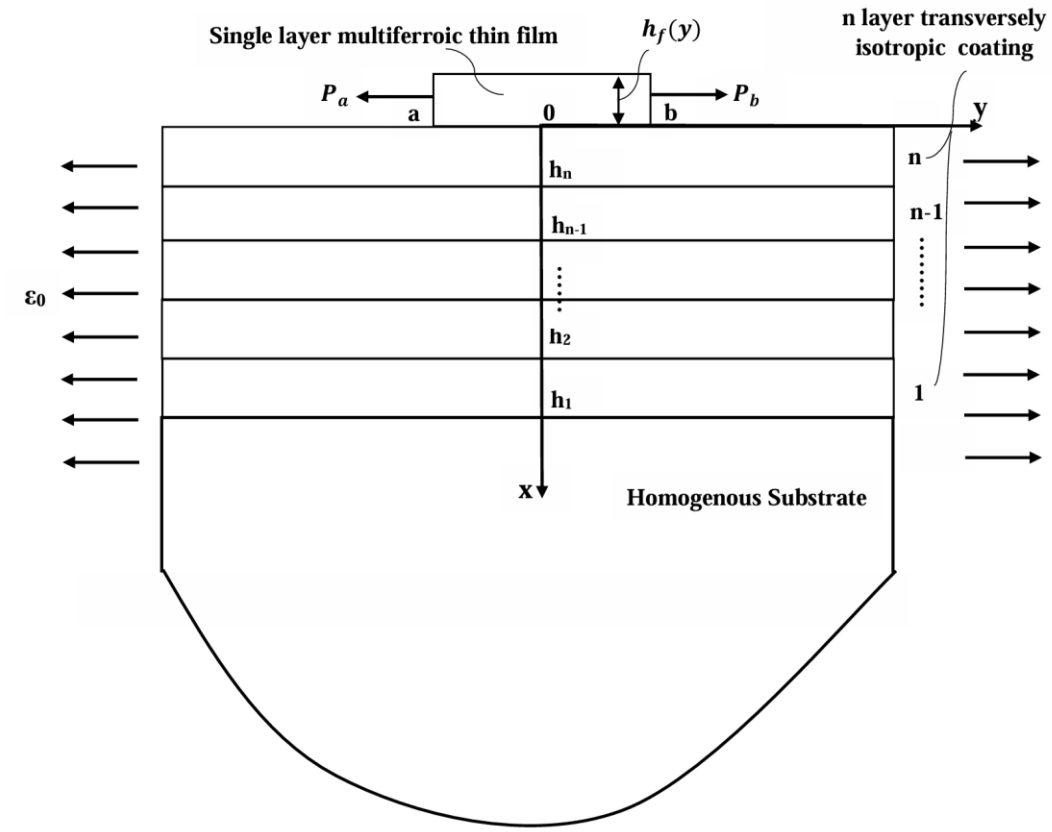

Figure 2-1. Geometry of the problem

2.2 Formulation

In this section, stress-displacement relations are employed to derive the equations for the thin film, multilayer coating, and substrate, in that order. Subsequently, singular integral equations are derived using continuity and boundary conditions.

2.2.1 Thin Film

The thin film in this study is accepted as multiferroic and poled along the x-axis. The constitutive equations for this material model can be expressed in (2.1) and (2.2) using elastic, piezoelectric and piezomagnetic material properties. The elastic stiffness coefficients of the thin film are represented by C_{11}^f, C_{12}^f, C_{22}^f. The

piezoelectric stiffness coefficients and piezomagnetic stiffness coefficients of the material are declared as e_{11}^f, e_{12}^f and h_{11}^f, h_{12}^f, respectively. The electric field and the magnetic field in x-direction are also stated as E_x^f and H_x^f, respectively.

$$\sigma_{xx}^f = C_{11}^f \varepsilon_{xx}^f + C_{12}^f \varepsilon_{yy}^f - e_{11}^f E_x^f - h_{11}^f H_x^f, \tag{2.1}$$

$$\sigma_{yy}^f = C_{12}^f \varepsilon_{xx}^f + C_{22}^f \varepsilon_{yy}^f - e_{12}^f E_x^f - h_{12}^f H_x^f. \tag{2.2}$$

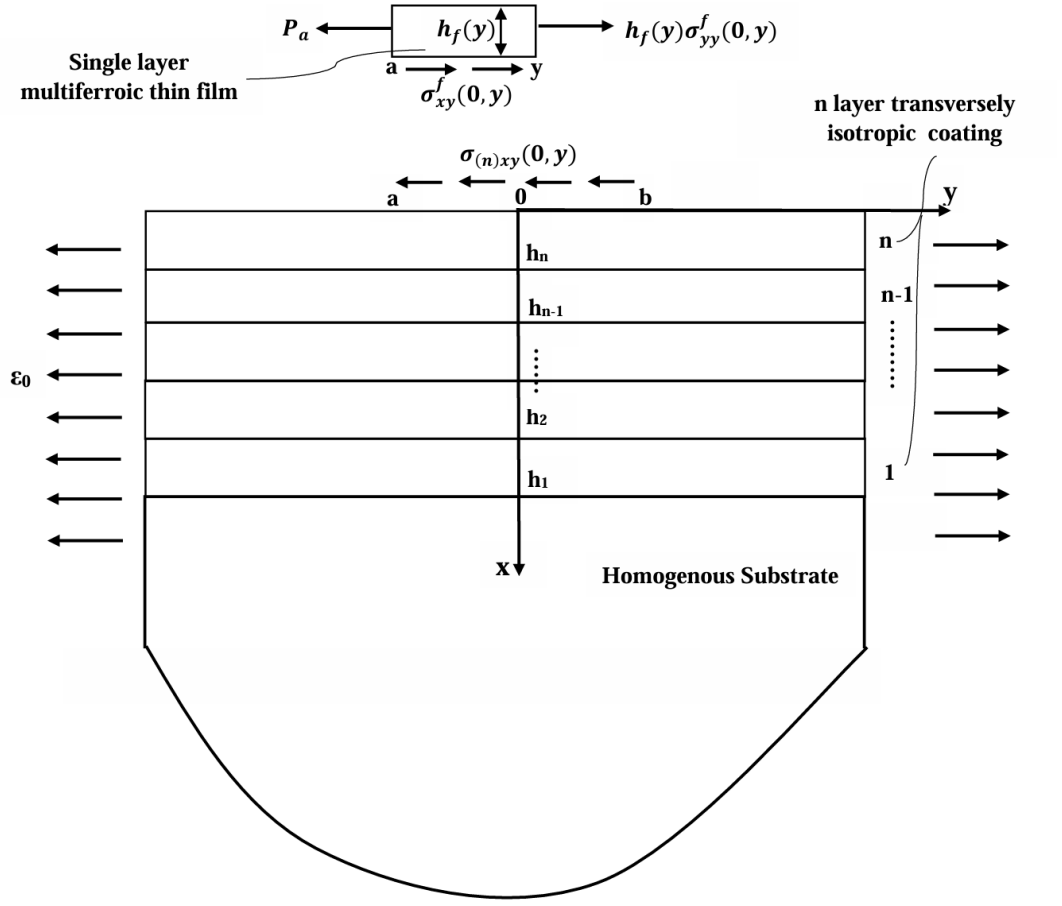

Figure 2-2. Free body diagram for the thin film

Free body diagram of the thin film is illustrated in **Figure 2-2**. The normal and shear stresses at the contact surface for the n-th layer coating are written as follows according to the membrane model of the thin film.

$$\sigma_{(n)xx}(0,y) = 0, \qquad -\infty < y < \infty, \tag{2.3}$$

$$\sigma_{(n)xy}(0,y) = \begin{cases} 0, & y < a \; and \; y > b, \\ f(y), & a < y < b, \end{cases} \tag{2.4}$$

The ratio of the normal force to the unit width of the thin film in the x-direction can be assumed uniform along with the thickness. Hence, one can obtain force equilibrium equations for the thin film in the following forms.

$$-\int_a^y \sigma_{xy}^f(0,t)dt + P_a = h_f(y)\sigma_{yy}^f(y), \tag{2.5}$$

$$\int_a^b \sigma_{xy}^f(0,t)dt + P_b = P_a. \tag{2.6}$$

The boundary conditions between the thin film and the coating can be derived as follows since all the layers are desired perfectly bonded.

$$\sigma_{(n)xy}(0,y) = \sigma_{xy}^f(0,y), \tag{2.7}$$

$$\sigma_{(n)xx}(0,y) = \sigma_{xx}^f(0,y). \tag{2.8}$$

The force equilibrium equations for the thin film in (2.5) and (2.6) can be redeclared considering (2.4) and the first boundary condition in (2.7) as below.

$$\sigma_{yy}^f(y) = \frac{1}{h_f(y)}(P_a - \int_a^y f(t)dt), \tag{2.9}$$

$$\int_a^b f(t)dt = P_a - P_b. \tag{2.10}$$

One can express the normal strain in x-direction considering the constitutive relation in (2.1) since the normal stress for the thin film in the x-direction is zero.

$$\varepsilon_{xx}^f(y) = (-C_{12}^f \varepsilon_{yy}^f(y) + e_{11}^f E_x^f + h_{11}^f H_x^f)/C_{11}^f \tag{2.11}$$

When the equation (2.11) is substituted into the constitutive relation in (2.2), a new expression for the normal stress in y-direction is accessed in the following form.

$$\sigma_{yy}^f(0,y) = (C_{22}^f - \frac{C_{12}^{f\,2}}{C_{11}^f})\,\varepsilon_{yy}^f(0,y) + \left(\frac{C_{12}^f e_{11}^f}{C_{11}^f} - e_{12}^f\right)E_x^f + \left(\frac{C_{12}^f h_{11}^f}{C_{11}^f} - h_{12}^f\right)H_x^f. \tag{2.12}$$

Finally, one can obtain the expression for the normal strain in y-direction by using the right-hand side of the (2.9) and (2.12).

$$\varepsilon_{yy}^{f}(0,y) = \frac{\frac{1}{h_f(y)}(P_a - \int_a^y f(t)dt) - \left(\frac{C_{12}^f e_{11}^f}{C_{11}^f} - e_{12}^f\right)E_x^f - \left(\frac{C_{12}^f h_{11}^f}{C_{11}^f} - h_{12}^f\right)H_x^f}{(C_{22}^f - \frac{C_{12}^{f\,2}}{C_{11}^f})}. \tag{2.13}$$

2.2.2 Multilayer Coating

The stress-strain relations related to each of the sub-layers for the transversely isotropic coatings are declared by the following matrix form:

$$\begin{bmatrix}\sigma_{(i)xx}\\ \sigma_{(i)yy}\\ \sigma_{(i)xy}\end{bmatrix} = \begin{bmatrix}C_{(i)11} & C_{(i)12} & 0\\ C_{(i)12} & C_{(i)22} & 0\\ 0 & 0 & C_{(i)55}\end{bmatrix}\begin{bmatrix}\varepsilon_{(i)xx}\\ \varepsilon_{(i)yy}\\ 2\varepsilon_{(i)xy}\end{bmatrix} \tag{2.14}$$

The elastic stiffnesses in (2.14) can be represented in terms of independent elastic parameters for both plain strain and plane stress cases in transversely isotropic material model. The number of these parameters are five for plain strain and four for plain stress. The elastic stiffnesses are formulated with these parameters in the following forms.

$$C_{(i)11} = \begin{cases}\frac{E_{(i)x}^2}{E_{(i)x} - v_{(i)xy}^2 E_{(i)y}} & for\ plane\ stress\\ \frac{(1 - v_{(i)yz}{}^2)E_{(i)x}^2}{\Delta} & for\ plane\ strain\end{cases}, \tag{2.15}$$

$$C_{(i)12} = \begin{cases}\frac{v_{(i)xy}E_{(i)x}E_{(i)y}}{E_{(i)x} - v_{(i)xy}^2 E_{(i)y}} & for\ plane\ stress\\ \frac{(v_{(i)xy} + v_{(i)xy}v_{(i)yz})E_{(i)x}E_{(i)y}}{\Delta} & for\ plane\ strain\end{cases}, \tag{2.16}$$

$$C_{(i)22} = \begin{cases}\frac{E_{(i)x}E_{(i)y}}{E_{(i)x} - v_{(i)xy}^2 E_{(i)y}} & for\ plane\ stress\\ \frac{(1 - v_{(i)yx}v_{(i)xy})E_{(i)x}E_{(i)y}}{\Delta} & for\ plane\ strain\end{cases}, \tag{2.17}$$

$$C_{(i)55} = \mu_{(i)xy}. \tag{2.18}$$

where,

$$\Delta = E_{(i)x}\left(1 - {v_{(i)yz}}^2 - v_{(i)xy}v_{(i)yx} + {v_{(i)yz}}^2 v_{(i)xy}v_{(i)yx}\right)$$
$$-E_{(i)y}(v_{(i)xy}^2 + 2v_{(i)xy}^2 v_{(i)yz} + v_{(i)xy}^2 v_{(i)yz}^2) \tag{2.19}$$

The equations are defined for these relations as follows.

$$\frac{v_{(i)ab}}{E_{(i)a}} = \frac{v_{(i)ba}}{E_{(i)b}}, \quad a, b = x, y, z. \tag{2.20}$$

The equilibrium equations for each sub-layer and the substrate can be stated as follows since there is no body force on the system.

$$\frac{\partial \sigma_{xx}}{\partial x} + \frac{\partial \sigma_{xy}}{\partial y} = 0 \tag{2.21}$$

$$\frac{\partial \sigma_{yy}}{\partial y} + \frac{\partial \sigma_{xy}}{\partial x} = 0 \tag{2.22}$$

When the stress equation in (2.14) is substituted into governing equilibrium equations (2.20) and (2.21), the following Navier's equations for displacements in each sub-layer yields in the partial differential equation form.

$$C_{(i)11}\frac{\partial^2 u_{(i)}}{\partial x^2} + C_{(i)55}\frac{\partial^2 u_{(i)}}{\partial y^2} + (C_{(i)12} + C_{(i)55})\frac{\partial^2 v_{(i)}}{\partial x \partial y} = 0, \tag{2.23}$$

$$C_{(i)22}\frac{\partial^2 v_i}{\partial y^2} + C_{(i)55}\frac{\partial^2 v_{(i)}}{\partial x^2} + (C_{(i)12} + C_{(i)55})\frac{\partial^2 u_{(i)}}{\partial x \partial y} = 0. \tag{2.24}$$

The displacements for each sublayer coating and the substrate can be explained in the following forms by applying Fourier transform in y direction.

$$u(x, y) = \frac{1}{2\pi}\int_{-\infty}^{\infty} U(x, \omega)e^{I\omega y}d\omega, \tag{2.25}$$

$$v(x, y) = \frac{1}{2\pi}\int_{-\infty}^{\infty} V(x, \omega)e^{I\omega y}d\omega. \tag{2.26}$$

where $I = \sqrt{-1}$ and $U(x, \omega)$ and $V(x, \omega)$ are Fourier transforms of u(x,y) and v(x,y) in y direction, respectively.

When the Fourier Transforms of the displacements are substituted into Navier's equations, one can transform these partial differential equations into the following ordinary differential equations.

$$C_{(i)11}\frac{d^2U_{(i)}}{dx^2} - C_{(i)55}\omega^2 U_{(i)} + (C_{(i)12} + C_{(i)55})\frac{dV_{(i)}}{dx} I\omega = 0, \tag{2.27}$$

$$-C_{(i)22}\omega^2 V_{(i)} + C_{(i)55}\frac{d^2V_{(i)}}{dx^2} + (C_{(i)12} + C_{(i)55})\frac{dU_{(i)}}{dx} I\omega = 0. \tag{2.28}$$

The solution forms for $U_{(i)}$ and $V_{(i)}$ can be suggested as follows.

$$U_{(i)}(x,\omega) = \sum_{j=1}^{4} M_{(i)j} e^{s_{(i)j}x}, \qquad i = 1,\dots,n-1, h_{(i+1)} < x < h_{(i)},$$

$$i = n,\ 0 < x < h_{(n)}, \tag{2.29}$$

$$V_{(i)}(x,\omega) = \sum_{j=1}^{4} M_{(i)j} N_{(i)j} e^{s_{(i)j}x}, \qquad i = 1,\dots,n-1, h_{(i+1)} < x < h_{(i)},$$

$$i = n,\ 0 < x < h_{(n)}. \tag{2.30}$$

The two partial differential equations can be modified into the following matrix system with the replacement of solution of the displacements in these equations.

$$\begin{bmatrix} I\omega s_{(i)j}(C_{(i)12} + C_{(i)55}) & C_{(i)11}s_{(i)j}^2 - C_{(i)55}\omega^2 \\ C_{(i)55}s_{(i)j}^2 - C_{(i)22}\omega^2 & (C_{(i)12} + C_{(i)55})I\omega s_{(i)j} \end{bmatrix} \begin{bmatrix} M_{(i)j}N_{(i)j} \\ M_{(i)j} \end{bmatrix} = 0. \tag{2.31}$$

The determinant of this matrix gives the following fourth order characteristic equation.

$$s_{(i)j}^4 + \left(\frac{C_{(i)12}^2}{C_{(i)11}C_{(i)55}} - \frac{C_{(i)22}}{C_{(i)55}} + \frac{2C_{(i)12}}{C_{(i)11}}\right)\omega^2 s_{(i)j}^2 + \frac{C_{(i)22}}{C_{(i)11}}\omega^4 = 0. \tag{2.32}$$

The solution of these characteristic equations yields the following roots.

$$s_{(i)1} = A_{(i)}|\omega|, \qquad \Re(s_{(i)1}) > 0, \tag{2.33}$$

$$s_{(i)2} = -A_{(i)}|\omega|, \quad \Re(s_{(i)2}) < 0, \tag{2.34}$$

$$s_{(i)3} = B_{(i)}|\omega|, \quad \Re(s_{(i)3}) > 0, \tag{2.35}$$

$$s_{(i)4} = -B_{(i)}|\omega|, \quad \Re(s_{(i)4}) < 0. \tag{2.36}$$

where $A_{(i)}$ and $B_{(i)}$ constants depend on the elastic stiffness coefficients with the given relations.

$$A_{(i)} = \frac{\sqrt{-2\left(\frac{c_{(i)12}^2}{c_{(i)11}c_{(i)55}} - \frac{c_{(i)22}}{c_{(i)55}} + \frac{2c_{(i)12}}{c_{(i)11}}\right) + 2\sqrt{\frac{c_{(i)12}^4}{c_{(i)11}^2 c_{(i)55}^2} - 2\frac{c_{(i)12}^2 c_{(i)22}}{c_{(i)11}c_{(i)55}^2} + 4\frac{c_{(i)12}^3}{c_{(i)11}^2 c_{(i)55}} + \frac{c_{(i)22}^2}{c_{(i)55}^2} - 4\frac{c_{(i)12}c_{(i)22}}{c_{(i)11}c_{(i)55}} + 4\frac{c_{(i)12}^2}{c_{(i)11}^2} - 4\frac{c_{(i)22}}{c_{(i)11}}}}}{2}, \tag{2.37}$$

$$B_{(i)} = \frac{\sqrt{-2\left(\frac{c_{(i)12}^2}{c_{(i)11}c_{(i)55}} - \frac{c_{(i)22}}{c_{(i)55}} + \frac{2c_{(i)12}}{c_{(i)11}}\right) - 2\sqrt{\frac{c_{(i)12}^4}{c_{(i)11}^2 c_{(i)55}^2} - 2\frac{c_{(i)12}^2 c_{(i)22}}{c_{(i)11}c_{(i)55}^2} + 4\frac{c_{(i)12}^3}{c_{(i)11}^2 c_{(i)55}} + \frac{c_{(i)22}^2}{c_{(i)55}^2} - 4\frac{c_{(i)12}c_{(i)22}}{c_{(i)11}c_{(i)55}} + 4\frac{c_{(i)12}^2}{c_{(i)11}^2} - 4\frac{c_{(i)22}}{c_{(i)11}}}}}{2}. \tag{2.38}$$

The expression for $N_{(i)j}$'s can be stated in the following relation by substituting the obtained roots in the matrix equation.

$$N_{(i)j} = I\frac{c_{(i)11}s_{(i)j}^2 - c_{(i)55}\omega^2}{(c_{(i)12}+c_{(i)55})\omega s_{(i)j}}. \tag{2.39}$$

2.2.3 Substrate

The stress-displacement relations for the homogenous substrate are given by the following notations.

$$\sigma_{xx}^s(x,y) = \frac{\mu^s}{(\kappa^s-1)}\left[(\kappa^s+1)\frac{\partial u^s}{\partial x} + (3-\kappa^s)\frac{\partial v^s}{\partial y}\right], \tag{2.40}$$

$$\sigma_{yy}^{s}(x,y) = \frac{\mu^{s}}{(\kappa^{s}-1)}[(3-\kappa^{s})\frac{\partial u^{s}}{\partial x} + (\kappa^{s}+1)\frac{\partial v^{s}}{\partial y}], \tag{2.41}$$

$$\sigma_{xy}^{s}(x,y) = \mu^{s}\left[\frac{\partial u^{s}}{\partial y} + \frac{\partial v^{s}}{\partial x}\right]. \tag{2.42}$$

where μ^{s} is the shear modulus of the substrate and κ^{s} is the Kolosov constant defined by the following definitions.

$$\kappa^{s} = \begin{cases} 3-4\nu^{s} & \text{for plane strain,} \\ \frac{3-\nu^{s}}{1+\nu^{s}} & \text{for plane stress.} \end{cases} \tag{2.43}$$

One can obtain the equilibrium equations for the substrate as follows.

$$\frac{\kappa^{s}+1}{\kappa^{s}-1}\frac{\partial^{2}u^{s}}{\partial x^{2}} + \frac{\partial^{2}u^{s}}{\partial y^{2}} + \frac{2}{\kappa^{s}-1}\frac{\partial^{2}v^{s}}{\partial x \partial y} = 0, \tag{2.44}$$

$$\frac{\kappa^{s}+1}{\kappa^{s}-1}\frac{\partial^{2}v^{s}}{\partial y^{2}} + \frac{\partial^{2}v^{s}}{\partial x^{2}} + \frac{2}{\kappa^{s}-1}\frac{\partial^{2}u^{s}}{\partial x \partial y} = 0. \tag{2.45}$$

Same procedure applies for the transformation of the partial differential equations into the ordinary differential equations. The Navier equations for the displacement in substrate take the following ordinary differential equations forms.

$$\frac{\kappa^{s}+1}{\kappa^{s}-1}\frac{d^{2}U^{s}}{dx^{2}} - \omega^{2}U^{s} + \frac{2}{\kappa^{s}-1}\frac{dV^{s}}{dx}I\omega = 0, \tag{2.46}$$

$$-\omega^{2}\frac{\kappa^{s}+1}{\kappa^{s}-1}V^{s} + \frac{d^{2}V^{s}}{dx^{2}} + \frac{2}{\kappa^{s}-1}\frac{dU^{s}}{dx}I\omega = 0. \tag{2.47}$$

The solutions are assumed similarly as follows.

$$U^{s}(x,\omega) = \sum_{k=1}^{4} M_{k}^{s} e^{s_{k}x}, \tag{2.48}$$

$$V^{s}(x,\omega) = \sum_{k=1}^{4} M_{k}^{s} N_{k}^{s} e^{s_{k}x}. \tag{2.49}$$

The ordinary differential equations can be summarized in the form of a matrix by using the solutions of the Fourier transform of the displacements.

$$\begin{bmatrix} \frac{2}{\kappa^{s}-1}I\omega s_{k} & \frac{\kappa^{s}+1}{\kappa^{s}-1}s_{k}^{2} - \omega^{2} \\ s_{k}^{2} - \frac{\kappa^{s}+1}{\kappa^{s}-1}\omega^{2} & \frac{2}{\kappa^{s}-1}I\omega s_{k} \end{bmatrix} \begin{bmatrix} M_{k}^{s} N_{k}^{s} \\ M_{k}^{s} \end{bmatrix} = 0. \tag{2.50}$$

The following characteristic equation is accessed from the matrix.

$$(1-(\kappa^s)^2)s_k^4 - 2(1-(\kappa^s)^2)\omega^2 s_k^2 + (1-(\kappa^s)^2)\omega^4 = 0. \quad (2.51)$$

The roots of this characteristic equations are,

$$s_{1,2} = |\omega|, \qquad s_{3,4} = -|\omega|. \quad (2.52)$$

One can reach the relationship between M_k^s's and N_k^s's with the following statements.

$$N_1^s = I\frac{|\omega|M_1^s + \kappa^s M_2^s}{\omega M_1^s}, \quad (2.53)$$

$$N_2^s = I\frac{|\omega|}{\omega}, \quad (2.54)$$

$$N_3^s = -I\frac{|\omega|M_3^s - \kappa^s M_4^s}{\omega M_3^s}, \quad (2.55)$$

$$N_4^s = -I\frac{|\omega|}{\omega}. \quad (2.56)$$

The values of M_1^s and M_2^s are taken as zero since the stresses for the substrate should be limited as the values of x and y approach to infinity. In this way, the Fourier transforms of the displacements reduce to the following structures.

$$U^s(x,\omega) = M_3^s e^{s_3 x} + xM_4^s e^{s_4 x}, \quad (2.57)$$

$$V^s(x,\omega) = M_3^s N_3^s e^{s_3 x} + xM_4^s N_4^s e^{s_4 x}. \quad (2.58)$$

2.2.4 Determination of Unknown Constants

The continuity and boundary conditions must be satisfied to extract the unknown functions $M_{(i)j}$ and M_k^s. The number of the equations required to define $4N+2$ unknown functions is $4N+2$. One can define $4N$ continuity conditions at each interface between the layers. 2 boundary conditions can be specified at the upper interface.

2.2.4.1 Continuity Conditions

The perfect bonding between the layers achieves the continuity conditions. These conditions can begin to be defined with the interface between the substrate and the first layer of the coating. For the first interface, four conditions are defined as follows.

$$u_{(1)}(h_1, y) = u^s(h_1, y), \tag{2.59}$$

$$v_{(1)}(h_1, y) = v^s(h_1, y), \tag{2.60}$$

$$\sigma_{(1)xx}(h_1, y) = \sigma^s_{xx}(h_1, y), \tag{2.61}$$

$$\sigma_{(1)xy}(h_1, y) = \sigma^s_{xy}(h_1, y). \tag{2.62}$$

When the Fourier transforms of the displacements and the equation (2.55) are fitted to the first two continuity conditions, the following matrix is produced. N_3^S is defined with respect to the unknown functions M_3^S and M_4^S. Hence, the open form of it is used to derive this matrix.

$$\begin{bmatrix} e^{s_3 h_1} & 0 \\ 0 & e^{s_4 h_1} \end{bmatrix} \begin{Bmatrix} M_3^S \\ M_4^S \end{Bmatrix} = \begin{bmatrix} 1 & h_1 \\ -\dfrac{I|\omega|}{\omega} & h_1 N_{\mathbf{4}}^S + \dfrac{\boldsymbol{I}\kappa^S}{\omega} \end{bmatrix}^{-1} \begin{bmatrix} 1 & 1 & 1 & 1 \\ N_{(1)\mathbf{1}} & N_{(1)\mathbf{2}} & N_{(1)\mathbf{3}} & N_{(1)\mathbf{4}} \end{bmatrix}$$
$$\begin{bmatrix} e^{s_{(1)1} h_1} & 0 & 0 & 0 \\ 0 & e^{s_{(1)2} h_1} & 0 & 0 \\ 0 & 0 & e^{s_{(1)3} h_1} & 0 \\ 0 & 0 & 0 & e^{s_{(1)4} h_1} \end{bmatrix} \begin{bmatrix} M_{(1)\mathbf{1}} \\ M_{(1)\mathbf{2}} \\ M_{(1)\mathbf{3}} \\ M_{(1)\mathbf{4}} \end{bmatrix}. \tag{2.63}$$

The last two continuity conditions, which refer to stresses, can also be transformed into the matrix form, after a few mathematical manipulations, as follows.

$$\left[r^{(s)}\right] \begin{bmatrix} e^{s_3 h_1} & 0 \\ 0 & e^{s_4 h_1} \end{bmatrix} \begin{Bmatrix} M_3^S \\ M_4^S \end{Bmatrix} = \left[r_{(1)}\right] \begin{bmatrix} e^{s_{(1)1} h_1} & 0 & 0 & 0 \\ 0 & e^{s_{(1)2} h_1} & 0 & 0 \\ 0 & 0 & e^{s_{(1)3} h_1} & 0 \\ 0 & 0 & 0 & e^{s_{(1)4} h_1} \end{bmatrix} \begin{bmatrix} M_{(1)1} \\ M_{(1)2} \\ M_{(1)3} \\ M_{(1)4} \end{bmatrix}. \tag{2.64}$$

where,

$$\left[r^{(s)}\right] = \begin{bmatrix} r_1^{(s)} & r_2^{(s)} \\ r_3^{(s)} & r_4^{(s)} \end{bmatrix}, \tag{2.65}$$

$$r_1^{(s)} = \frac{\mu^s}{(\kappa^s - 1)}[(\kappa^s + 1)s_3 + (3 - \kappa^s)|\omega|], \tag{2.66}$$

$$r_2^{(s)} = \frac{\mu^s}{(\kappa^s - 1)}[(\kappa^s + 1)(1 + h_1 s_4) + I\omega(3 - \kappa^s)h_1 N_4^s + \kappa^s(\kappa^s - 3)], \tag{2.67}$$

$$r_3^{(s)} = I\mu^s(\omega - \frac{|\omega|}{\omega}s_3), \tag{2.68}$$

$$r_4^{(s)} = \mu^s[I\omega h_1 + N_4^s(1 + h_1 s_4) + \frac{I\kappa^s}{\omega}s_4]. \tag{2.69}$$

$$\left[r_{(1)}\right] = \begin{bmatrix} r_{(1)1} & r_{(1)2} & r_{(1)3} & r_{(1)4} \\ r_{(1)5} & r_{(1)6} & r_{(1)7} & r_{(1)8} \end{bmatrix}, \tag{2.70}$$

$$r_{(1)1} = C_{(1)11}s_{(1)1} + I\omega C_{(1)12}N_{(1)1}, \tag{2.71}$$

$$r_{(1)2} = C_{(1)11}s_{(1)2} + I\omega C_{(1)12}N_{(1)2}, \tag{2.72}$$

$$r_{(1)3} = C_{(1)11}s_{(1)3} + I\omega C_{(1)12}N_{(1)3}, \tag{2.73}$$

$$r_{(1)4} = C_{(1)11}s_{(1)4} + I\omega C_{(1)12}N_{(1)4}, \tag{2.74}$$

$$r_{(1)5} = C_{(1)55}(I\omega + N_{(1)1}s_{(1)1}), \tag{2.75}$$

$$r_{(1)6} = C_{(1)55}(I\omega + N_{(1)2}s_{(1)2}), \tag{2.76}$$

$$r_{(1)7} = C_{(1)55}(I\omega + N_{(1)3}s_{(1)3}), \tag{2.77}$$

$$r_{(1)8} = C_{(1)55}(I\omega + N_{(1)4}s_{(1)4}). \tag{2.78}$$

M_3^s and M_4^s are attained in terms of $M_{(1)j}$'s with equation system (2.63). Hence, the equation system (2.64) provides $M_{(1)1}$ and $M_{(1)3}$ to be described with respect to $M_{(1)2}$ and $M_{(1)4}$ after the mathematical procedures shown in the following steps.

A new matrix $q_{(1)}$ can be prescribed in the following way.

$$\left[q_{(1)}\right]=\left[r^{(s)}\right]\begin{bmatrix}1 & h_1\\ -\frac{I|\omega|}{\omega} & h_1N_{\mathbf{4}}^{s}+\frac{I\kappa^{s}}{\omega}\end{bmatrix}^{-1}\begin{bmatrix}1 & 1 & 1 & 1\\ N_{(1)1} & N_{(1)\mathbf{2}} & N_{(1)\mathbf{3}} & N_{(1)\mathbf{4}}\end{bmatrix}, \tag{2.79}$$

$$\left[q_{(1)}\right]=\begin{bmatrix}q_{(1)1} & q_{(1)2} & q_{(1)3} & q_{(1)4}\\ q_{(1)5} & q_{(1)6} & q_{(1)7} & q_{(1)8}\end{bmatrix}. \tag{2.80}$$

The next step is to express the matrix $\left[w_{(1)}\right]$, which establishes the relationship between the $M_{(1)j}$'s.

$$\begin{bmatrix}e^{s_{(1)1}h_1} & 0\\ 0 & e^{s_{(1)3}h_1}\end{bmatrix}\begin{bmatrix}M_{(1)1}\\ M_{(1)\mathbf{3}}\end{bmatrix}=\begin{bmatrix}w_{(1)1} & w_{(1)2}\\ w_{(1)3} & w_{(1)4}\end{bmatrix}\begin{bmatrix}e^{s_{(1)2}h_1} & 0\\ 0 & e^{s_{(1)4}h_1}\end{bmatrix}\begin{bmatrix}M_{(1)\mathbf{2}}\\ M_{(1)\mathbf{4}}\end{bmatrix}, \tag{2.81}$$

$$\begin{bmatrix}\mathrm{w}_{(1)1} & \mathrm{w}_{(1)2}\\ \mathrm{w}_{(1)3} & \mathrm{w}_{(1)4}\end{bmatrix}=\begin{bmatrix}\mathrm{q}_{(1)1}-\mathrm{r}_{(1)1} & \mathrm{q}_{(1)3}-\mathrm{r}_{(1)3}\\ \mathrm{q}_{(1)5}-\mathrm{r}_{(1)5} & \mathrm{q}_{(1)7}-\mathrm{r}_{(1)7}\end{bmatrix}^{-1}\begin{bmatrix}\mathrm{r}_{(1)2}-\mathrm{q}_{(1)2} & \mathrm{r}_{(1)4}-\mathrm{q}_{(1)4}\\ \mathrm{r}_{(1)6}-\mathrm{q}_{(1)6} & \mathrm{r}_{(1)8}-\mathrm{q}_{(1)8}\end{bmatrix}. \tag{2.82}$$

Finally, to move the relationships from the lower interface to the upper interface of the first layer, a $\left[z_{(1)}\right]$ matrix is defined.

$$\begin{bmatrix}e^{s_{(1)1}h_2} & 0\\ 0 & e^{s_{(1)3}h_2}\end{bmatrix}\begin{bmatrix}M_{(1)1}\\ M_{(1)\mathbf{3}}\end{bmatrix}=\begin{bmatrix}z_{(1)1} & z_{(1)2}\\ z_{(1)3} & z_{(1)4}\end{bmatrix}\begin{bmatrix}e^{s_{(1)2}h_2} & 0\\ 0 & e^{s_{(1)4}h_2}\end{bmatrix}\begin{bmatrix}M_{(1)\mathbf{2}}\\ M_{(1)\mathbf{4}}\end{bmatrix}, \tag{2.83}$$

$$\begin{bmatrix}z_{(1)1} & z_{(1)2}\\ z_{(1)3} & z_{(1)4}\end{bmatrix}=\begin{bmatrix}e^{s_{(1)1}(h_2-h_1)} & 0\\ 0 & e^{s_{(1)3}(h_2-h_1)}\end{bmatrix}\begin{bmatrix}w_{(1)1} & w_{(1)2}\\ w_{(1)3} & w_{(1)4}\end{bmatrix}\begin{bmatrix}e^{s_{(1)2}(h_1-h_2)} & 0\\ 0 & e^{s_{(1)4}(h_1-h_2)}\end{bmatrix}. \tag{2.84}$$

The following statements are used to formulate the continuity conditions between the interfaces of the multilayer coatings.

$$u_{(i)}(h_{i+1},y)=u_{(i+1)}(h_{i+1},y),\qquad i=1,\dots,n-1,\quad -\infty<y<\infty, \tag{2.85}$$

$$v_{(i)}(h_{i+1},y)=v_{(i+1)}(h_{i+1},y),\qquad i=1,\dots,n-1,\quad -\infty<y<\infty, \tag{2.86}$$

$$\sigma_{(i)xx}(h_{i+1},y)=\sigma_{(i+1)xx}(h_{i+1},y),\quad i=1,\dots,n-1,\quad -\infty<y<\infty, \tag{2.87}$$

$$\sigma_{(i)xy}(h_{i+1}, y) = \sigma_{(i+1)xy}(h_{i+1}, y), \;\; i = 1, \ldots, n-1, \;\; -\infty < y < \infty. \qquad (2.88)$$

A similar approach to the previous example can be applied for the continuity conditions of the multilayer coatings. The following matrix can be constructed with the help of the two displacement equations in (2.85) and (2.86).

$$\begin{aligned}\left[K_{(i)}\right]\begin{bmatrix} e^{s_{(i)1}h_{(i+1)}} & 0 \\ 0 & e^{s_{(i)3}h_{(i+1)}} \end{bmatrix}\begin{bmatrix} M_{(i)1} \\ M_{(i)\mathbf{3}} \end{bmatrix} + \left[L_{(i)}\right]\begin{bmatrix} e^{s_{(i)2}h_{(i+1)}} & 0 \\ 0 & e^{s_{(i)4}h_{(i+1)}} \end{bmatrix}\begin{bmatrix} M_{(i)\mathbf{2}} \\ M_{(i)\mathbf{4}} \end{bmatrix} \\ = \left[M^*_{(i)}\right]\begin{bmatrix} e^{s_{(i+1)1}h_{(i+1)}} & 0 \\ 0 & e^{s_{(i+1)3}h_{(i+1)}} \end{bmatrix}\begin{bmatrix} M_{(i+1)1} \\ M_{(i+1)\mathbf{3}} \end{bmatrix} \\ + \left[N^*_{(i)}\right]\begin{bmatrix} e^{s_{(i+1)2}h_{(i+1)}} & 0 \\ 0 & e^{s_{(i+1)4}h_{(i+1)}} \end{bmatrix}\begin{bmatrix} M_{(i+1)\mathbf{2}} \\ M_{(i+1)\mathbf{4}} \end{bmatrix}.\end{aligned} \qquad (2.89)$$

where $\left[K_{(i)}\right]$, $\left[L_{(i)}\right]$, $\left[M^*_{(i)}\right]$ and $\left[N^*_{(i)}\right]$ are the matrices defined as follows.

$$\left[K_{(i)}\right] = \begin{bmatrix} 1 & 1 \\ N_{(i)1} & N_{(i)\mathbf{3}} \end{bmatrix}, \qquad (2.90)$$

$$\left[L_{(i)}\right] = \begin{bmatrix} 1 & 1 \\ N_{(i)2} & N_{(i)\mathbf{4}} \end{bmatrix}, \qquad (2.91)$$

$$\left[M^*_{(i)}\right] = \begin{bmatrix} 1 & 1 \\ N_{(\boldsymbol{i+1})1} & N_{(\boldsymbol{i+1})\mathbf{3}} \end{bmatrix}, \qquad (2.92)$$

$$\left[N^*_{(i)}\right] = \begin{bmatrix} 1 & 1 \\ N_{(\boldsymbol{i+1})2} & N_{(\boldsymbol{i+1})\mathbf{4}} \end{bmatrix}. \qquad (2.93)$$

$[M_{(i)\mathbf{2}} \quad M_{(i)\mathbf{4}}]^T$ and $[M_{(i)\mathbf{1}} \quad M_{(i)\mathbf{3}}]^T$ can be related in the following form.

$$\begin{bmatrix} e^{s_{(i)1}h_{(i+1)}} & 0 \\ 0 & e^{s_{(i)3}h_{(i+1)}} \end{bmatrix}\begin{bmatrix} M_{(i)1} \\ M_{(i)\mathbf{3}} \end{bmatrix} = \begin{bmatrix} z_{(i)1} & z_{(i)2} \\ z_{(i)3} & z_{(i)4} \end{bmatrix}\begin{bmatrix} e^{s_{(i)2}h_{(i+1)}} & 0 \\ 0 & e^{s_{(i)4}h_{(i+1)}} \end{bmatrix}\begin{bmatrix} M_{(i)\mathbf{2}} \\ M_{(i)\mathbf{4}} \end{bmatrix}. \qquad (2.94)$$

One can easily define $[M_{(i)\mathbf{2}} \quad M_{(i)\mathbf{4}}]^T$ in terms of $M_{(\boldsymbol{i+1})_j}$'s by the substitution of (2.94) in (2.89) as follows.

$$\begin{bmatrix} e^{s_{(i)2}h_{(i+1)}} & 0 \\ 0 & e^{s_{(i)4}h_{(i+1)}} \end{bmatrix} \begin{bmatrix} M_{(i)\mathbf{2}} \\ M_{(i)\mathbf{4}} \end{bmatrix}$$
$$= \left[O_{(i)}\right]^{-1}\left[M^{*}_{(i)}\right] \begin{bmatrix} e^{s_{(i+1)1}h_{(i+1)}} & 0 \\ 0 & e^{s_{(i+1)3}h_{(i+1)}} \end{bmatrix} \begin{bmatrix} M_{(i+1)1} \\ M_{(i+1)\mathbf{3}} \end{bmatrix}$$
$$+ \left[O_{(i)}\right]^{-1}\left[N^{*}_{(i)}\right] \begin{bmatrix} e^{s_{(i+1)2}h_{(i+1)}} & 0 \\ 0 & e^{s_{(i+1)4}h_{(i+1)}} \end{bmatrix} \begin{bmatrix} M_{(i+1)\mathbf{2}} \\ M_{(i+1)\mathbf{4}} \end{bmatrix}. \quad (2.95)$$

where,

$$\left[O_{(i)}\right] = \left[\left[K_{(i)}\right] \begin{bmatrix} z_{(i)1} & z_{(i)2} \\ z_{(i)3} & z_{(i)4} \end{bmatrix} + \left[L_{(i)}\right]\right]. \quad (2.96)$$

The following matrix declaration is used to express stress related continuity conditions in (2.87) and (2.88).

$$\left[P_{(i)}\right] \begin{bmatrix} e^{s_{(i)1}h_{(i+1)}} & 0 \\ 0 & e^{s_{(i)3}h_{(i+1)}} \end{bmatrix} \begin{bmatrix} M_{(i)1} \\ M_{(i)\mathbf{3}} \end{bmatrix} + \left[R_{(i)}\right] \begin{bmatrix} e^{s_{(i)2}h_{(i+1)}} & 0 \\ 0 & e^{s_{(i)4}h_{(i+1)}} \end{bmatrix} \begin{bmatrix} M_{(i)\mathbf{2}} \\ M_{(i)\mathbf{4}} \end{bmatrix}$$
$$= \left[S_{(i)}\right] \begin{bmatrix} e^{s_{(i+1)1}h_{(i+1)}} & 0 \\ 0 & e^{s_{(i+1)3}h_{(i+1)}} \end{bmatrix} \begin{bmatrix} M_{(i+1)1} \\ M_{(i+1)\mathbf{3}} \end{bmatrix}$$
$$+ \left[T_{(i)}\right] \begin{bmatrix} e^{s_{(i+1)2}h_{(i+1)}} & 0 \\ 0 & e^{s_{(i+1)4}h_{(i+1)}} \end{bmatrix} \begin{bmatrix} M_{(i+1)\mathbf{2}} \\ M_{(i+1)\mathbf{4}} \end{bmatrix}. \quad (2.97)$$

where the matrices $\left[P_{(i)}\right]$, $\left[R_{(i)}\right]$, $\left[S_{(i)}\right]$ and $\left[T_{(i)}\right]$ are given below.

$$\left[P_{(i)}\right] = \begin{bmatrix} C_{(i)11}s_{(i)1} + I\omega C_{(i)12}N_{(i)1} & C_{(i)11}s_{(i)3} + I\omega C_{(i)12}N_{(i)3} \\ C_{(i)55}(I\omega + N_{(i)1}s_{(i)1}) & C_{(i)55}(I\omega + N_{(i)3}s_{(i)3}) \end{bmatrix}, \quad (2.98)$$

$$\left[R_{(i)}\right] = \begin{bmatrix} C_{(i)11}s_{(i)2} + I\omega C_{(i)12}N_{(i)2} & C_{(i)11}s_{(i)4} + I\omega C_{(i)12}N_{(i)4} \\ C_{(i)55}(I\omega + N_{(i)2}s_{(i)2}) & C_{(i)55}(I\omega + N_{(i)4}s_{(i)4}) \end{bmatrix}, \quad (2.99)$$

$$\left[S_{(i)}\right]$$
$$= \begin{bmatrix} C_{(i+1)11}s_{(i+1)1} + I\omega C_{(i+1)12}N_{(i+1)1} & C_{(i+1)11}s_{(i+1)3} + I\omega C_{(i+1)12}N_{(i+1)3} \\ C_{(i+1)55}(I\omega + N_{(i+1)1}s_{(i+1)1}) & C_{(i+1)55}(I\omega + N_{(i+1)3}s_{(i+1)3}) \end{bmatrix}, \quad (2.100)$$

$$[T_{(i)}]$$
$$= \begin{bmatrix} C_{(i+1)11}s_{(i+1)2} + I\omega C_{(i+1)12}N_{(i+1)2} & C_{(i+1)11}s_{(i+1)4} + I\omega C_{(i+1)12}N_{(i+1)4} \\ C_{(i+1)55}(I\omega + N_{(i+1)2}s_{(i+1)2}) & C_{(i+1)55}(I\omega + N_{(i+1)4}s_{(i+1)4}) \end{bmatrix}.$$

(2.101)

$[W_{(i)}]$ matrix is attained, which allows $[M_{(i+1)2} \quad M_{(i+1)4}]^T$ to be written in $[M_{(i+1)1} \quad M_{(i+1)3}]^T$ dependent form using (2.94) and (2.95) in these continuity conditions.

$$\begin{bmatrix} e^{s_{(i+1)1}h_{(i+1)}} & 0 \\ 0 & e^{s_{(i+1)3}h_{(i+1)}} \end{bmatrix} \begin{bmatrix} M_{(i+1)1} \\ M_{(i+1)3} \end{bmatrix} = [W_{(i)}] \begin{bmatrix} e^{s_{(i+1)2}h_{(i+1)}} & 0 \\ 0 & e^{s_{(i+1)4}h_{(i+1)}} \end{bmatrix} \begin{bmatrix} M_{(i+1)2} \\ M_{(i+1)4} \end{bmatrix}. \quad (2.102)$$

where,

$$[W_{(i)}] = \left[[U_{(i)}] - [S_{(i)}]\right]^{-1} \left[[T_{(i)}] - [V_{(i)}]\right], \quad (2.103)$$

$$[U_{(i)}] = \left[[P_{(i)}] \begin{bmatrix} z_{(i)1} & z_{(i)2} \\ z_{(i)3} & z_{(i)4} \end{bmatrix} + [R_{(i)}]\right] [O_{(i)}]^{-1} [M^*_{(i)}], \quad (2.104)$$

$$[V_{(i)}] = \left[[P_{(i)}] \begin{bmatrix} z_{(i)1} & z_{(i)2} \\ z_{(i)3} & z_{(i)4} \end{bmatrix} + [R_{(i)}]\right] [O_{(i)}]^{-1} [N^*_{(i)}]. \quad (2.105)$$

The final step is to extract the $[Z_{(i+1)}]$ matrix, which represents the transition from the $h_{(i+1)}$ interface to the $h_{(i+2)}$ interface.

$$\begin{bmatrix} e^{s_{(i+1)1}h_{(i+2)}} & 0 \\ 0 & e^{s_{(i+1)3}h_{(i+2)}} \end{bmatrix} \begin{bmatrix} M_{(i+1)1} \\ M_{(i+1)3} \end{bmatrix} = \begin{bmatrix} z_{(i+1)1} & z_{(i+1)2} \\ z_{(i+1)3} & z_{(i+1)4} \end{bmatrix} \begin{bmatrix} e^{s_{(i+1)2}h_{(i+2)}} & 0 \\ 0 & e^{s_{(i+1)4}h_{(i+2)}} \end{bmatrix} \begin{bmatrix} M_{(i+1)2} \\ M_{(i+1)4} \end{bmatrix}. \quad (2.106)$$

where,

$$\begin{bmatrix} z_{(i+1)1} & z_{(i+1)2} \\ z_{(i+1)3} & z_{(i+1)4} \end{bmatrix} = \begin{bmatrix} e^{s_{(i+1)1}(h_{(i+2)} - h_{(i+1)})} & 0 \\ 0 & e^{s_{(i+1)3}(h_{(i+2)} - h_{(i+1)})} \end{bmatrix}$$

$$[W_{(i)}]\begin{bmatrix} e^{s_{(i+1)2}(h_{(i+1)}-h_{(i+2)})} & 0 \\ 0 & e^{s_{(i+1)4}(h_{(i+1)}-h_{(i+2)})} \end{bmatrix}. \quad (2.107)$$

Consequently, the relationships at the topmost layer can be defined in the following form.

$$\begin{bmatrix} M_{(n)1} \\ M_{(n)\mathbf{3}} \end{bmatrix} = \begin{bmatrix} z_{(n)1} & z_{(n)2} \\ z_{(n)3} & z_{(n)4} \end{bmatrix} \begin{bmatrix} M_{(n)\mathbf{2}} \\ M_{(n)\mathbf{4}} \end{bmatrix}, \quad (2.108)$$

$$\begin{bmatrix} z_{(n)1} & z_{(n)2} \\ z_{(n)3} & z_{(n)4} \end{bmatrix} = \begin{bmatrix} e^{-s_{(n)1}h_n} & 0 \\ 0 & e^{-s_{(n)3}h_n} \end{bmatrix} [W_{(n-1)}] \begin{bmatrix} e^{s_{(n)2}h_n} & 0 \\ 0 & e^{s_{(n)4}h_n} \end{bmatrix}. \quad (2.109)$$

All the unknown functions in the problem can only be described in terms of $M_{(n)\mathbf{2}}$ and $M_{(n)\mathbf{4}}$.

2.2.4.2 Boundary Conditions

The boundary conditions are determined with the help of the free surface condition of the uppermost face and the continuity conditions between the thin film and the uppermost layer. These conditions are specified in the equations (2.3) and (2.4) at the upper interface of the uppermost layer. The following expressions are obtained by applying the Fourier transform to these equations.

$$\int_{-\infty}^{\infty} \sigma_{(n)xx}(0,t)\, e^{-I\omega t} dt = 0, \quad (2.110)$$

$$\int_{-\infty}^{\infty} \sigma_{(n)xy}(0,t)\, e^{-I\omega t} dt = \int_{a}^{b} f(t)\, e^{-I\omega t} dt = Q(\omega). \quad (2.111)$$

The equations (2.110) and (2.111) can be summarized as follows in matrix form.

$$\begin{bmatrix} M_{(n)\mathbf{2}} \\ M_{(n)\mathbf{4}} \end{bmatrix} = [\Theta] \begin{bmatrix} 0 \\ Q(\omega) \end{bmatrix}, \quad (2.112)$$

where $[\Theta]$ is given below as a function of $[P_{(n)}]$ and $[R_{(n)}]$ matrices declared by means of the formulae (2.98) and (2.99) for $i = n$.

$$[\Theta] = \left[[P_{(n)}][z_{(n)}] + [R_{(n)}] \right]^{-1}. \quad (2.113)$$

Ultimately, all hitherto unknown functions are defined in terms of $Q(\omega)$.

2.2.5 Derivation of Singular Integral Equation

The singular integral equation is obtained at the end of this part. The formulation commences with the derivative of displacements with respect to y-coordinate.

$$\lim_{x\to 0}\frac{\partial u_{(n)}(x,y)}{\partial y}=\lim_{x\to 0}\frac{1}{2\pi}\int_{-\infty}^{\infty} I\omega\sum_{J=1}^{4} M_{(n)j}\, e^{s_{(n)j}x+I\omega y}d\omega, \tag{2.114}$$

$$\lim_{x\to 0}\frac{\partial v_{(n)}(x,y)}{\partial y}=\lim_{x\to 0}\frac{1}{2\pi}\int_{-\infty}^{\infty} I\omega\sum_{J=1}^{4} M_{(n)j}N_{(n)j}\, e^{s_{(n)j}x+I\omega y}d\omega. \tag{2.115}$$

The aforementioned derivatives can be modified into the following forms in order to establish a relationship between $f(t)$.

$$\lim_{x\to 0} 2\pi\frac{\partial u_{(n)}(x,y)}{\partial y}=\int_{-\infty}^{\infty} J_1(x,y,t)f(t)\,dt, \tag{2.116}$$

$$\lim_{x\to 0} 2\pi\frac{\partial v_{(n)}(x,y)}{\partial y}=\int_{-\infty}^{\infty} J_2(x,y,t)f(t)\,dt. \tag{2.117}$$

where the functions J_1 and J_2 are defined in the following manner.

$$J_1=\lim_{x\to 0}\int_{-\infty}^{\infty} o_1(x,\omega)\, e^{-I\omega(t-y)}d\omega, \tag{2.118}$$

$$J_2=\lim_{x\to 0}\int_{-\infty}^{\infty} o_2(x,\omega)\, e^{-I\omega(t-y)}d\omega. \tag{2.119}$$

The functions o_1 and o_2 are defined in terms of the parameter, which contains the coefficient with respect to $Q(\omega)$, as follows.

$$o_1(x,\omega)=\text{coeff}\left[I\omega\sum_{J=1}^{4} M_{(n)j}\, e^{s_{(n)j}x}, Q(\omega)\right], \tag{2.120}$$

$$o_2(x,\omega)=\text{coeff}\left[I\omega\sum_{J=1}^{4} M_{(n)j}N_{(n)j}\, e^{s_{(n)j}x}, Q(\omega)\right]. \tag{2.121}$$

An asymptotic analysis must be conducted to ascertain the strength of the singularity in the singular integral in this step. In this study, the functions are illustrated as ω approaches infinity with the use of the infinity symbol in superscript form.

$z_{(n)}$ matrix can be written in the following explicit form.

$$\begin{bmatrix} z_{(n)1} & z_{(n)2} \\ z_{(n)3} & z_{(n)4} \end{bmatrix} = \begin{bmatrix} e^{(s_{(n)2}-s_{(n)1})h_n} W_{(n-1)1} & e^{(s_{(n)4}-s_{(n)1})h_n} W_{(n-1)2} \\ e^{(s_{(n)2}-s_{(n)3})h_n} W_{(n-1)3} & e^{(s_{(n)4}-s_{(n)3})h_n} W_{(n-1)4} \end{bmatrix}. \tag{2.122}$$

In consequence of the definition of the real parts of the roots, the exponents of the exponential functions tend to minus infinity, which implies that the $z_{(n)}$ matrix assumes a value of zero. Accordingly, $M_{(n)1}^{\infty}$ and $M_{(n)3}^{\infty}$ are calculated to be equal to zero and $M_{(n)2}^{\infty}$ and $M_{(n)4}^{\infty}$ are extracted in the following form.

$$\begin{bmatrix} M_{(n)2}^{\infty} \\ M_{(n)4}^{\infty} \end{bmatrix} = [\Theta]^{\infty} \begin{bmatrix} 0 \\ Q(\omega) \end{bmatrix}. \tag{2.123}$$

where,

$$[\Theta]^{\infty} = \left[R_{(n)}\right]^{-1}. \tag{2.124}$$

As a result of asymptotic analysis o_1^{∞} and o_2^{∞} can be expressed in the following form.

$$o_1^{\infty}(x,\omega) = p_{11} e^{s_{(n)2}x} + p_{12} e^{s_{(n)4}x}, \tag{2.125}$$

$$o_2^{\infty}(x,\omega) = I\frac{\omega}{|\omega|} p_{21} e^{s_{(n)2}x} + I\frac{\omega}{|\omega|} p_{22} e^{s_{(n)4}x}. \tag{2.126}$$

p constants depend on only the elastic stiffness coefficients. J_1^{∞} and J_2^{∞} are obtained by using equations (2.125) and (2.126).

$$J_1^{\infty} = \lim_{x\to 0}\left(p_{11}\int_{-\infty}^{\infty} e^{-A|\omega|x}\, e^{-I\omega(t-y)} d\omega\right) + \lim_{x\to 0}\left(p_{12}\int_{-\infty}^{\infty} e^{-B|\omega|x}\, e^{-I\omega(t-y)} d\omega\right), \tag{2.127}$$

$$J_2^{\infty} = \lim_{x\to 0}\left(p_{21}\int_{-\infty}^{\infty} I\frac{\omega}{|\omega|} e^{-A|\omega|x}\, e^{-I\omega(t-y)} d\omega\right) + \lim_{x\to 0}\left(p_{22}\int_{-\infty}^{\infty} I\frac{\omega}{|\omega|} e^{-B|\omega|x}\, e^{-I\omega(t-y)} d\omega\right). \tag{2.128}$$

The following steps illustrate the streamlining of the aforementioned two functions.

Exponential function can be expressed in trigonometric forms by using Euler formula.

$$e^{-I\omega(t-y)} = \cos\big(\omega(t-y)\big) - I\sin(\omega(t-y)). \tag{2.129}$$

The following equations can be derived by employing this formula and the odd-even characteristics of functions.

$$\int_{-\infty}^{\infty} e^{|\omega|x}\, e^{-I\omega(t-y)} d\omega = 2\int_{0}^{\infty} e^{\omega x}\, cos\big(\omega(t-y)\big)\, d\omega, \tag{2.130}$$

$$\int_{-\infty}^{\infty} I\frac{\omega}{|\omega|} e^{|\omega|x}\, e^{-I\omega(t-y)} d\omega = 2\int_{0}^{\infty} e^{\omega x}\, sin\big(\omega(t-y)\big)\, d\omega. \tag{2.131}$$

The following integral rules are put forth by Abramowitz and Stegun [47].

$$\int_{0}^{\infty} e^{-ax}\sin(bx)\, dx = \frac{b}{a^2+b^2}, \qquad \int_{0}^{\infty} e^{-ax}\cos(bx)\, dx = \frac{a}{a^2+b^2}. \tag{2.132}$$

The equations (2.130) and (2.131) can be updated by employing the aforementioned rules.

$$2\int_{0}^{\infty} e^{\omega x} cos\,(\omega(t-y))d\omega = \frac{-2x}{x^2+(t-y)^2}, \tag{2.133}$$

$$2\int_{0}^{\infty} e^{\omega x}\sin\big(\omega(t-y)\big)\, d\omega = \frac{2(t-y)}{x^2+(t-y)^2}. \tag{2.134}$$

One can express J_1^{∞} and J_2^{∞} by using (2.133) and (2.134) as follows.

$$J_1^{\infty} = 2p_{11}\lim_{x\to 0}\left(\frac{Ax}{(Ax)^2+(t-y)^2}\right) + 2p_{12}\lim_{x\to 0}\left(\frac{Bx}{(Bx)^2+(t-y)^2}\right), \tag{2.135}$$

$$J_2^{\infty} = 2p_{21}\lim_{x\to 0}\left(\frac{(t-y)}{(Ax)^2+(t-y)^2}\right) + 2p_{22}\lim_{x\to 0}\left(\frac{(t-y)}{(Bx)^2+(t-y)^2}\right). \tag{2.136}$$

The two equations can be transformed into their final form by determining the limits.

$$J_1^{\infty} = 2(p_{11}+p_{12})\,\pi\delta(t-y), \tag{2.137}$$

$$J_2^{\infty} = \frac{2(p_{21}+p_{22})}{t-y}. \tag{2.138}$$

where δ represents the Dirac delta function.

The derivative of the displacements can be defined by means of asymptotic values of the kernels in the following ways.

$$\lim_{x\to 0} 2\pi \frac{\partial u_{(n)}(x,y)}{\partial y} = \int_{-\infty}^{\infty}[J_1(x,y,t) - J_1^{\infty}(x,y,t)]f(t)\,dt + \int_{-\infty}^{\infty} J_1^{\infty}(x,y,t)f(t)dt, \quad (2.139)$$

$$\lim_{x\to 0} 2\pi \frac{\partial v_{(n)}(x,y)}{\partial y} = \int_{-\infty}^{\infty}[J_2(x,y,t) - J_2^{\infty}(x,y,t)]f(t)\,dt + \int_{-\infty}^{\infty} J_2^{\infty}(x,y,t)f(t)dt. \quad (2.140)$$

The second integral in equation (2.139) can be simplified as follows by using the sifting property of Dirac delta function. The second integral in (2.140) is also shown as below.

$$\int_{-\infty}^{\infty} J_1^{\infty}(x,y,t)f(t)dt = 2\pi p_1 f(y). \quad (2.141)$$

$$\int_{-\infty}^{\infty} J_2^{\infty}(x,y,t)f(t)dt = 2p_2 \int_{-\infty}^{\infty} \frac{1}{t-y} f(t)dt. \quad (2.142)$$

where,

$$p_1 = p_{11} + p_{12}, \quad (2.143)$$

$$p_2 = p_{21} + p_{22}, \quad (2.144)$$

These two parameters are obtained from the asymptotic analysis and expressed as follows.

$$p_1 = -\frac{(C_{(n)11}A_{(i)}B_{(i)} - C_{(n)12})(C_{(n)12} + C_{(n)55})}{C_{(n)55}(C_{(n)11}{B_{(i)}}^2 + C_{(n)12})(C_{(n)11}{A_{(i)}}^2 + C_{(n)12})}, \quad (2.145)$$

$$p_2 = -\frac{C_{(n)11}(A_{(i)} + B_{(i)})(C_{(n)12} + C_{(n)55})}{C_{(n)55}(C_{(n)11}{B_{(i)}}^2 + C_{(n)12})(C_{(n)11}{A_{(i)}}^2 + C_{(n)12})}. \quad (2.146)$$

In light of the definitions of $A_{(i)}$ and $B_{(i)}$ in equations (2.37) and (2.38), which pertain to the elastic stiffness coefficients, it follows that, p_1 and p_2 are solely contingent upon these coefficients.

The singular integral equations are derived by modifying the integral limits in accordance with the definition of $f(t)$ and employing the expressions in (2.141), (2.142), as detailed below.

$$\frac{\partial u_{(n)}(x,y)}{\partial y} = \frac{1}{\pi}\int_a^b k_1(t,y)f(t)\,dt + p_1\,f(y), \tag{2.147}$$

$$\frac{\partial v_{(n)}(x,y)}{\partial y} = \frac{1}{\pi}\int_a^b \left[k_2(t,y) + \frac{p_2}{t-y}\right] f(t)dt. \tag{2.148}$$

where $k_1(t,y)$ and $k_2(t,y)$ are the Fredholm kernels defined as below. The numerical solutions of these kernels are provided in Chapter 3.

$$k_1(t,y) = \int_0^\infty (o_1(0,\omega) - p_1)\cos\big(\omega(t-y)\big)\,d\omega, \tag{2.149}$$

$$k_2(t,y) = \int_0^\infty (o_2(0,\omega) - p_2)\sin\big(\omega(t-y)\big)\,d\omega. \tag{2.150}$$

The second integral will be subjected to subsequent analysis in order to extract stress relations. The following compatibility condition can be defined at $x = 0$, given that the far-field loading is present solely on the multi-layer coating and substrate system, rather than on the thin film and for perfect bonding condition.

$$\varepsilon_{(n)yy} - \varepsilon_{yy}^f = \varepsilon_0, \tag{2.151}$$

This equation can be updated by substituting.

$$\frac{1}{\pi}\int_a^b \left[k_2(t,y) + \frac{p_2}{t-y}\right] f(t)dt - \frac{\frac{1}{h_{f(y)}}(P_a - \int_a^y f(t)dt) - \left(\frac{C_{12}^f e_{11}^f}{C_{11}^f} - e_{12}^f\right)E_x^f - \left(\frac{C_{12}^f h_{11}^f}{C_{11}^f} - h_{12}^f\right)H_x^f}{\left(C_{22}^f - \frac{C_{12}^{f\,2}}{C_{11}^f}\right)} = \varepsilon_0. \tag{2.152}$$

After a simple manipulation the final form of the singular integral equation is declared in the following form. One can attain the normal stress in y-direction and the lateral stress in thin film using the solution of this singular integral equation.

$$\frac{1}{\pi}\left(C_{22}^{f}-\frac{C_{12}^{f\,2}}{C_{11}^{f}}\right)\int_{a}^{b}\left[k_2(t,y)+\frac{p_2}{t-y}\right]f(t)dt+\frac{1}{h_f(y)}\int_{a}^{y}f(t)dt$$

$$=\frac{P_a}{h_f(y)}+\left(\frac{C_{12}^{f}e_{11}^{f}}{C_{11}^{f}}-e_{12}^{f}\right)E_x^f+\left(\frac{C_{12}^{f}h_{11}^{f}}{C_{11}^{f}}-h_{12}^{f}\right)H_x^f+\left(C_{22}^{f}-\frac{C_{12}^{f\,2}}{C_{11}^{f}}\right)\varepsilon_0.$$

(2.153)

CHAPTER 3

NUMERICAL SOLUTION

The objective of this chapter is to develop solutions for the singular integral equation of the problem. The singular integral equation has been normalized to accommodate a change in the integration limits, which is an adaptation to collocation methods. The Gauss-Legendre quadrature polynomial expansion is employed for the computation of the Fredholm kernels. The final equation is expanded using Chebyshev polynomials and the solution is searched for the coefficients of this expansion. The following section provides the numerical solution techniques mentioned above, with a focus on two distinct loading conditions.

3.1 Normalization and Numerical Solution for Fredholm Kernel

It is essential to normalize the interval of the singular integral equation, which is given by (a, b), to the interval $(-1,1)$ in order to be able to solve the equation. It is assumed that h_f is constant. The new variables and functions are also defined to adapt the existing variables in (2.153) to this normalization. The following is a description of the process.

$$y = \frac{b-a}{2} r + \frac{b+a}{2}, \qquad t = \frac{b-a}{2} s + \frac{b+a}{2}, \qquad -1 < \mathrm{r} < 1, -1 < s < 1. \tag{3.1}$$

$$(C_{22}^f - \frac{C_{12}^{f\,2}}{C_{11}^f}) \frac{1}{\pi} \int_{-1}^{1} \left[K_2(s,r) + \frac{p_2}{s-r} \right] f(s)\, ds + \frac{b-a}{2h_f} \int_{-1}^{r} f(s) ds = D \tag{3.2}$$

where,

$$D = \frac{p_a}{h_f} + \left(\frac{C_{12}^f e_{11}^f}{C_{11}^f} - e_{12}^f \right) E_x^f + \left(\frac{C_{12}^f h_{11}^f}{C_{11}^f} - h_{12}^f \right) H_x^f + \left(C_{22}^f - \frac{C_{12}^{f\,2}}{C_{11}^f} \right) \varepsilon_0, \tag{3.3}$$

$$K_2(s,r) = \frac{b-a}{2} k_2(t,y). \tag{3.4}$$

The new Kernel $K_2(s,r)$, which guarantees the validity of proposition (3.4), can be declared with the following definitions.

$$\omega = \frac{2}{b-a}\omega^*, \quad o_2(0,\omega) = {o_2}^*(0,\omega^*), \qquad p_2 = {p_2}^*. \tag{3.5}$$

$$K_2(s,r) = \int_0^\infty ({o_2}^*(0,\omega^*) - {p_2}^*)\sin\big(\omega^*(s-r)\big)\,d\omega^*. \tag{3.6}$$

Given that the Kernel is constituted by an integral with an infinite upper limit, the integral is partitioned into two constituent parts, as detailed below, in order to attain a solution. A^* is defined as the cut-off point of the integral. When this value is set to a sufficiently high level, the first integral identified in right hand side of the (3.7) can be regarded as zero.

$$\begin{aligned} K_2(s,r) = {} & \int_{A^*}^\infty ({o_2}^*(0,\omega^*) - {p_2}^*)\sin\big(\omega^*(s-r)\big)\,d\omega^* \\ & + \int_0^{A^*} ({o_2}^*(0,\omega^*) - {p_2}^*)\sin\big(\omega^*(s-r)\big)\,d\omega^*. \end{aligned} \tag{3.7}$$

One more normalization is carried out with the following description and the kernel is calculated approximately by using the Gauss-Legendre quadrature collocation method, as follows.

$$\omega^* = \frac{A^*}{2}\xi + \frac{A^*}{2}, \tag{3.8}$$

$$\begin{aligned} K_2(s,r) &= \frac{A^*}{2}\int_{-1}^{1}\left({o_2}^*\left(0,\left(\frac{A^*}{2}\xi + \frac{A^*}{2}\right)\right) - {p_2}^*\right)\sin\left(\left(\frac{A^*}{2}\xi + \frac{A^*}{2}\right)(s-r)\right)d\xi \\ &\cong \frac{A^*}{2}\sum_{k=1}^{t} w_k n(\xi_k), \end{aligned} \tag{3.9}$$

$$n(\xi_k) = \left({o_2}^*\left(0,\left(\frac{A^*}{2}\xi_k + \frac{A^*}{2}\right)\right) - {p_2}^*\right)\sin\left(\left(\frac{A^*}{2}\xi_k + \frac{A^*}{2}\right)(s-r)\right). \tag{3.10}$$

where w_k's are quadrature weight functions and ξ_k's are the roots of the t-th Legendre polynomial. The quadrature weight functions are presented in the following manner where P_n denotes the Legendre polynomials.

$$w_k = \frac{2}{(1-\xi_k^2)\left[P_n'(\xi_k)\right]^2}\,. \tag{3.11}$$

In this study, the integration interval is partitioned into numerous segments to minimize the computational burden, and the collocation is conducted through the utilization of 20 points.

3.2 Numerical Solution for Single End Loading Condition

It is assumed that a loading only exists at the right end of the thin film and that no strain is present at the ends of the multilayer coating and substrate assembly in this version of the problem. Consequently, the integral equation can be updated to reflect the following single end loading conditions.

$$P_a = 0, \qquad P_b = P, \qquad \varepsilon_0 = 0. \tag{3.12}$$

One can define $f(s)$ with the following new parameters.

$$f(s) = g_1 g(s), \tag{3.13}$$

where,

$$g_1 = \left(\frac{C_{12}^f e_{11}^f}{C_{11}^f} - e_{12}^f\right) E_x^f + \left(\frac{C_{12}^f h_{11}^f}{C_{11}^f} - h_{12}^f\right) H_x^f + \frac{P}{h_f}. \tag{3.14}$$

The solution in the following form is proposed for the function $g(s)$.

$$g(s) = \phi(s) w(s). \tag{3.15}$$

where $\phi(s)$ is a continous, bounded function within the $(-1,1)$ interval and $w(s)$ denotes the weight function associated with the Chebyshev polynomials of the first kind.

In accordance with the findings of Erdoğan and Gupta, the functions $\phi(s)$ and $w(s)$ can be expressed in the following forms [40]:

$$\phi(s) = \sum_{n=0}^{\infty} A_n T_n(s), \tag{3.16}$$

$$w(s) = \frac{1}{\sqrt{1-s^2}}. \tag{3.17}$$

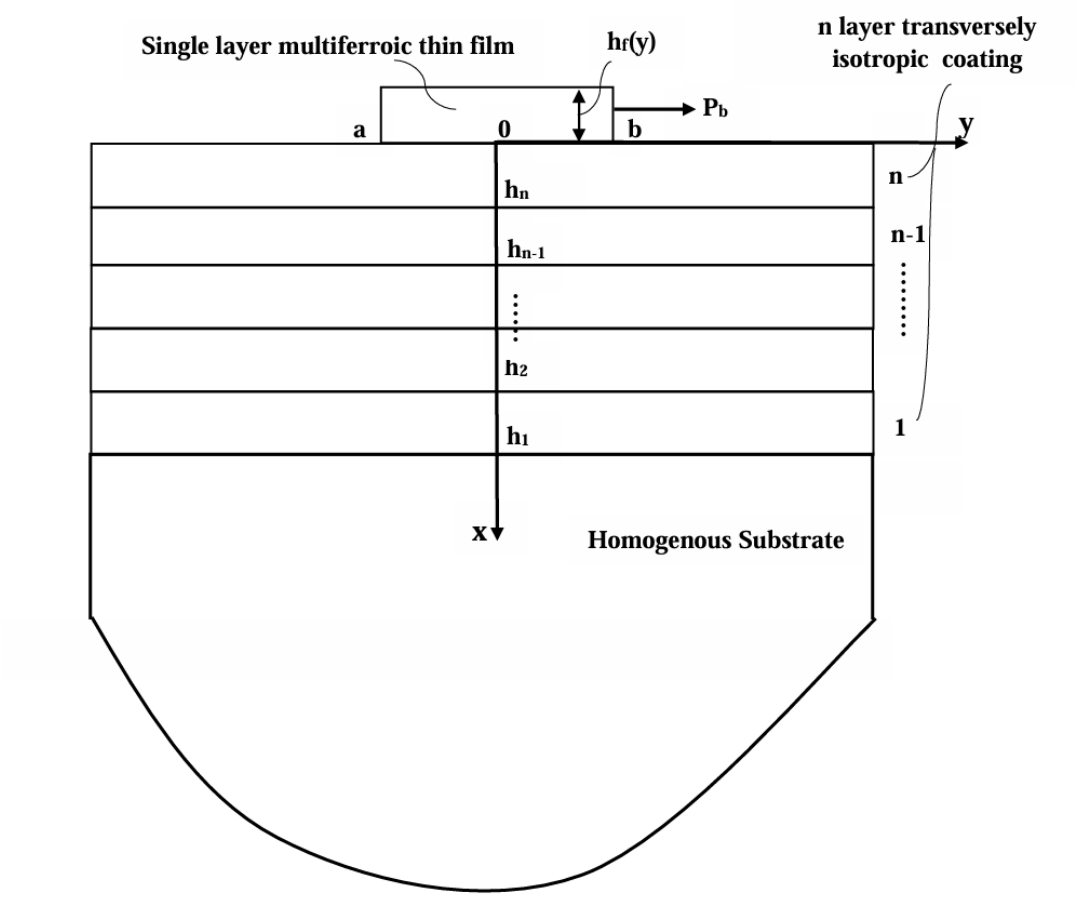

Figure 3-1. Geometry of the single end loading problem

The Chebyshev polynomials possess the following properties, wherein $U_n(r)$ represents the Chebyshev polynomials of the second kind.

$$\frac{1}{\pi}\int_{-1}^{1}\frac{T_n(s)}{(s-r)\sqrt{1-s^2}}ds=\begin{cases}0, & n=0,\\ U_{n-1}(r), & n>0.\end{cases} \tag{3.18}$$

$$\int_{-1}^{r}\frac{T_n(s)}{\sqrt{1-s^2}}ds=\begin{cases}\pi-\cos^{-1}(r), & n=0,\\ -\frac{1}{n}U_{n-1}(r)\sqrt{1-r^2}, & n>0.\end{cases} \tag{3.19}$$

The integral in (3.3) can be modified as follows.

$$(C_{22}^{f}-\frac{C_{12}^{f\,2}}{C_{11}^{f}})\frac{1}{\pi}\int_{-1}^{1}\left[K_2(s,r)+\frac{p_2}{s-r}\right]g(s)\,ds+\frac{b-a}{2h_f}\int_{-1}^{r}g(s)ds=E, \tag{3.20}$$

$$E=1-\frac{\frac{P}{h_f}}{\left(\frac{C_{12}^{f}e_{11}^{f}}{C_{11}^{f}}-e_{12}^{f}\right)E_x^f+\left(\frac{C_{12}^{f}h_{11}^{f}}{C_{11}^{f}}-h_{12}^{f}\right)H_x^f+\frac{P}{h_f}}. \tag{3.21}$$

It is evident that if the electrical and magnetic parameters are assumed to be zero, the right-hand side of the equation is also zero.

The equation (2.10) can be modified as follows by using Chebyshev expansion.

$$\frac{a-b}{2}g_1\sum_{n=0}^{\infty}A_n\int_{-1}^{1}\frac{T_n(s)}{\sqrt{1-s^2}}ds=\ P. \tag{3.22}$$

The value of A_0 can be obtained in the following way by making use of the property (3.19).

$$A_0=\frac{2P}{\pi g_1(a-b)}. \tag{3.23}$$

The integral equation in (3.20) can be transformed into a linear equation system by employing the Chebyshev polynomial expansion of $g(s)$ and the properties of it as outlined in (3.18) and (3.19).

$$\sum_{n=1}^{\infty}A_n[LU_{n-1}(r)+R_n(r)]=F(r), \tag{3.24}$$

where,

$$R_n(r)=\frac{(a-b)}{2h_f n}U_{n-1}(r)\sqrt{1-r^2}+(C_{22}^{f}-\frac{C_{12}^{f\,2}}{C_{11}^{f}})\frac{1}{\pi}\int_{-1}^{1}K_2(s,r)\frac{T_n(s)}{\sqrt{1-s^2}}ds, \tag{3.25}$$

$$F(r)=\frac{P}{\pi h_f g_1}(\pi-\cos^{-1}(r))+(C_{22}^{f}-\frac{C_{12}^{f\,2}}{C_{11}^{f}})\frac{2P}{\pi^2(b-a)g_1}\int_{-1}^{1}\frac{K_2(s,r)}{\sqrt{1-s^2}}ds+E, \tag{3.26}$$

$$L=\left(C_{22}^{f}-\frac{C_{12}^{f\,2}}{C_{11}^{f}}\right)p_2. \tag{3.27}$$

Some modifications have been made to (3.24) to facilitate the attainment of a solution approximately. The upper limit of the summation in this equation is

constrained by a sufficiently large N value and the values that make the Chebyshev polynomials of the first kind zero ($T_n(r_i) = 0$) are selected for the r values. After these modifications, the equation takes the following final form.

$$\sum_{n=1}^{N} A_n[LU_{n-1}(r_i) + R_n(r_i)] = F(r_i), \tag{3.28}$$

where,

$$r_i = \cos\left[(2i-1)\frac{\pi}{2N}\right]. \tag{3.29}$$

The aforementioned equation yields a set of N equations for each value of r_i, and the A_n's are determined by solving each equation.

As a result, the shear and the lateral stress values for the thin film at $x = 0$ can be defined in the non-dimensional form according to the following equations.

$$\frac{\sigma_{xy}^{f}(0,r)}{g_1} = \frac{\sum_{n=0}^{N} A_n T_n(r)}{\sqrt{1-r^2}}. \tag{3.30}$$

$$\frac{\sigma_{yy}^{f}(r)}{g_1} = \frac{b-a}{2h_f}\int_{-1}^{r} \frac{\sum_{n=0}^{N} A_n T_n(s)}{\sqrt{1-s^2}}\, ds, \tag{3.31}$$

The equation (3.31) takes the following final form after simplification.

$$\frac{\sigma_{yy}^{f}(r)}{g_1} = \frac{b-a}{2h_f}\left[\frac{2P}{\pi g_1(a-b)}(\pi - \cos^{-1}(r)) - \sum_{n=1}^{N}\frac{A_n}{n}U_{n-1}(r)\sqrt{1-r^2}\right]. \tag{3.32}$$

The results for the single end loading condition at the other end can be calculated on the assumption that the results in equations (3.30) and (3.32) are symmetric about point $(0, \frac{a+b}{2})$. Consequently, the double end loading condition can be determined by superimposing the results in these two single end conditions.

The singularities located at the left and right ends of the thin film can be regarded as analogous to a crack problem under in-plane shear mode, given that both of these problems possess a square root expression. Hence, one can define the mode II stress intensity factors at these points as follows.

$$k_{II,a} = \lim_{y \to a} \sqrt{2(y-a)}\, \sigma_{xy}^{f}(0,y). \tag{3.33}$$

$$k_{II,b} = \lim_{y \to b} \sqrt{2(b-y)}\, \sigma_{xy}^{f}(0,y). \tag{3.34}$$

The limits in the equations can be modified using the Chebyshev expansion of the $f(y)$. The final forms for stress intensity factors are obtained in the following expressions.

$$\frac{k_{II,a}}{g_1\sqrt{\frac{b-a}{2}}} = \sum_{n=0}^{N} A_n T_n(-1), \tag{3.35}$$

$$\frac{k_{II,b}}{g_1\sqrt{\frac{b-a}{2}}} = \sum_{n=0}^{N} A_n T_n(1). \tag{3.36}$$

The equation (3.36) may be modified since $T_n(1)$ is always equal to 1, which will yield the final expression.

$$\frac{k_{II,b}}{g_1\sqrt{\frac{b-a}{2}}} = \sum_{n=0}^{N} A_n. \tag{3.37}$$

3.3 Numerical Solution for Far-Field Loading Condition

In the context of a far-field loading problem, it is presumed that the loading occurs due to a constant strain present at the ends of the multilayer coating and substrate assembly, and that the thin film is not subjected to edge loading. The end conditions and $f(s)$ can be defined as follows.

$$P_a = 0, \qquad P_b = 0. \tag{3.38}$$

$$f(s) = g_2 g(s), \tag{3.39}$$

where $g(s)$ has the same definition as previous part and g_2 is given below.

$$g_2 = \left(\frac{C_{12}^{f} e_{11}^{f}}{C_{11}^{f}} - e_{12}^{f}\right) E_x^{f} + \left(\frac{C_{12}^{f} h_{11}^{f}}{C_{11}^{f}} - h_{12}^{f}\right) H_x^{f} + (C_{22}^{f} - \frac{C_{12}^{f\,2}}{C_{11}^{f}})\varepsilon_0. \tag{3.40}$$

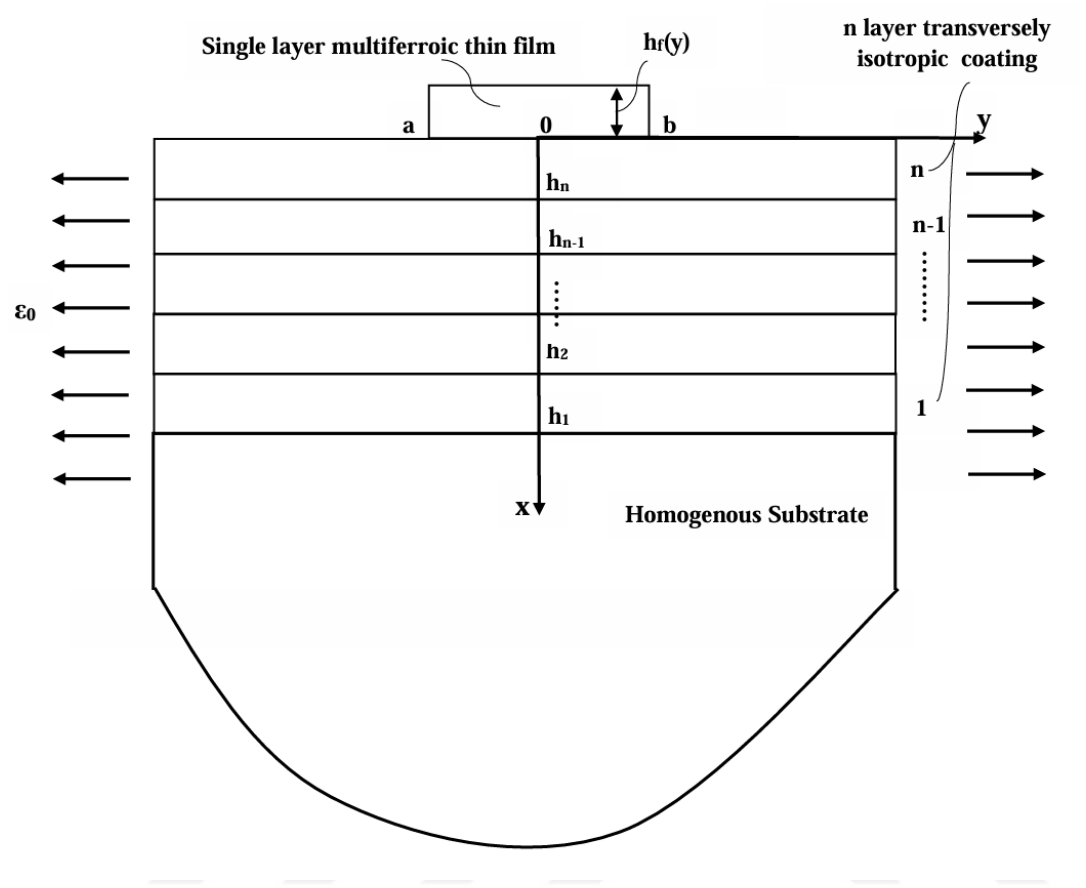

Figure 3-2. Geometry of the far-field loading problem

One can alter the equation (2.10) to accommodate this version of the problem in the following way.

$$\sum_{n=0}^{\infty} A_n \int_{-1}^{1} \frac{T_n(s)}{\sqrt{1-s^2}} ds = 0. \tag{3.41}$$

In accordance with (3.19), this equation suggests that A_0 is equal to zero. The equation takes the following definition.

$$\sum_{n=1}^{\infty} A_n [L U_{n-1}(r) + R_n(r)] = 1. \tag{3.42}$$

where,

$$R_n(r) = \frac{(a-b)}{2h_f n} U_{n-1}(r)\sqrt{1-r^2} + (C_{22}^f - \frac{C_{12}^{f\,2}}{C_{11}^f}) \frac{1}{\pi} \int_{-1}^{1} K_2(s,r) \frac{T_n(s)}{\sqrt{1-s^2}} ds, \tag{3.43}$$

$$L = \left(C_{22}^{f} - \frac{C_{12}^{f\,2}}{C_{11}^{f}}\right) p_2. \tag{3.44}$$

A_n's are determined by implementing the specified procedure in the context of the single end loading condition. Subsequently, one can declare stresses in the following equations.

$$\frac{\sigma_{xy}^{f}(0,r)}{g_2} = \frac{\sum_{n=1}^{N} A_n T_n(r)}{\sqrt{1-r^2}}, \tag{3.45}$$

$$\frac{\sigma_{yy}^{f}(r)}{g_2} = \frac{a-b}{2h_f} \sum_{n=1}^{N} \frac{A_n}{n} U_{n-1}(r)\sqrt{1-r^2}. \tag{3.46}$$

The mode II stress intensity factors in this version of problem can be stated as follows.

$$\frac{k_{II,a}}{g_2\sqrt{\frac{b-a}{2}}} = \sum_{n=1}^{N} A_n T_n(-1), \tag{3.47}$$

$$\frac{k_{II,b}}{g_2\sqrt{\frac{b-a}{2}}} = \sum_{n=1}^{N} A_n. \tag{3.48}$$

CHAPTER 4

NUMERICAL RESULTS

This chapter presents the results obtained through the application of the procedures outlined in Chapters 2 and 3, as illustrated in tables and figures. Among the significant outputs of the problems are the normal and lateral contact stresses for the thin film, uppermost layer and mode-II stress intensity factors at the singularity points. The solution obtained in Chapter 3 is verified in Section 4.1. The parametric studies with different models are presented in Section 4.2.

4.1 Verification

The comparisons are presented with the results of previously documented cases in the literature in order to validate the developed analytical and numerical procedures.

The initial series of comparisons has been derived from an analysis of the thin film problem as solved by Chen et al. in 2016 [46]. The interface stresses in a thin film bonded to an isotropic substrate with an arbitrarily graded coating are analyzed when there is a constant strain present at the ends of the multilayer coating and substrate assembly in this comparison study as illustrated in **Figure 4-1**. The grading functions are selected as linear and exponential for the shear modulus in the comparison study. In the present study, the Young's moduli in the x and y directions are also determined by the grading functions to be able to determine the elastic stiffness coefficients for transversely isotropic coating and thin film model, in addition to the shear modulus. Furthermore, in order to obtain solutions that align with the principles outlined in this material model, the ratios for elastic moduli and the Poisson’s ratios are defined as being very slightly different from the ratios of shear moduli and the Poisson’s ratio for the substrate , as illustrated in **Table 4-1**, **Table 4-2** and **Table 4-3**. The elastic modulus in the x and y directions and the shear modulus at the uppermost

surface is represented by E_{0x}, E_{0y} and μ_0, respectively. The material constant E^s, which is intrinsic to the substrate, is employed in both the elastic modulus in the x and y directions for the bottom surface of the coating. Similarly, μ^s is used at this surface as shear modulus. These values for each layer are derived from these values by using the grading functions.

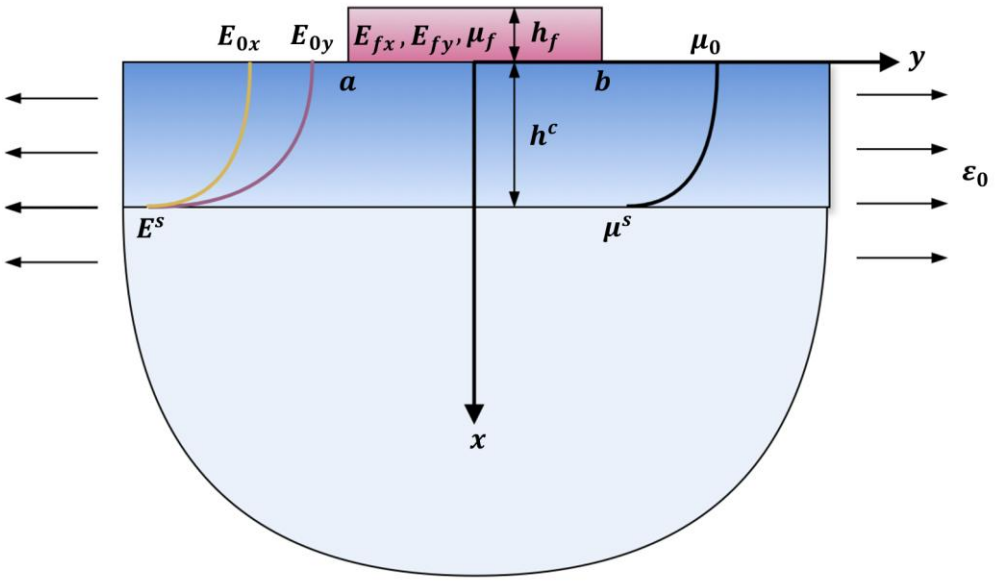

Figure 4-1. Geometry of the verification problem-1

Table 4-1. The declaration of the ratio of elastic moduli with respect to the ratio of shear modulus for coating

$\frac{\mu^s}{\mu_0}$	$\frac{E^s}{E_{0x}}$	$\frac{E^s}{E_{0y}}$
7	6.999	7.001
$\frac{1}{7}$	$\frac{1}{6.999}$	$\frac{1}{7.001}$

Table 4-2. The declaration of the ratio of elastic moduli with respect to the ratio of shear modulus for thin film

$\frac{\mu_f}{\mu_0}$	$\frac{E_{fx}}{E_{0x}}$	$\frac{E_{fy}}{E_{0y}}$
28	27.999	28.001

Table 4-3. The declaration of Poisson's ratio for the entire system

v^s	v_{xy}^f	v_{yz}^f	v_{0xy}	v_{0yz}
0.3	0.299	0.301	0.299	0.301

The coating is divided into N layers. The arithmetic mean of the coordinates of the bottom and top surfaces at each layer is employed to ascertain the material properties of the layer in question. The linear variation in the material properties for the multi-layer coating system is defined by the following equations.

$$\mu_{(i)} = \mu_0 + (\mu^s - \mu_0)\left(\frac{x_{(i)}}{h^c}\right) \tag{4.1}$$

$$E_{(i)x} = E_{0x} + (E^s - E_{0x})\left(\frac{x_{(i)}}{h^c}\right) \tag{4.2}$$

$$E_{(i)y} = E_{0x} + (E^s - E_{0y})\left(\frac{x_{(i)}}{h^c}\right) \tag{4.3}$$

$$v_{(i)xy} = v_{0xy} + (v^s - v_{0xy})\left(\frac{x_{(i)}}{h^c}\right) \tag{4.4}$$

$$v_{(i)yz} = v_{0yz} + (v^s - v_{0yz})\left(\frac{x_{(i)}}{h^c}\right) \tag{4.5}$$

The subsequent equations are employed for exponential gradation.

$$\mu_{(i)} = \mu_0 e^{\ln\left(\frac{\mu^s}{\mu_0}\right)\left(\frac{x_{(i)}}{h^c}\right)} \tag{4.6}$$

$$E_{(i)x} = E_{0x} e^{\ln\left(\frac{E^s}{E_{0x}}\right)\left(\frac{x_{(i)}}{h^c}\right)} \tag{4.7}$$

$$E_{(i)y} = E_{0y} e^{\ln\left(\frac{E^S}{E_{0y}}\right)\left(\frac{x_{(i)}}{h^C}\right)} \tag{4.8}$$

$$\upsilon_{(i)xy} = \upsilon_{0xy} e^{\ln\left(\frac{\upsilon^S}{\upsilon_{0xy}}\right)\left(\frac{x_{(i)}}{h^C}\right)} \tag{4.9}$$

$$\upsilon_{(i)yz} = \upsilon_{0yz} e^{\ln\left(\frac{\upsilon^S}{\upsilon_{0yz}}\right)\left(\frac{x_{(i)}}{h^C}\right)} \tag{4.10}$$

The normalization constant h_1 for the thin film is declared as follows without multiferroic parameters.

$$h_1 = \frac{\mu_0}{1-\upsilon^S}\varepsilon_0. \tag{4.11}$$

The shear, lateral stress and stress intensity factors for the thin film are declared as follows with new variables.

$$S_{xy}^f(s) = \sigma_{xy}^f\left(0, \frac{b-a}{2}s + \frac{b+a}{2}\right)\frac{1}{h_1}, \tag{4.12}$$

$$S_{yy}^f(s) = \sigma_{yy}^f\left(0, \frac{b-a}{2}s + \frac{b+a}{2}\right)\frac{1}{h_1}, \tag{4.13}$$

$$K_{II,a} = \frac{k_{II,a}}{\sqrt{\frac{b-a}{2}}}\frac{1}{h_1}, \tag{4.14}$$

$$K_{II,b} = \frac{k_{II,b}}{\sqrt{\frac{b-a}{2}}}\frac{1}{h_1}. \tag{4.15}$$

The number of layers is determined by using the percentage error in the results of successive iterations as illustrated in **Table 4-4**. The number of layers is selected as 200 for the analysis. It is also observed that the run time of the program is dependent on the number of layers linearly.

Table 4-4. Number of layers, normalized lateral stresses, stress intensity factors and percent approximate errors computed at s=0 for a linearly graded coating multilayer model with $2h^c/b-a=20,\ \mu^s/\mu_0=1/7, \mu_f/\mu_0=28,\ b-a/2h_f=32$.

Number of Layers	**Approximate Error for $S_{yy}^f(s)$ (%)**	$S_{yy}^f(s)$	**Approximate Error for $K_{II,a}$ (%)**	$K_{II,a}$
20	-	12.367	-	0.8302
50	0.74	12.460	0.94	0.8381
100	0.16	12.480	0.26	0.8403
150	0.03	12.484	0.08	0.8410
200	0.01	12.486	0.04	0.8414

A comparative analysis is presented of the numerical results for the soft thin film in contact with a hard substrate and vice versa, for various values of $2h^c/b-a$ by using linear and exponential variation. A comparison of the results obtained in this study with those reported by Chen and his colleagues reveals a high degree of concordance, as illustrated in **Figure 4-2**, **Figure 4-3** and **Table 4-5**.

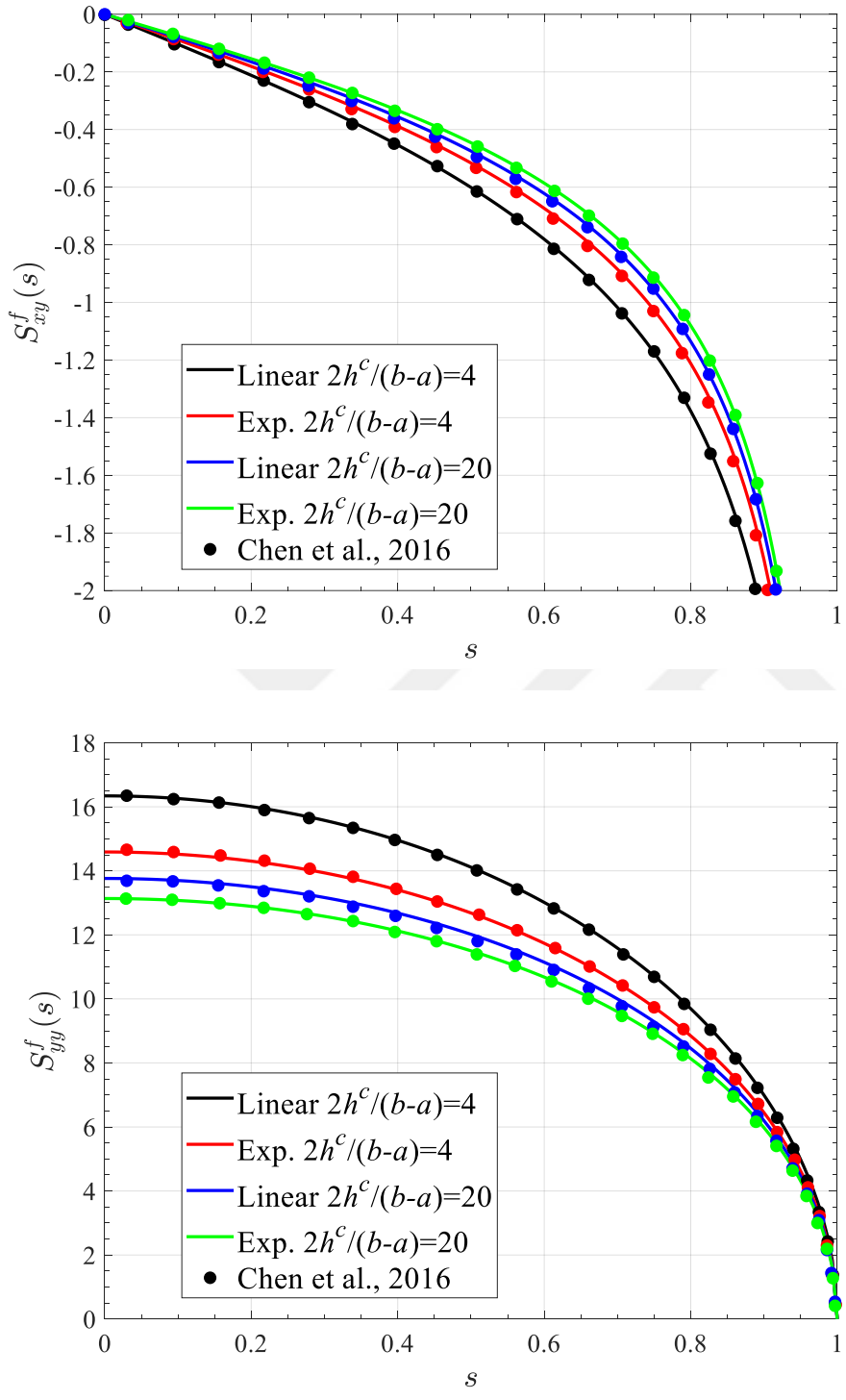

Figure 4-2. The comparison of the shear and lateral contact stresses derived in this study for a graded coating with $\mu^s/\mu_0 = 7$, $\mu_f/\mu_0 = 28$, $b - a/2h_f = 32$ to those given by Chen et al. (2016).

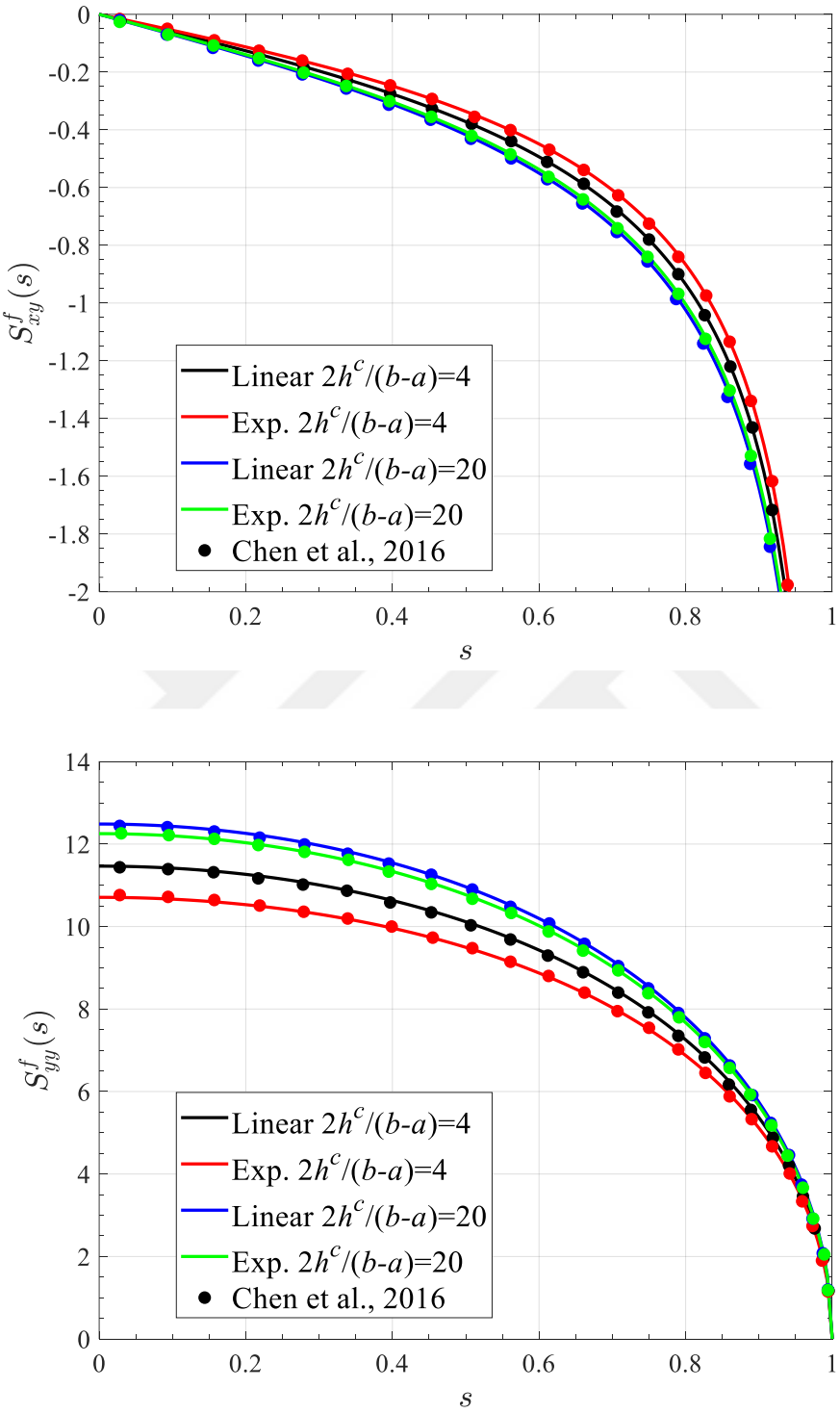

Figure 4-3. The comparison of the shear and lateral contact stresses derived in this study for a graded coating with $\mu^s/\mu_0 = 1/7$, $\mu_f/\mu_0 = 28$, $b - a/2h_f = 32$ to those given by Chen et al. (2016).

Table 4-5. The comparison of the normalized stress intensity factors at $s = -1$ derived in this study for a graded coating multilayer model with $\mu_f/\mu_0 = 28$, $b - a/2h_f = 32$ to those given by Chen et al. (2016).

	Chen et al. (2016)				**Present Study**			
	Exponential		**Linear**		**Exponential**		**Linear**	
$\frac{2h^c}{b-a}$	**4**	**20**	**4**	**20**	**4**	**20**	**4**	**20**
$\frac{\mu^s}{\mu_0} = 7$	0.9300	0.8712	0.9829	0.8931	0.9304	0.8734	0.99	0.9020
$\frac{\mu^s}{\mu_0} = \frac{1}{7}$	0.7633	0.8323	0.7917	0.8412	0.7610	0.8299	0.7922	0.8414

The final verification is conducted using the findings from the study of Chen et al. in 2018 [50]. This study analyses a theoretical model of a piezoelectric thin film attached to a graded half plane with an adhesive layer under an electrical loading. The present study is only compared with the aforementioned study in the context of perfect bonding and homogenous substrate.

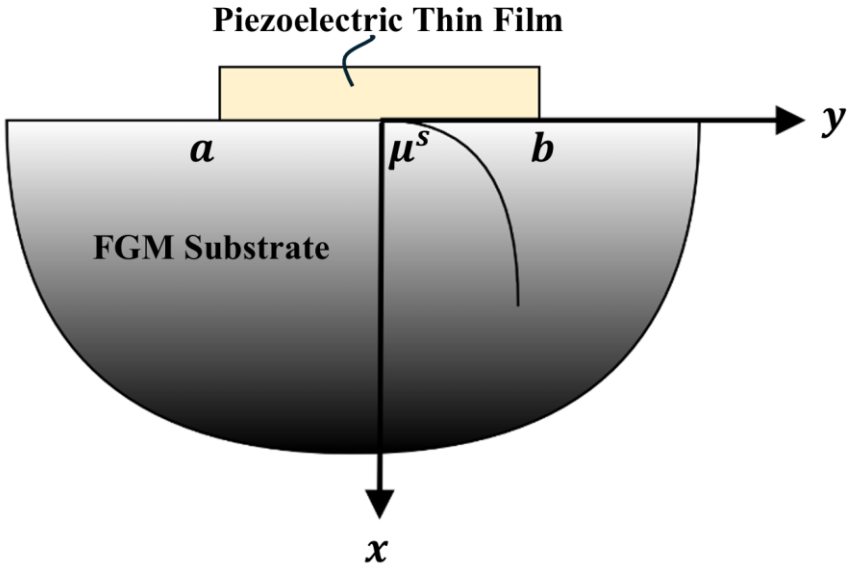

Figure 4-4. Geometry of the verification problem-2

The substrate is modeled as multilayer coating system with exponential gradation on a homogenous substrate in present study. The number of layers is selected as 200 for this multilayer system. The ratios for elastic moduli and the Poisson's ratios are defined in **Table 4-6** and **Table 4-3**, respectively.

Table 4-6. The declaration of the ratio of elastic moduli with respect to the ratio of shear modulus for coating

$\frac{\boldsymbol{\mu^s}}{\boldsymbol{\mu_0}}$	$\frac{\boldsymbol{E_{0x}}}{\boldsymbol{E^s}}$	$\frac{\boldsymbol{E_{0y}}}{\boldsymbol{E^s}}$
1	0.999	1.001

The constant h_2 for the thin film is declared in this analysis as follows since it is piezoelectric.

$$h_2 = \left(\frac{C_{12}^f e_{11}^f}{C_{11}^f} - e_{12}^f\right) E_x^f. \tag{4.16}$$

The shear, lateral stresses and the stress intensity factors for the thin film are declared as follows with the following expressions.

$$S_{xy}^f(s) = \sigma_{xy}^f \left(0, \frac{b-a}{2}s + \frac{b+a}{2}\right) \frac{1}{h_2}, \tag{4.17}$$

$$S_{yy}^f(s) = \sigma_{yy}^f \left(0, \frac{b-a}{2}s + \frac{b+a}{2}\right) \frac{1}{h_2}, \tag{4.18}$$

$$K_{II,a} = \frac{k_{II,a}}{\sqrt{\frac{b-a}{2}}} \frac{1}{h_2}, \tag{4.19}$$

$$K_{II,b} = \frac{k_{II,b}}{\sqrt{\frac{b-a}{2}}} \frac{1}{h_2}. \tag{4.20}$$

The elastic stiffness parameters for the thin film is defined with respect to the material parameters of the substrate as follows.

$$(C_{22}^f - \frac{C_{12}^{f\,2}}{C_{11}^f})/\mu^s = \pi/2.28(1 - \upsilon^s). \tag{4.21}$$

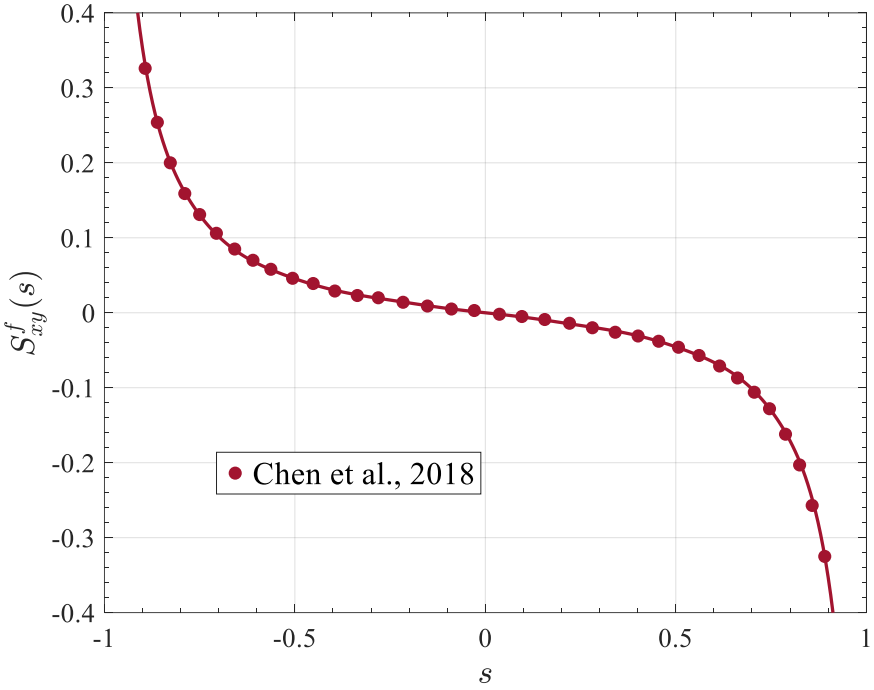

Figure 4-5. The comparison of the shear stress derived in this study for a graded substrate with $(C_{22}^f - \frac{C_{12}^{f\,2}}{C_{11}^f})/\mu^s = \pi/2.28(1-\upsilon^s)$, $b - a/2h_f = 5$ and $\upsilon^s = 0.3$ to those given by Chen et al. (2018).

A comparison of the result for the shear stress obtained in this study with that reported by Chen and his colleagues in 2018 demonstrates a strong degree of agreement.

4.2 Parametric Studies

The first parametric study is conducted on the multiferroic thin film bonded to an isotropic substrate with an arbitrarily graded transversely isotropic multi-layer coating system as illustrated in **Figure 4-6**. In this study, the edge loading and far-field loading conditions are assumed to be negligible in order to ascertain the effect of the multiferroicity of the thin film in isolation. The results are derived from linear, exponential and different power law gradation functions.

In a standard FGM, the volume proportions of the constituents are modified in a gradual manner over a macroscale geometrical dimension, such as coating thickness in order to meet the requirements of the material [51]. The definition of any material property in FGM, therefore, is contingent upon the volumetric fraction of ceramic and metal coatings. These volumetric fractions can be expressed as a function of the power index, denoted by η, and the coordinates [52]. The determination of the power index can be achieved by measuring the material properties at different locations. This can be accomplished through the utilization of various methodologies, encompassing the indentation test [53], thermal conductivity measurement [54] and the employment of Scanning Electron Microscopy (SEM) [55]. The exponent η for the power law gradation is designated as 0.4, 1 and 1.5 for metal-rich coating, linear coating and ceramic-rich coating, respectively in this study. The power law variation in the material properties for the multi-layer coating system is defined by the following equations.

$$\mu_{(i)} = \mu_0 + (\mu^s - \mu_0)\left(\frac{x_{(i)}}{h^c}\right)^{\eta} \tag{4.22}$$

$$E_{(i)x} = E_{0x} + (E^s - E_{0x})\left(\frac{x_{(i)}}{h^c}\right)^{\eta} \tag{4.23}$$

$$E_{(i)y} = E_{0x} + (E^s - E_{0y})\left(\frac{x_{(i)}}{h^c}\right)^{\eta} \tag{4.24}$$

$$\upsilon_{(i)xy} = \upsilon_{0xy} + (\upsilon^s - \upsilon_{0xy})\left(\frac{x_{(i)}}{h^c}\right)^{\eta} \tag{4.25}$$

$$\upsilon_{(i)yz} = \upsilon_{0yz} + (\upsilon^s - \upsilon_{0yz})\left(\frac{x_{(i)}}{h^c}\right)^{\eta} \tag{4.26}$$

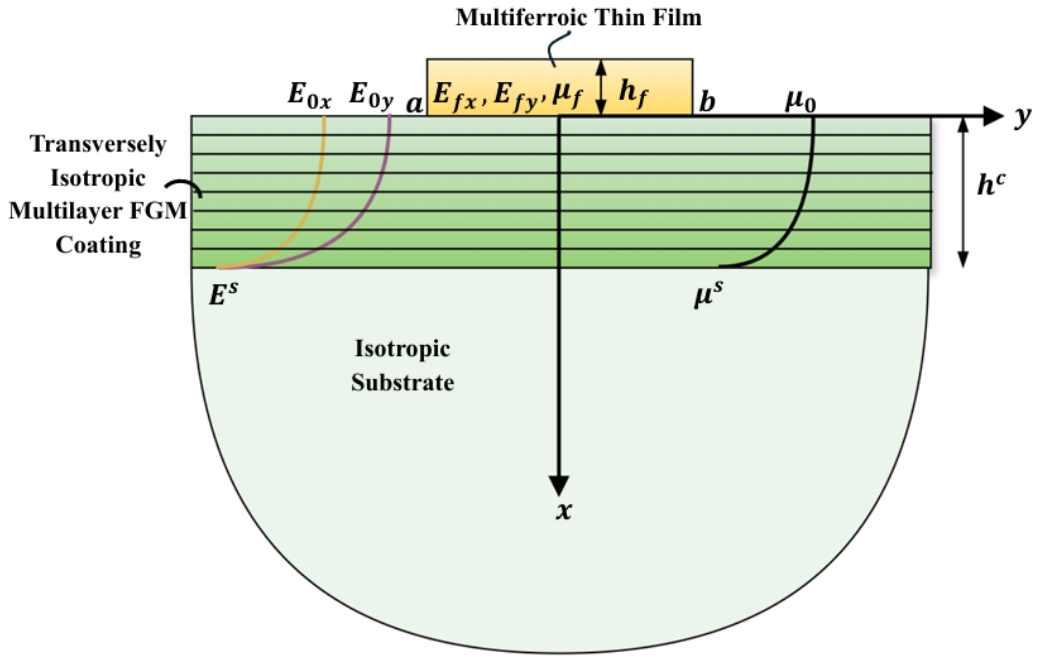

Figure 4-6. Geometry of the parametric study problem

The elastic modulus in the x and y directions at the uppermost surface take the E_{0x} and E_{0y} values, respectively. Similarly, the shear modulus is represented by μ_0 at this surface. The material constants of the substrate are used for the bottom surface of the coating and these values for each layer vary from the lowest to the highest layer of the pavement depending on the grading function.

In this analysis, the normalization constant h_3 for the thin film is declared as follows, given its multiferroic nature.

$$h_3 = \left(\frac{c_{12}^f e_{11}^f}{c_{11}^f} - e_{12}^f\right) E_x^f + \left(\frac{c_{12}^f h_{11}^f}{c_{11}^f} - h_{12}^f\right) H_x^f. \tag{4.27}$$

The shear and lateral stresses and the stress intensity factors for the thin film and the uppermost layer are declared as follows with the following expressions.

$$S_{xy}^f(s) = \sigma_{xy}^f \left(0, \frac{b-a}{2} s + \frac{b+a}{2}\right) \frac{1}{h_3}, \tag{4.28}$$

$$S_{yy}^{f}(s) = \sigma_{yy}^{f}\left(0, \frac{b-a}{2}s + \frac{b+a}{2}\right)\frac{1}{h_3}, \tag{4.29}$$

$$S_{(n)yy}(s) = \sigma_{(n)yy}\left(0, \frac{b-a}{2}s + \frac{b+a}{2}\right)\frac{1}{h_3}, \tag{4.30}$$

$$K_{II,a} = \frac{k_{II,a}}{\sqrt{\frac{b-a}{2}}}\frac{1}{h_3}, \tag{4.31}$$

$$K_{II,b} = \frac{k_{II,b}}{\sqrt{\frac{b-a}{2}}}\frac{1}{h_3}. \tag{4.32}$$

The results obtained by utilizing different parameters for the normalized stress intensity factors are presented in **Tables 4-7** to **4-11**. **Table 4-7** and **Table 4-8** demonstrate the influence of the ratio of the thickness of the coating to the width of the thin film ($2h^c/b-a$) using the different grading functions on the normalized SIF for $\mu^s/\mu_0 = 7$ and $\mu^s/\mu_0 = 1/7$, respectively. The increase in this ratio decreases the value of the SIFs for hard substrate-soft coating condition ($\mu^s/\mu_0 = 7$). A similar outcome is observed in the transition from a ($\eta = 0.4$) to ceramic-rich coating ($\eta = 1.5$). Conversely, the results obtained for the soft substrate-hard coating ($\mu^s/\mu_0 = 1/7$) condition are opposite. In addition, the hard substrate-soft coating model yields higher SIF values in comparison to the soft substrate-hard coating model when other material and geometrical parameters are kept the same. **Table 4-9** and **Table 4-10** reveal the effect of the ratio of the width of the thin film to the thickness of it ($b-a/h_f$) with the different grading functions on the normalized SIF for $\mu^s/\mu_0 = 7$. Thinner films (higher $b-a/h_f$ ratio) reduce SIF value for all grading functions. Furthermore, the metal-rich coating produces the highest SIF value compared to other ones. The effect of the modulus ratio E_{0x}/E_{0y} with the different grading functions on the normalized SIF for $\mu^s/\mu_0 = 7$ is shown in **Table 4-11**. The rise in this ratio causes higher SIF value. Nevertheless, the effect of this parameter is comparatively negligible in relation to the preceding parameters.

Table 4-7. The normalized stress intensity factors computed for the various grading functions with $\mu^s/\mu_0 = 7, \mu_f/\mu_0 = 5, b-a/h_f = 32, E^s/E_{0y} = 7, E_{0x}/E_{0y} = 2$.

	Exponential		**Linear**		$\boldsymbol{\eta = 0.4}$	$\boldsymbol{\eta = 1.5}$
$\boldsymbol{\frac{2h^c}{b-a}}$	**4**	**20**	**4**	**20**	**20**	**20**
$\boldsymbol{K_{II,a}}$	0.0578	0.0565	0.0593	0.0573	0.0744	0.0562
$\boldsymbol{K_{II,b}}$	-0.0578	-0.0565	-0.0593	-0.0573	-0.0744	-0.0562

Table 4-8. The normalized stress intensity factors computed for the various grading functions with $\mu^s/\mu_0 = 1/7, \mu_f/\mu_0 = 5, b-a/h_f = 32, E^s/E_{0y} = 1/7, E_{0x}/E_{0y} = 2$.

	Exponential		**Linear**		$\boldsymbol{\eta = 0.4}$	$\boldsymbol{\eta = 1.5}$
$\boldsymbol{\frac{2h^c}{b-a}}$	**4**	**20**	**4**	**20**	**20**	**20**
$\boldsymbol{K_{II,a}}$	0.0522	0.0550	0.0537	0.0554	0.0519	0.0557
$\boldsymbol{K_{II,b}}$	-0.0522	-0.0550	-0.0537	-0.0554	-0.0519	-0.0557

Table 4-9. The normalized stress intensity factors computed for the various grading functions with $\mu^s/\mu_0 = 7, \mu_f/\mu_0 = 5, 2h^c/b-a = 20, E^s/E_{0y} = 7, E_{0x}/E_{0y} = 2$.

	Linear				**Exponential**			
$\boldsymbol{\frac{b-a}{h_f}}$	**20**	**32**	**64**	**128**	**20**	**32**	**64**	**128**
$\boldsymbol{K_{II,a}}$	0.0677	0.0573	0.0429	0.0311	0.0664	0.0565	0.0425	0.0309
$\boldsymbol{K_{II,b}}$	-0.0677	-0.0573	-0.0429	-0.0311	-0.0664	-0.0565	-0.0425	-0.0309

Table 4-10. The normalized stress intensity factors computed for the various grading functions with $\mu^s/\mu_0 = 7$, $\mu_f/\mu_0 = 5$, $2h^c/b-a = 20$, $E^s/E_{0y} = 7$, $E_{0x}/E_{0y} = 2$.

	$\eta = 0.4$				$\eta = 1.5$			
$\frac{b-a}{h_f}$	**20**	**32**	**64**	**128**	**20**	**32**	**64**	**128**
$K_{II,a}$	0.0905	0.0744	0.0542	0.0387	0.0661	0.0562	0.0424	0.0308
$K_{II,b}$	-0.0905	-0.0744	-0.0542	-0.0387	-0.0661	-0.0562	-0.0424	-0.0308

Table 4-11. The normalized stress intensity factors computed for the various grading functions with $\mu^s/\mu_0 = 7$, $\mu_f/\mu_0 = 5$, $2h^c/b-a = 20$, $E^s/E_{0y} = 7$, $E_{0x}/E_{0y} = 2$, $b-a/h_f = 32$.

	Linear			**Exponential**		
$\frac{E_{0x}}{E_{0y}}$	**4**	**3**	**2**	**4**	**3**	**2**
$K_{II,a}$	0.0581	0.0578	0.0573	0.0573	0.0570	0.0565
$K_{II,b}$	-0.0581	-0.0578	-0.0573	-0.0573	-0.0570	-0.0565

The shear and lateral contact stresses for the thin film and uppermost layer, as influenced by different parameters, are presented in **Figures 4-7** to **4-20**. **Figure 4-7** and **Figures 4-8** depict the effect of the ratio of the thickness of the coating to the width of the thin film ($2h^c/b-a$) for the different grading functions on the normalized SIF for $\mu^s/\mu_0 = 7$ and $\mu^s/\mu_0 = 1/7$, respectively. For the hard substrate-soft coating condition, increasing this ratio has been shown to reduce the shear and lateral stress values of the thin film, while increasing the lateral stress value of the top layer. The lateral and shear stress values of the thin film for the linearly graded coating are higher than those for the exponential coating, while the lateral stress values for the top layer are lower. The opposite of the evaluations presented so far

applies to the case of soft substrate with hard coating. **Figure 4-9** and **Figure 4-10** give information on the influence of the exponent of the coating obeying the power law on the normalized SIF for $\mu^s/\mu_0 = 7$ and $\mu^s/\mu_0 = 1/7$, respectively. The metal-rich coating for hard substrate-soft coating condition has been shown to yield substantially elevated values in comparison with those of higher exponent coatings, particularly regarding the lateral stress value of the thin film. This type of coating shows interesting behavior for the lateral stress of the uppermost layer. It has higher stress values near the edge of the thin film and lower stress values in the other regions compared to the high exponent gradings. The inverse behavior for soft substrate-hard coating is also applicable in this case. The influence of the ratio of the shear modulus of the substrate to the coating (μ^s/μ_0) and the elastic modulus ratio (E^s/E_{0y}) for different grading functions on the resultant stresses are indicated in **Figure 4-11**, **Figure 4-12**, **Figure 4-13** and **Figure 4-14**. The results of the grading functions indicate that harder substrates result in higher stress values for the thin film and lower lateral stress for the uppermost layer. The application of a metal-rich coating to a harder substrate has been shown to result in the generation of significantly higher lateral stress values for the thin film in comparison to other grading functions. The change in the lateral stress behavior of the uppermost layer with respect to the ends of the thin film described in the previous case is exactly the same here. **Figure 4-15**, **Figure 4-16**, **Figure 4-17** and **Figure 4-18** illustrate the relation of the ratio of the width of the thin film to its thickness ($b - a/h_f$) by using the different grading functions with the stresses. The use of thinner films results in increased lateral stress values for the thin film, as well as reduced shear stress and lateral stress values in the uppermost layer. The maximum and minimum values are observed for the metal-rich coating, and the remaining grading functions yield analogous stress values. **Figure 4-19** and **Figure 4-20** show the effect of the elastic modulus ratio E_{0x}/E_{0y} with the different grading functions on the stresses. It is seen that change in this ratio doesn't have a significant impact on the stresses observed.

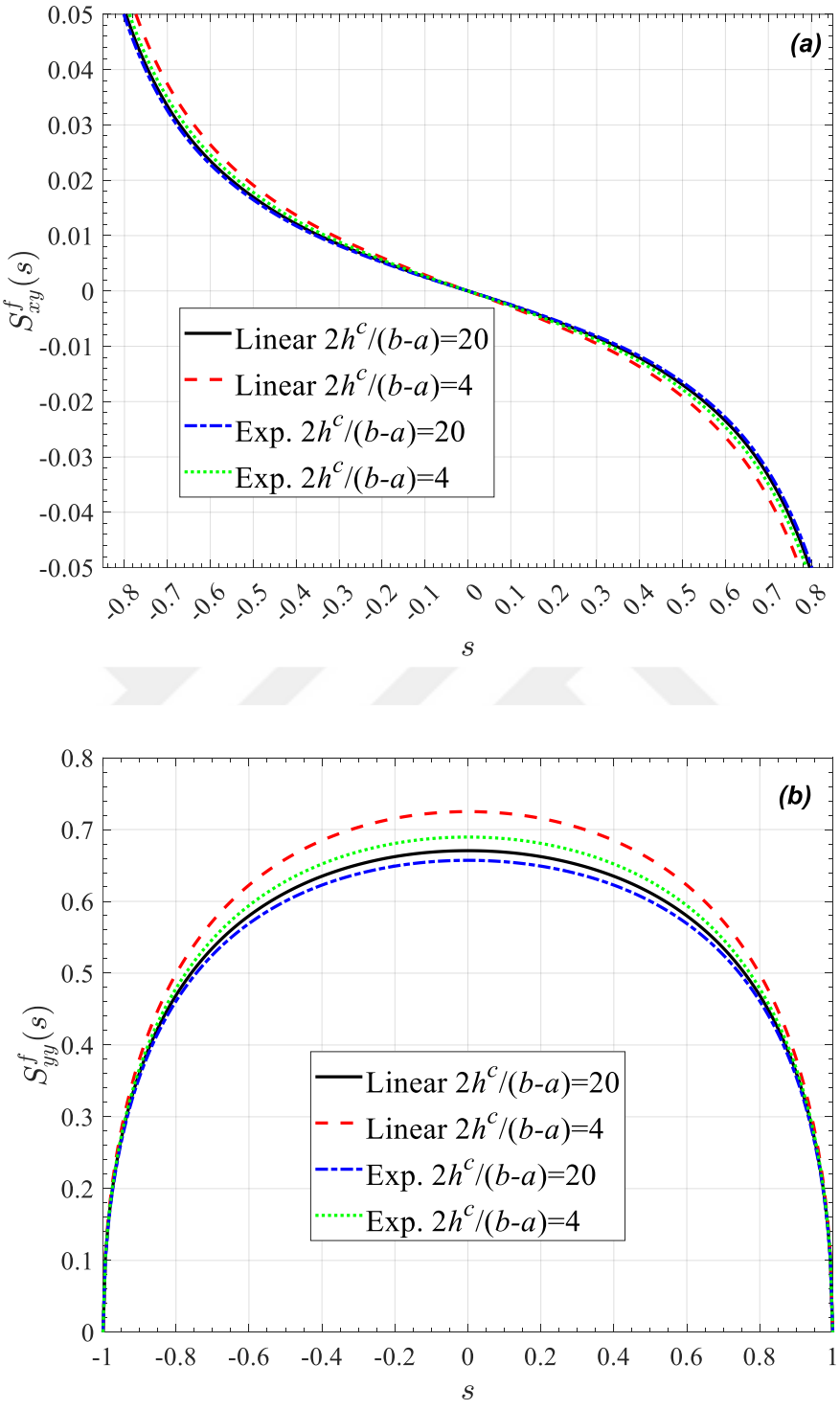

Figure 4-7. The computed shear stress ***(a)*** and the lateral stress ***(b)*** for the thin film and the lateral stress ***(c)*** for the uppermost layer by assuming a graded coating with $\mu^s/\mu_0 = 7, \mu_f/\mu_0 = 5, b - a/h_f = 32, E^s/E_{0y} = 7, E_{0x}/E_{0y} = 2$.

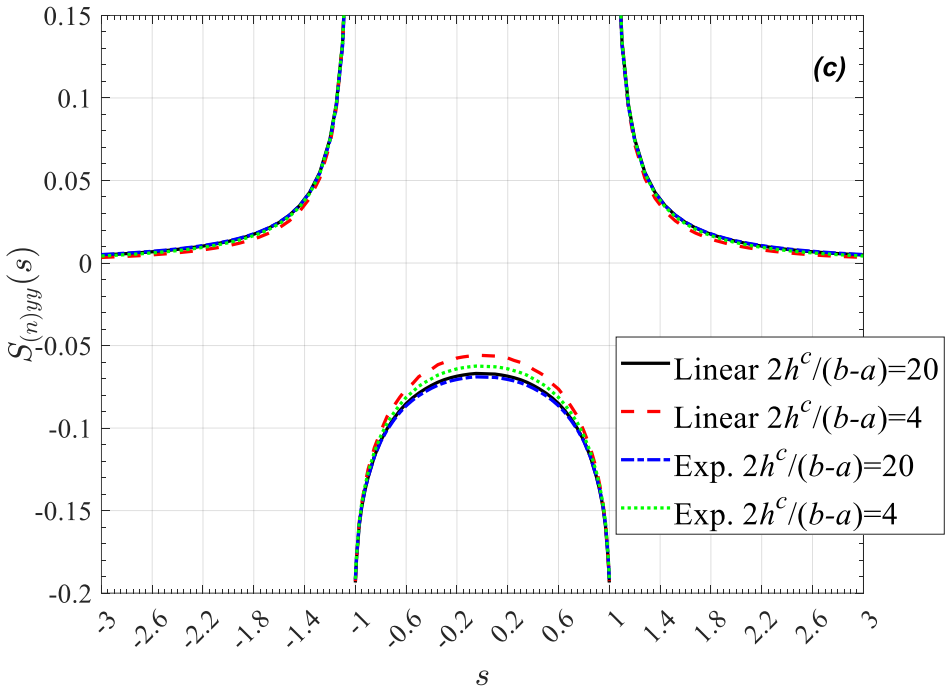

Figure 4-7. (continued)

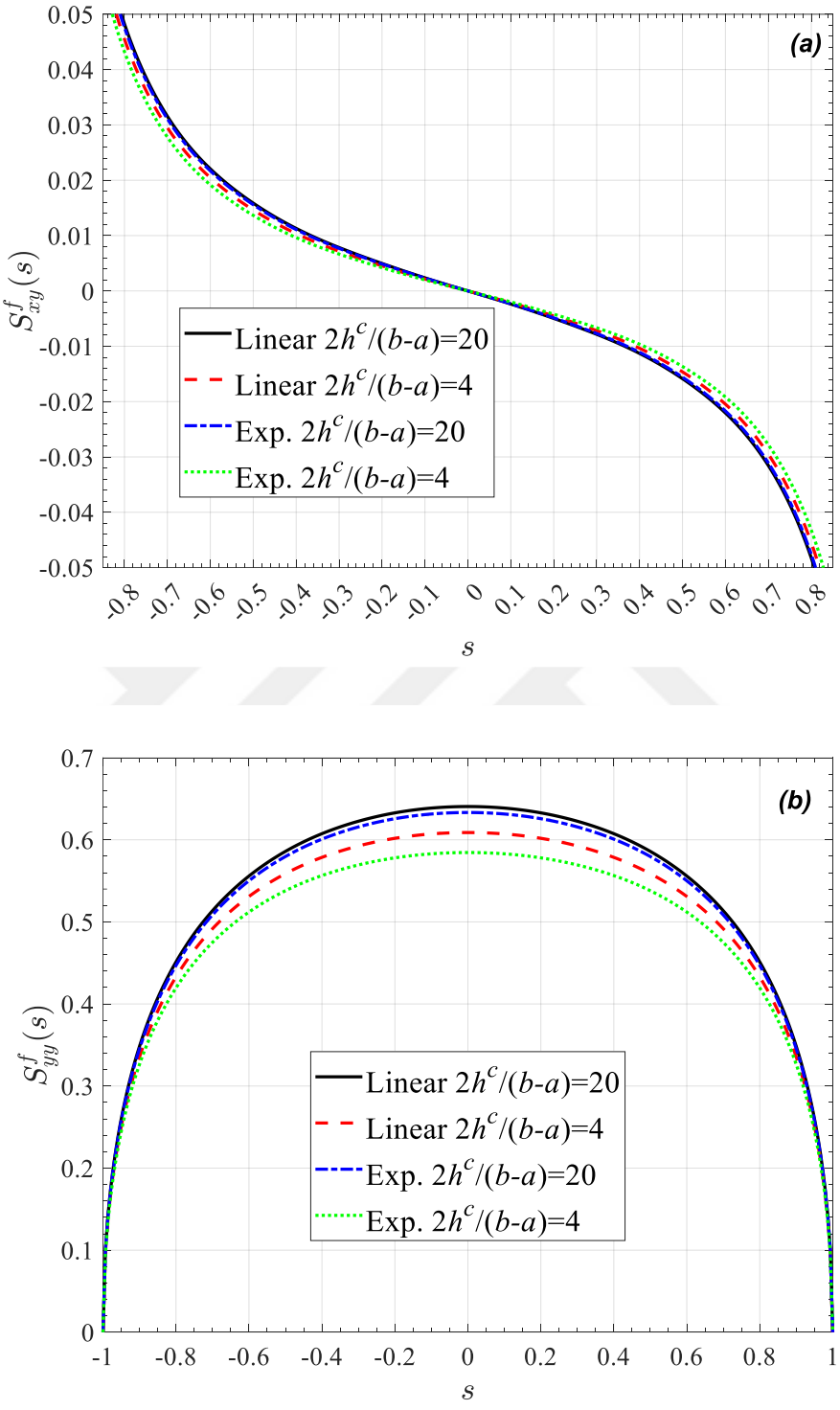

Figure 4-8. The computed shear stress ***(a)*** and the lateral stress ***(b)*** for the thin film and the lateral stress ***(c)*** for the uppermost layer by assuming a graded coating with $\mu^s/\mu_0 = 1/7, \mu_f/\mu_0 = 5, b - a/h_f = 32, E^s/E_{0y} = 1/7, E_{0x}/E_{0y} = 2$.

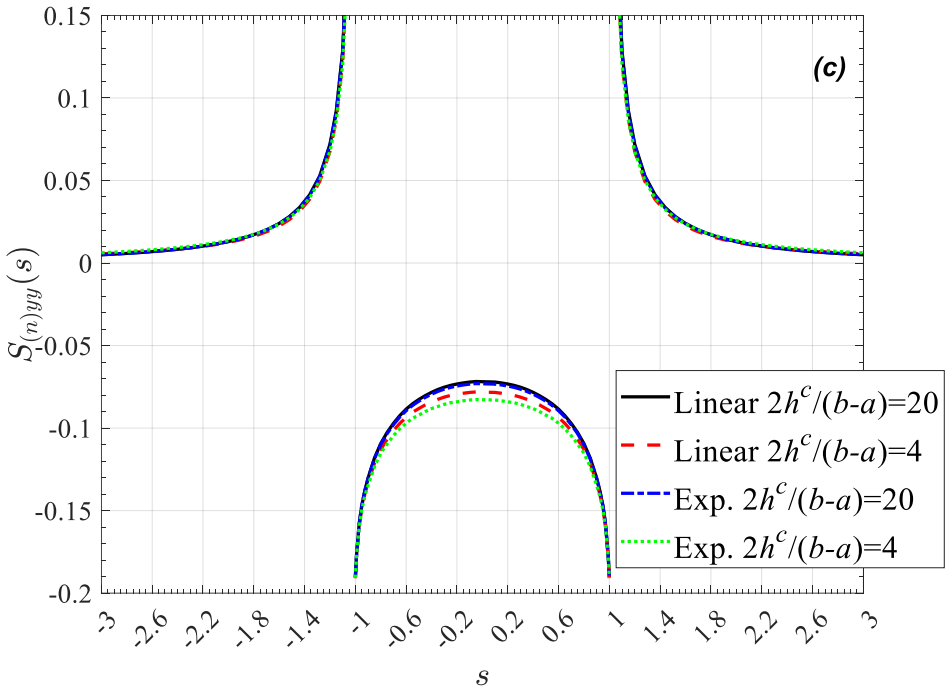

Figure 4-8. (continued)

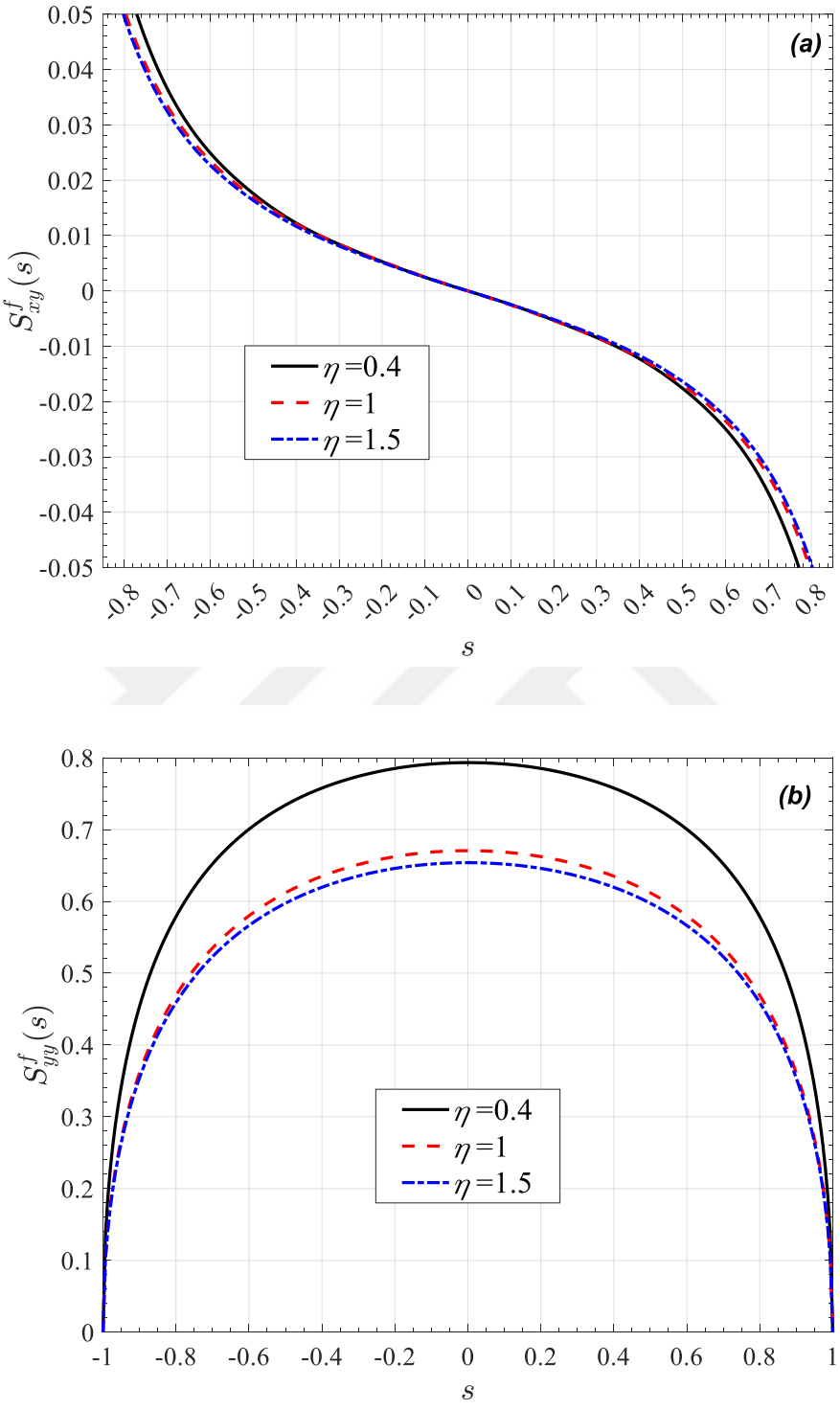

Figure 4-9. The computed shear stress ***(a)*** and the lateral stress ***(b)*** for the thin film and the lateral stress ***(c)*** for the uppermost layer by assuming a graded coating with $\mu^s/\mu_0 = 7, \mu_f/\mu_0 = 5, b - a/h_f = 32, 2h^c/b - a = 20, E^s/E_{0y} = 7, E_{0x}/E_{0y} = 2$.

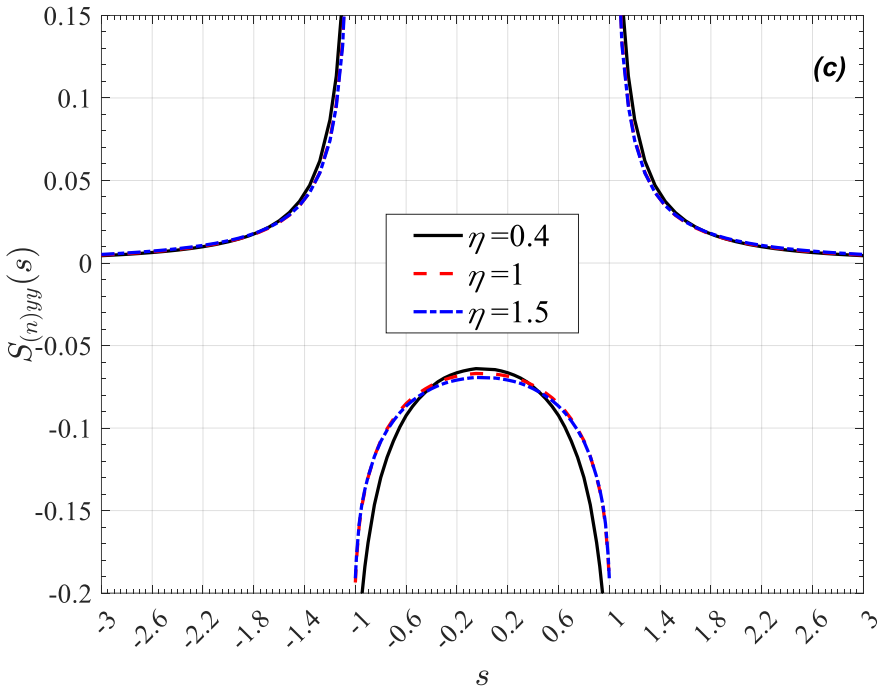

Figure 4-9. (continued)

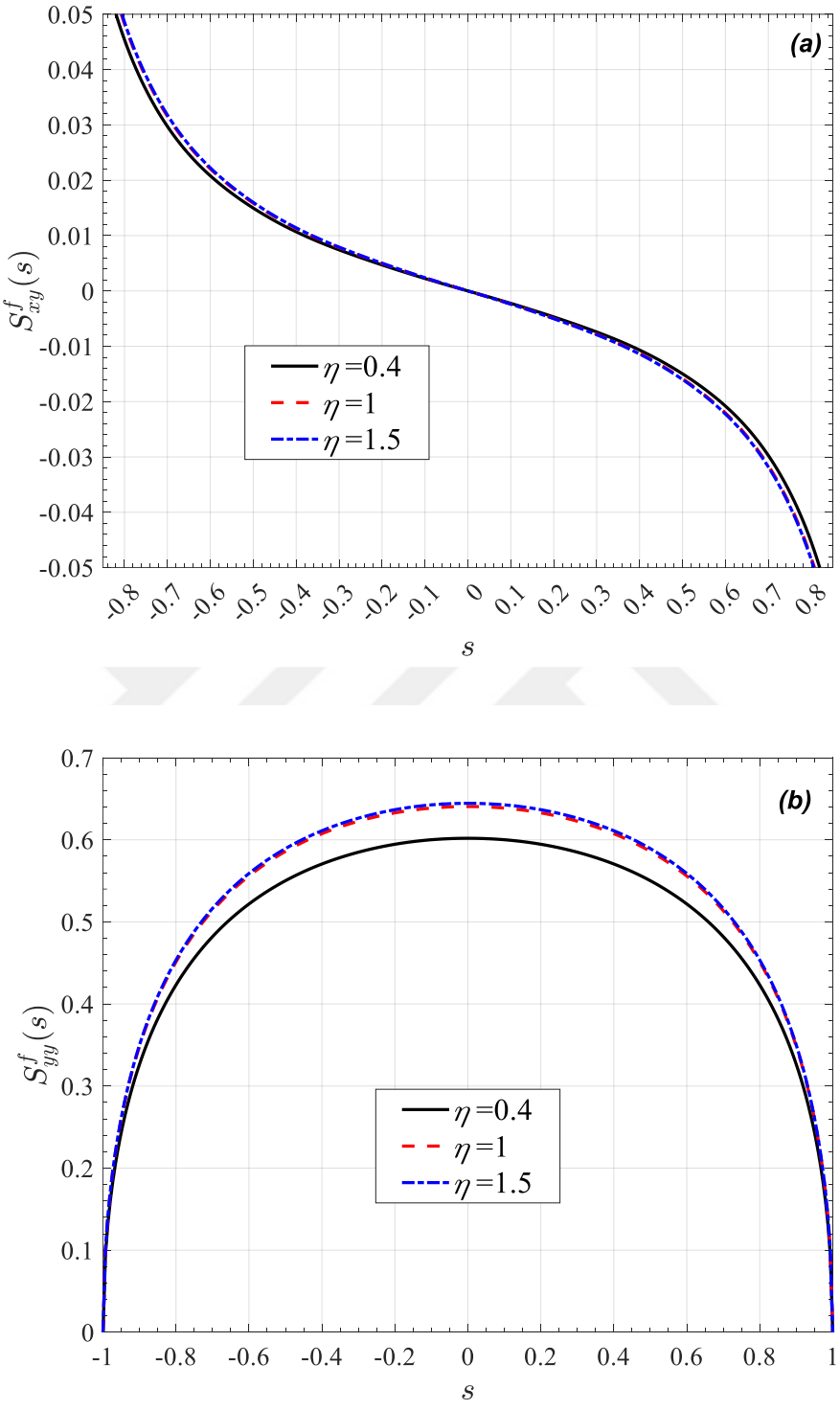

Figure 4-10. The computed shear stress ***(a)*** and the lateral stress ***(b)*** for the thin film and the lateral stress ***(c)*** for the uppermost layer by assuming a graded coating with $\mu^s/\mu_0 = 1/7, \mu_f/\mu_0 = 5, b - a/h_f = 32, 2h^c/b - a = 20, E^s/E_{0y} = 1/7, E_{0x}/E_{0y} = 2$.

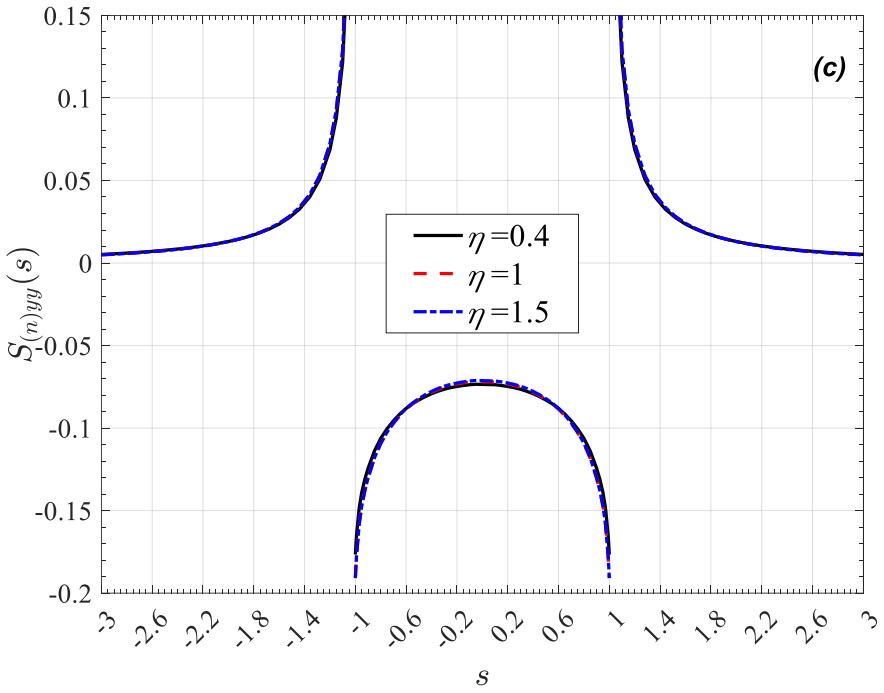

Figure 4-10. (continued)

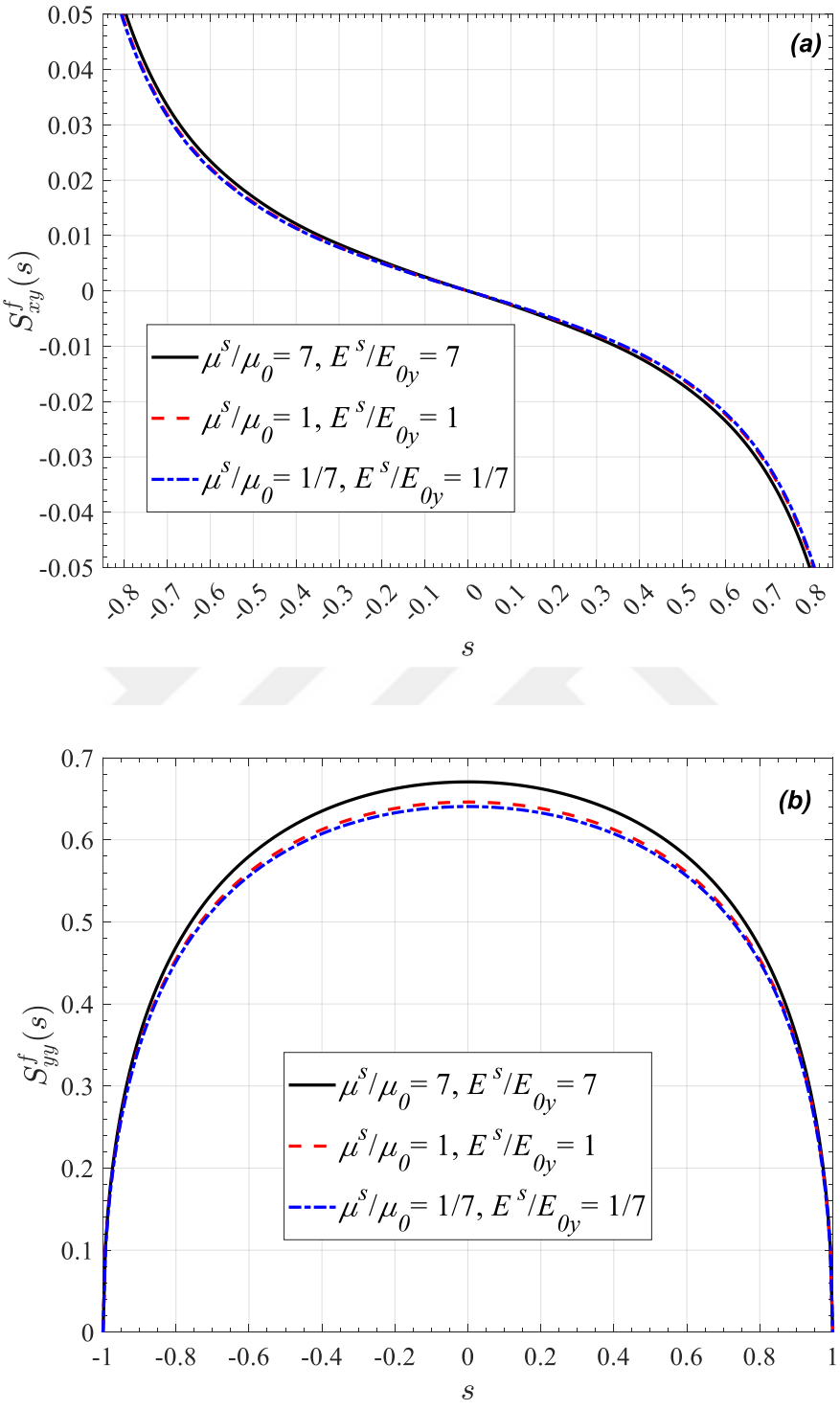

Figure 4-11. The computed shear stress ***(a)*** and the lateral stress ***(b)*** for the thin film and the lateral stress ***(c)*** for the uppermost layer by assuming a linearly graded coating with $\mu_f/\mu_0 = 5$, $b - a/h_f = 32$, $2h^c/b - a = 20$, $E_{0x}/E_{0y} = 2$**.**

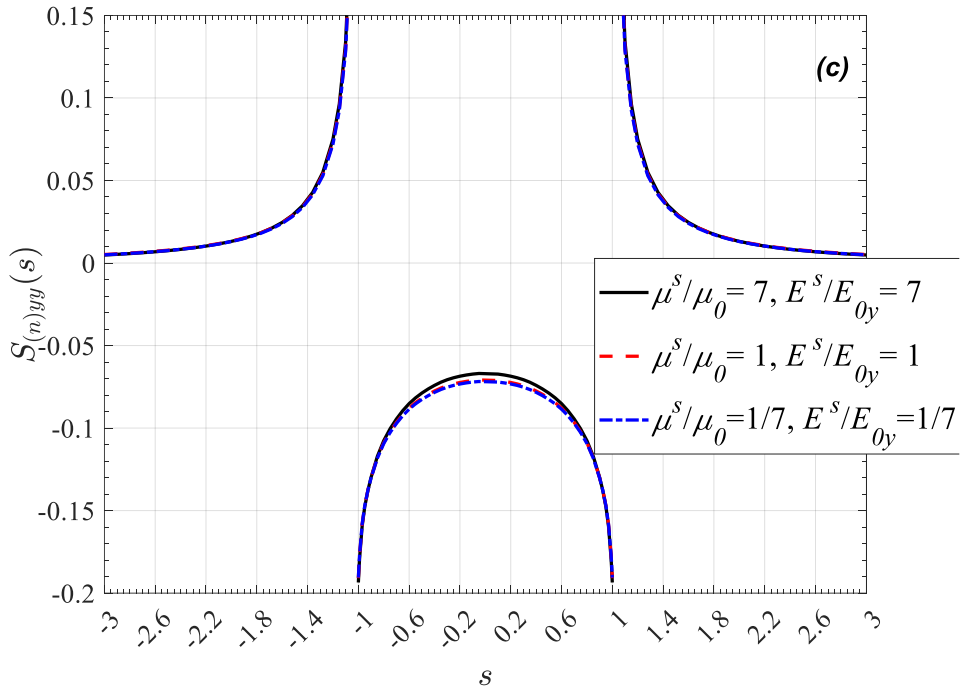

Figure 4-11. (continued)

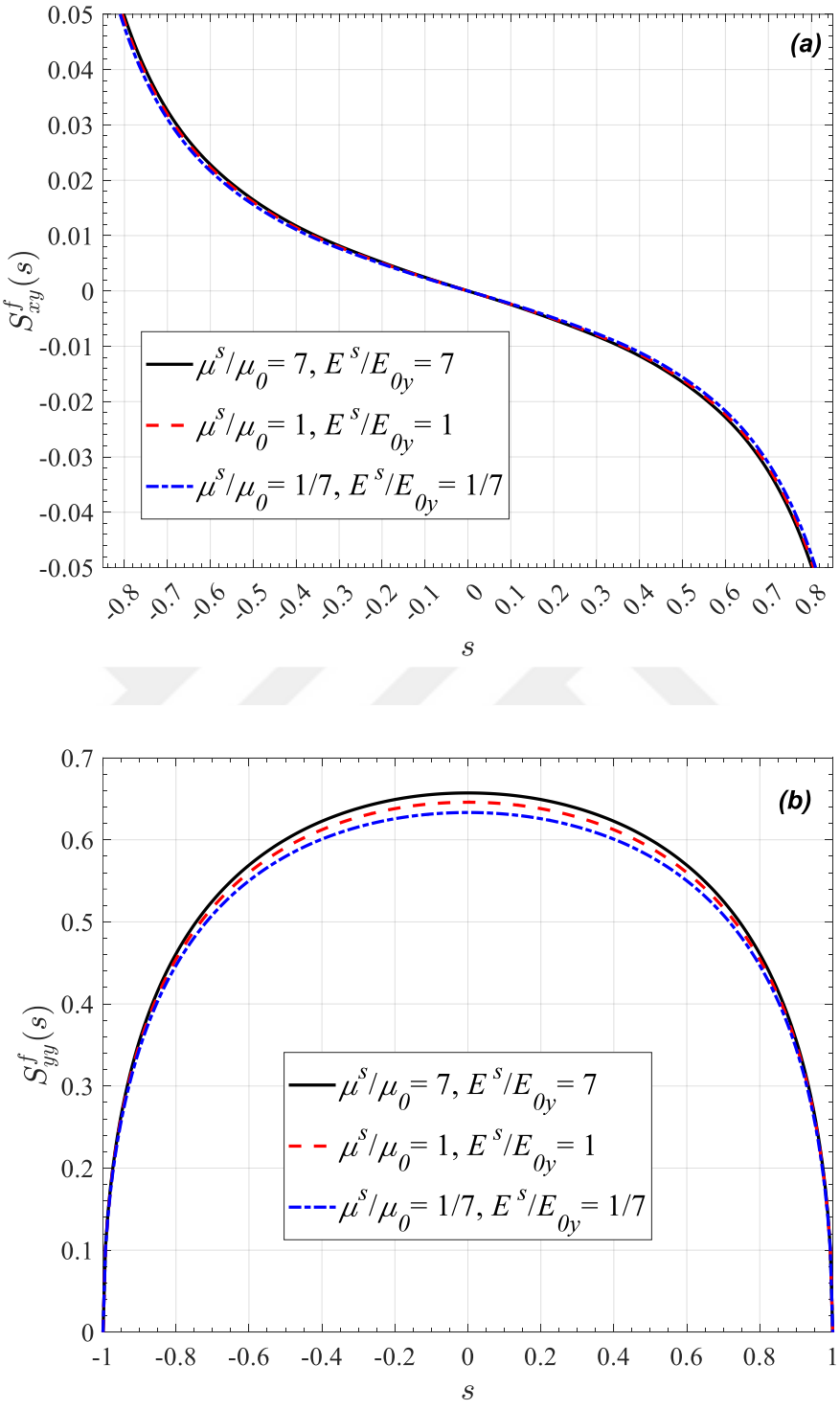

Figure 4-12. The computed shear stress ***(a)*** and the lateral stress ***(b)*** for the thin film and the lateral stress ***(c)*** for the uppermost layer by assuming an exponentially graded coating with $\mu_f/\mu_0 = 5$, $b - a/h_f = 32$, $2h^c/b - a = 20, E_{0x}/E_{0y} = 2$.

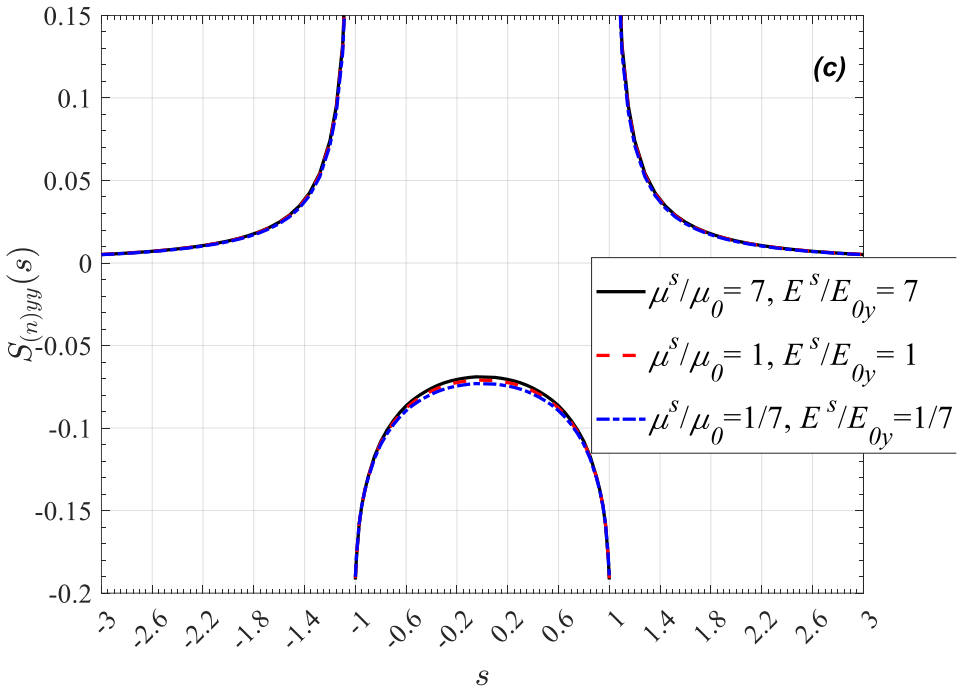

Figure 4-12. (continued)

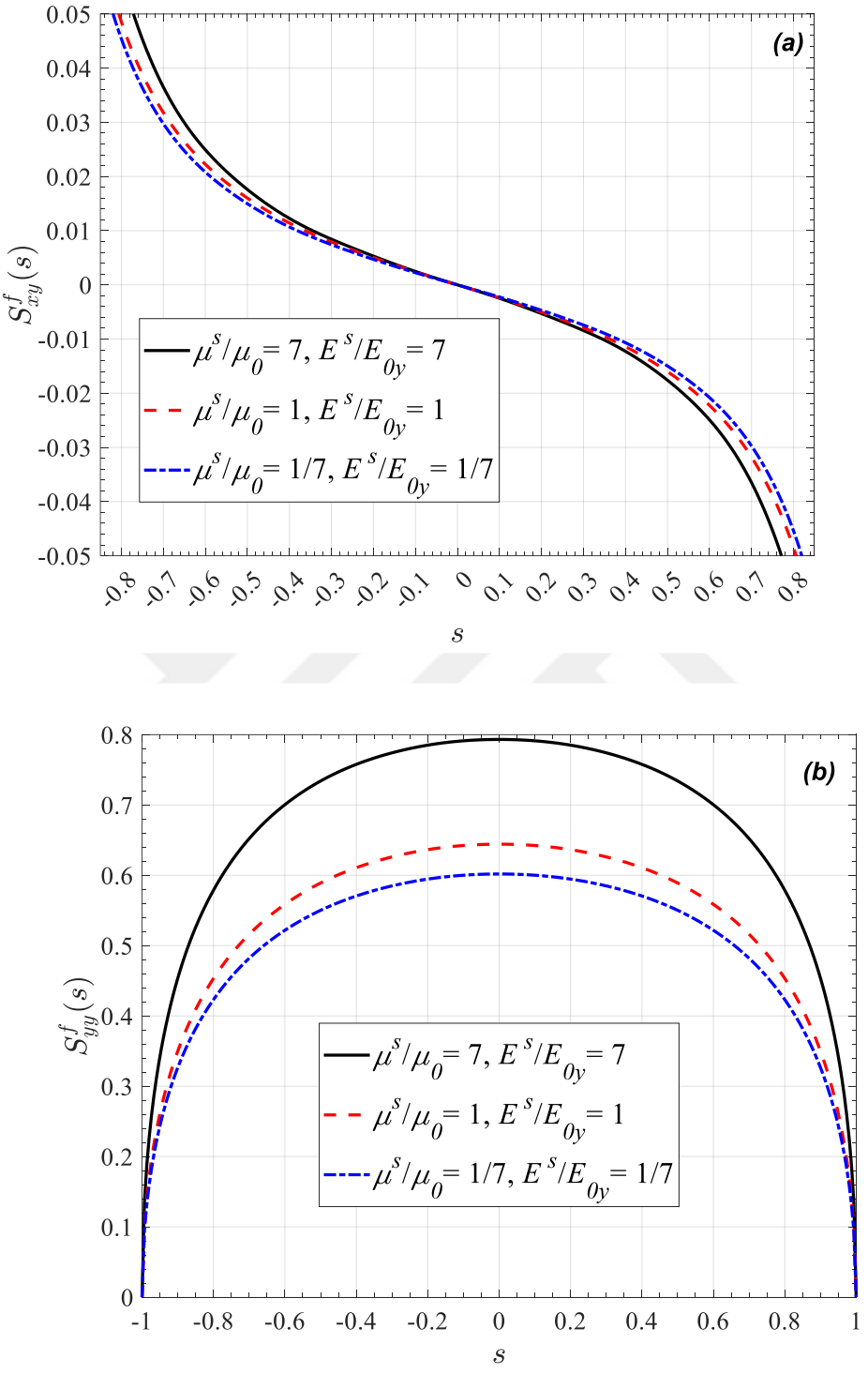

Figure 4-13. The computed shear stress ***(a)*** and the lateral stress ***(b)*** for the thin film and the lateral stress ***(c)*** for the uppermost layer by assuming graded coating with $\eta = 0.4, \mu_f/\mu_0 = 5, b - a/h_f = 32, 2h^c/b - a = 20, E_{0x}/E_{0y} =$ **2.**

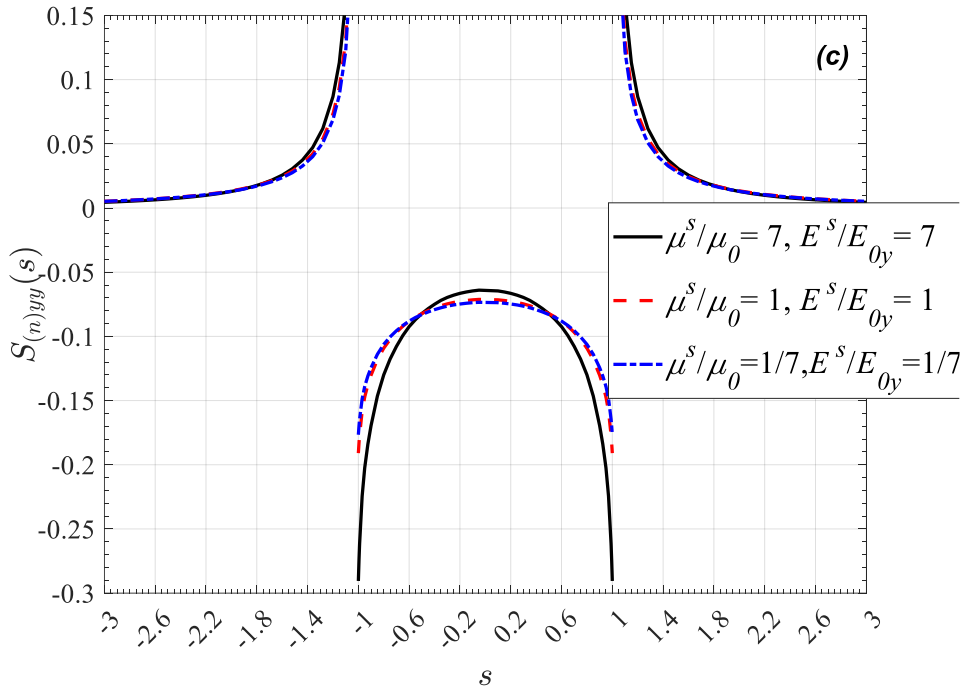

Figure 4-13. (continued)

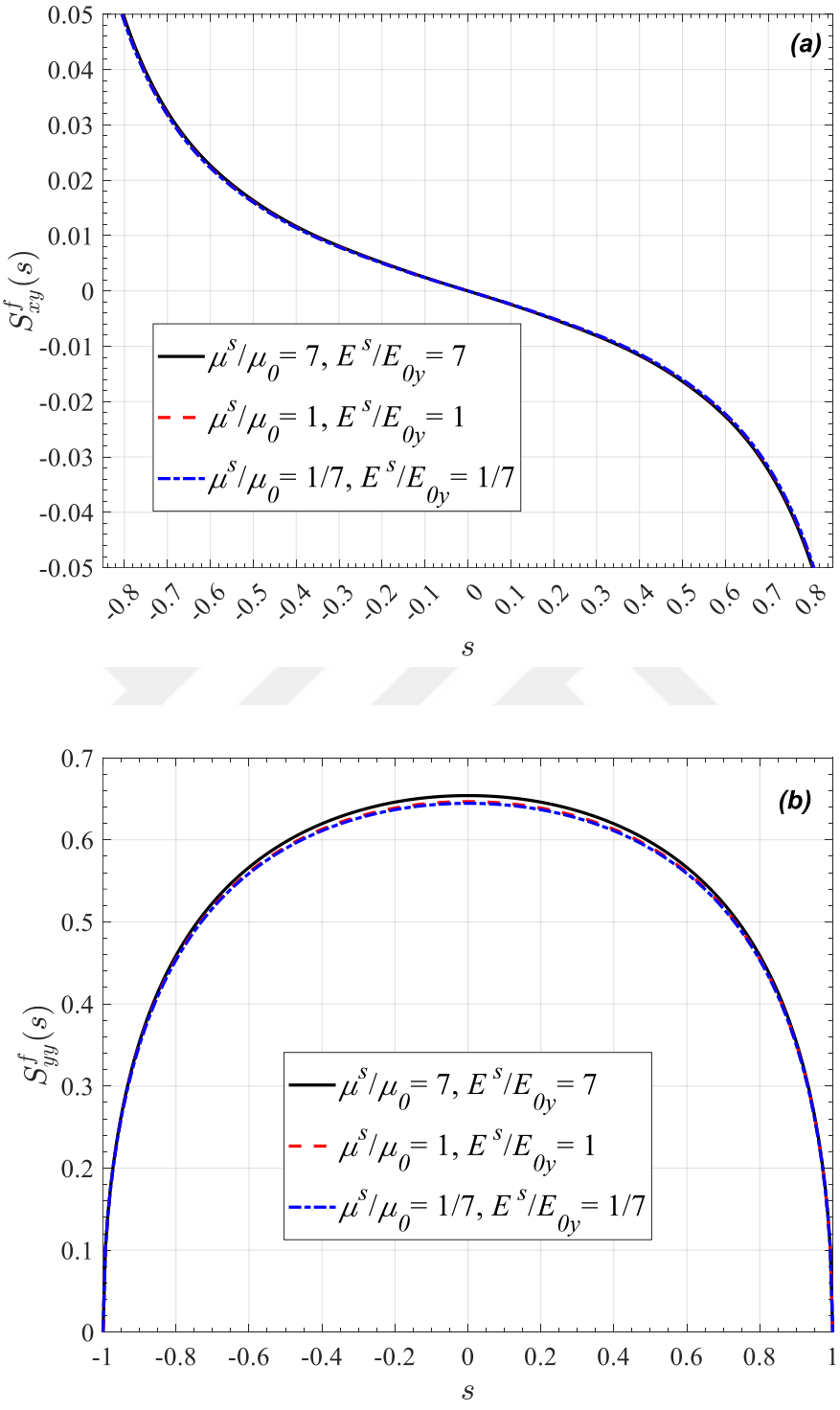

Figure 4-14. The computed shear stress ***(a)*** and the lateral stress ***(b)*** for the thin film and the lateral stress ***(c)*** for the uppermost layer by assuming graded coating with $\eta = 1.5, \mu_f/\mu_0 = 5, b - a/h_f = 32, 2h^c/b - a = 20, E_{0x}/E_{0y} =$ **2.**

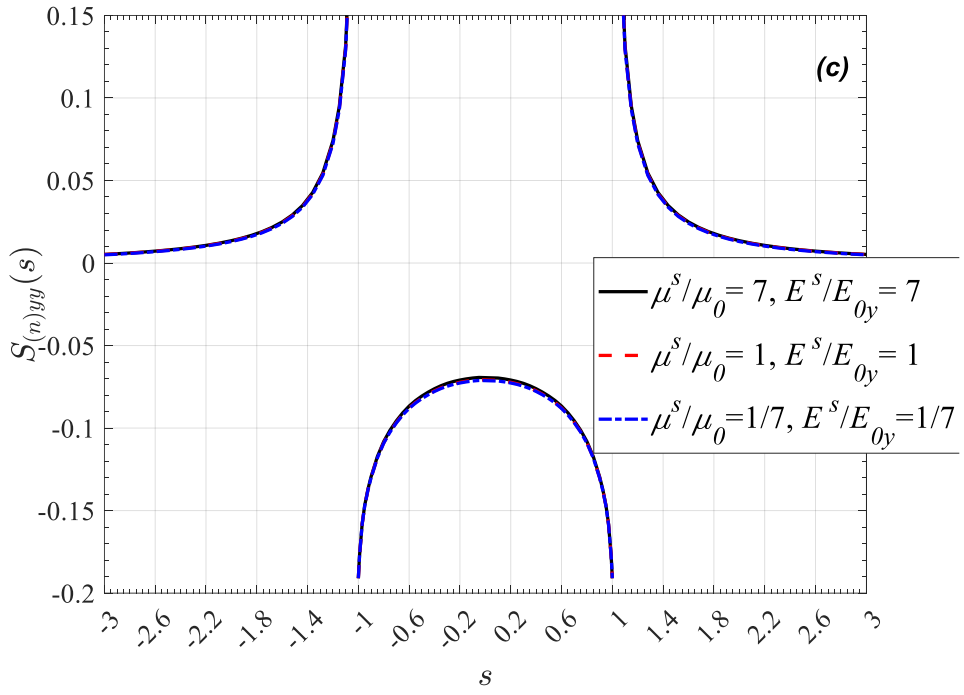

Figure 4-14. (continued)

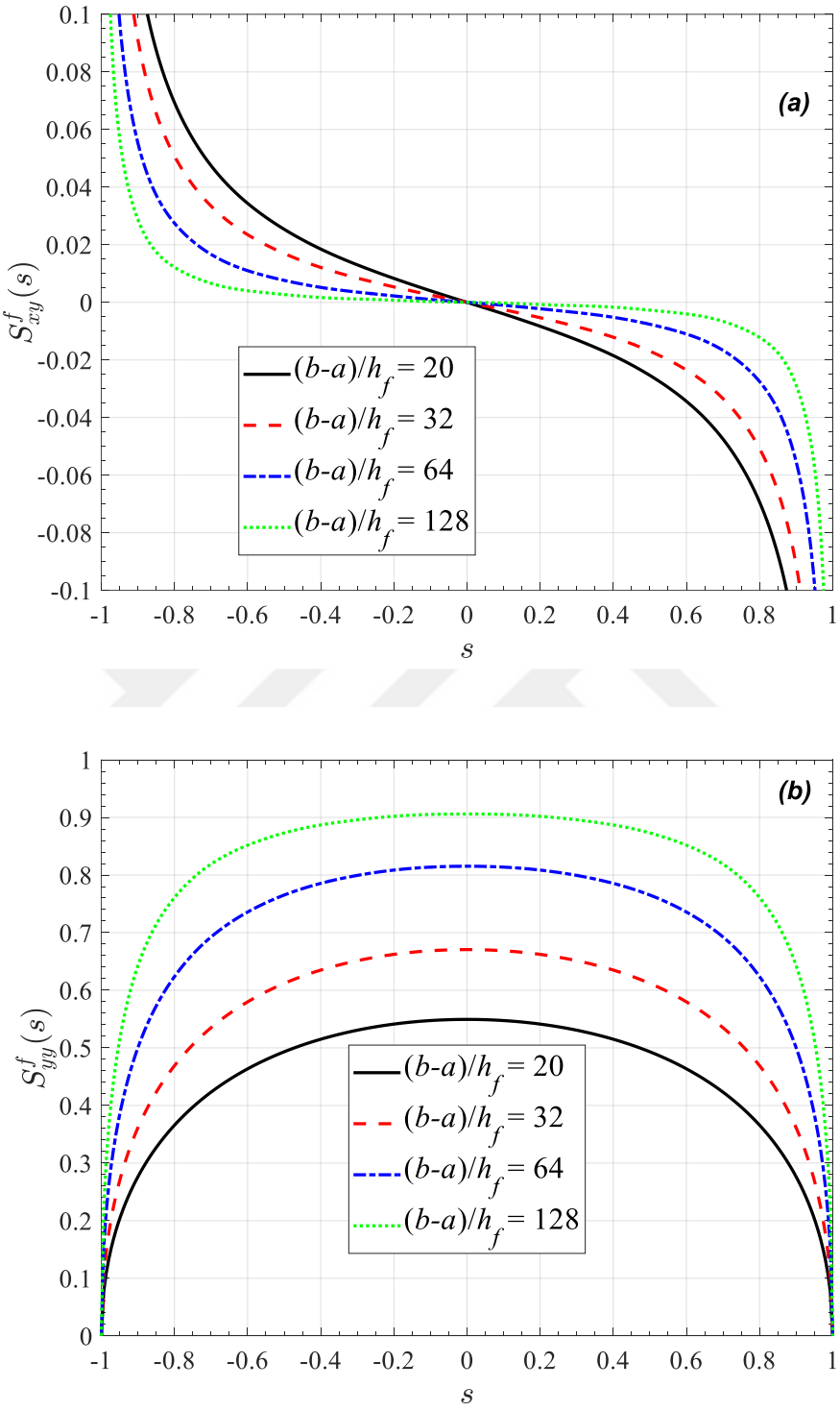

Figure 4-15. The computed shear stress ***(a)*** and the lateral stress ***(b)*** for the thin film and the lateral stress ***(c)*** for the uppermost layer by assuming a linearly graded coating with $\mu_f/\mu_0 = 5, \mu^s/\mu_0 = 7, 2h^c/b - a = 20, E^s/E_{0y} = \mathbf{7}, E_{0x}/E_{0y} = \mathbf{2}$.

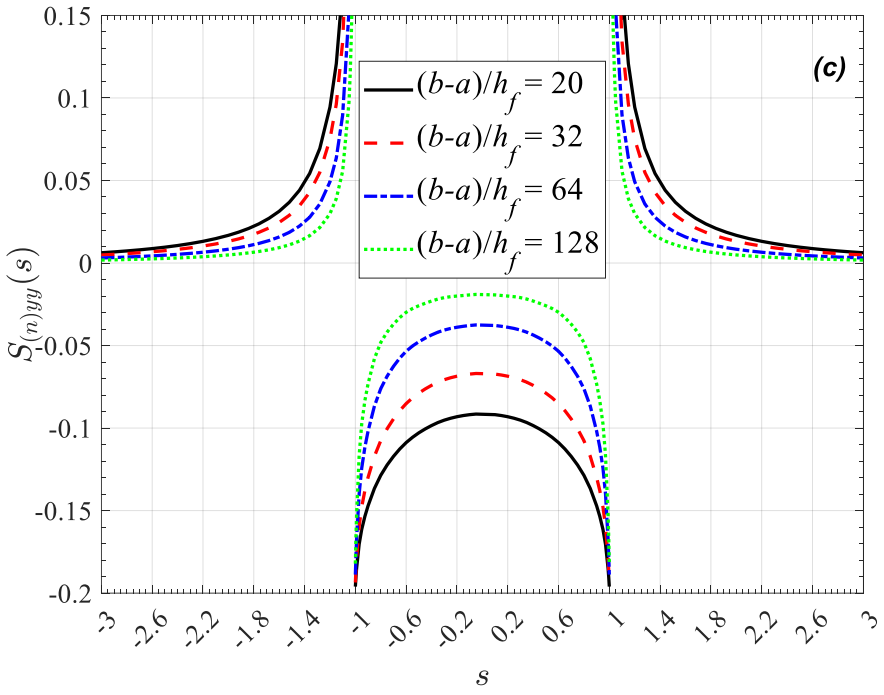

Figure 4-15. (continued)

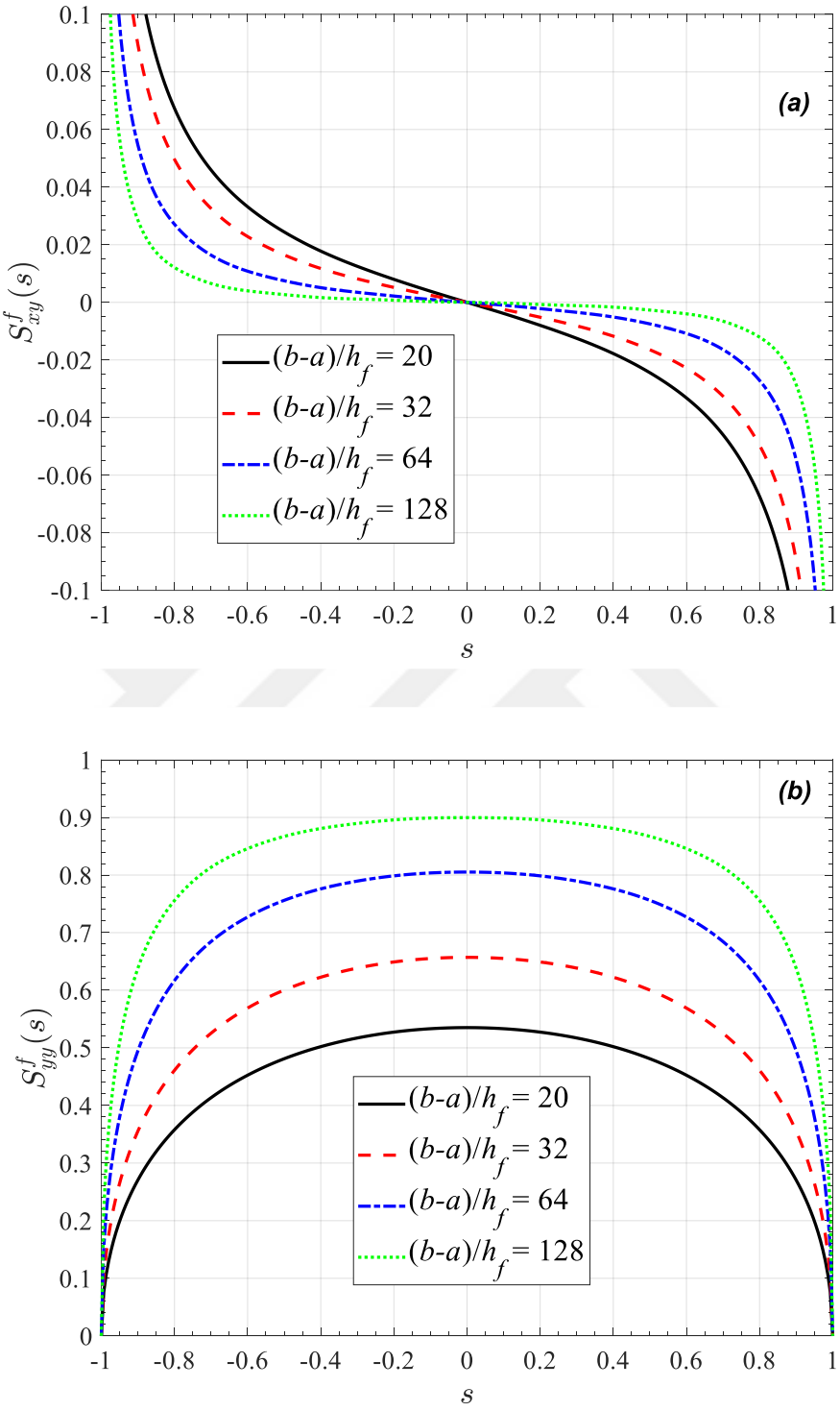

Figure 4-16. The computed shear stress ***(a)*** and the lateral stress ***(b)*** for the thin film and the lateral stress ***(c)*** for the uppermost layer by assuming an exponentially graded coating with $\mu_f/\mu_0 = 5$, $\mu^s/\mu_0 = 7$, $2h^c/b - a = 20$, $E^s/E_{0y} = \mathbf{7}$, $E_{0x}/E_{0y} = \mathbf{2}$.

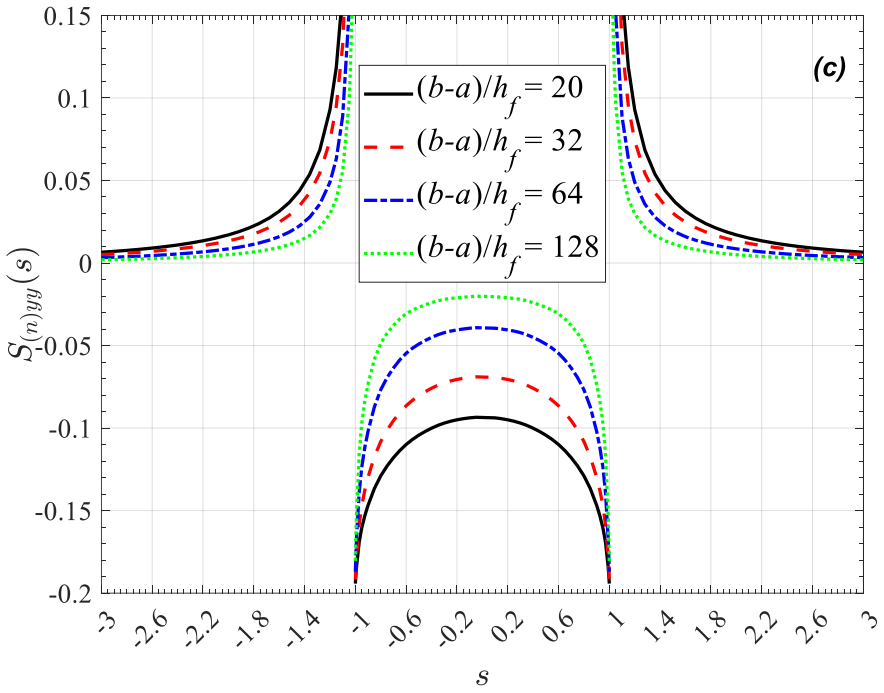

Figure 4-16. (continued)

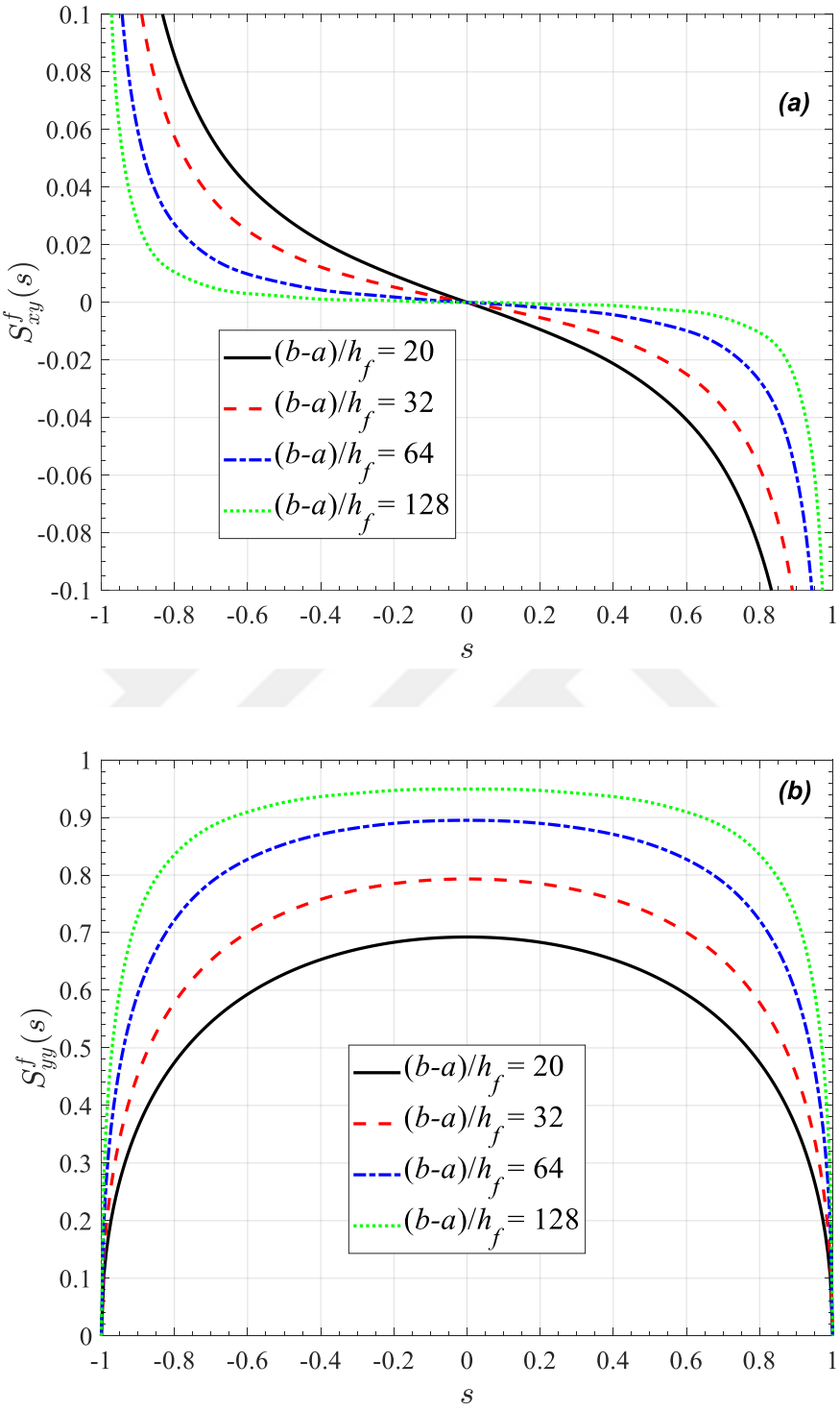

Figure 4-17. The computed shear stress ***(a)*** and the lateral stress ***(b)*** for the thin film and the lateral stress ***(c)*** for the uppermost layer by assuming a graded coating with $\eta = 0.4, \mu_f/\mu_0 = 5, \mu^s/\mu_0 = 7, 2h^c/b - a = 20, E^s/E_{0y} = \mathbf{7}, E_{0x}/E_{0y} = \mathbf{2}$.

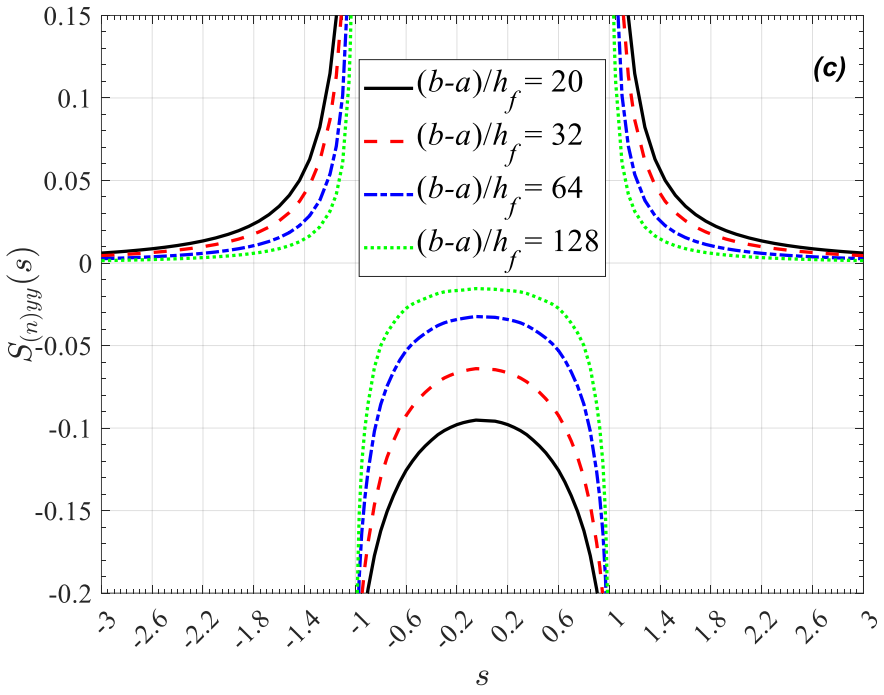

Figure 4-17. (continued)

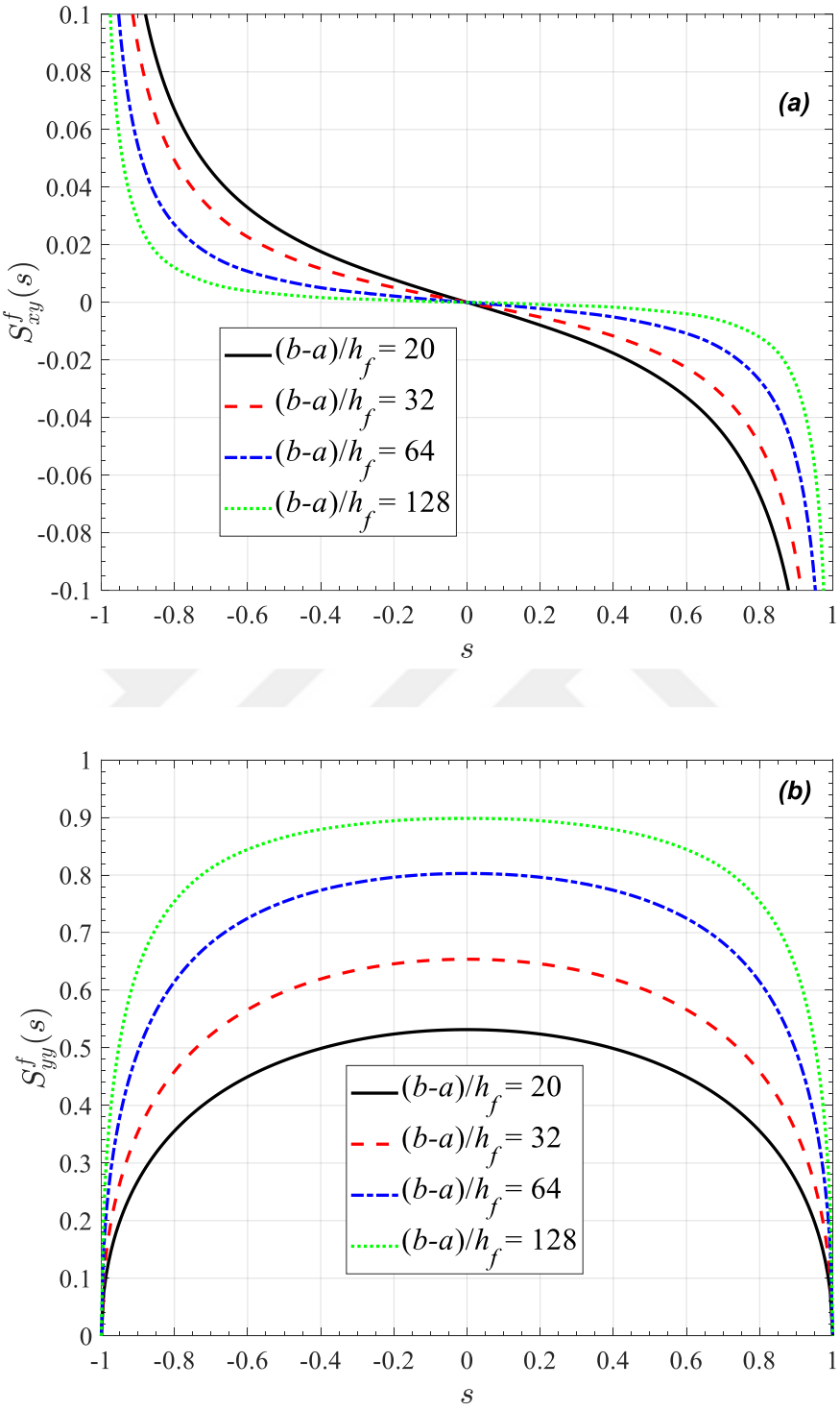

Figure 4-18. The computed shear stress ***(a)*** and the lateral stress ***(b)*** for the thin film and the lateral stress ***(c)*** for the uppermost layer by assuming a graded coating with $\eta = 1.5, \mu_f/\mu_0 = 5, \mu^s/\mu_0 = 7, 2h^c/b - a = 20, E^s/E_{0y} = \mathbf{7}, E_{0x}/E_{0y} = \mathbf{2}$.

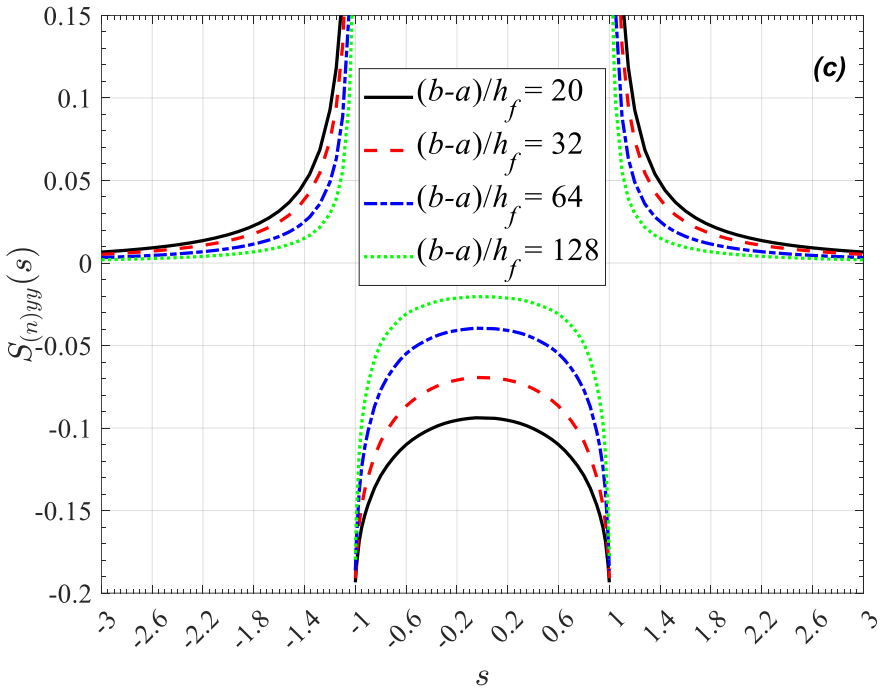

Figure 4-18. (continued)

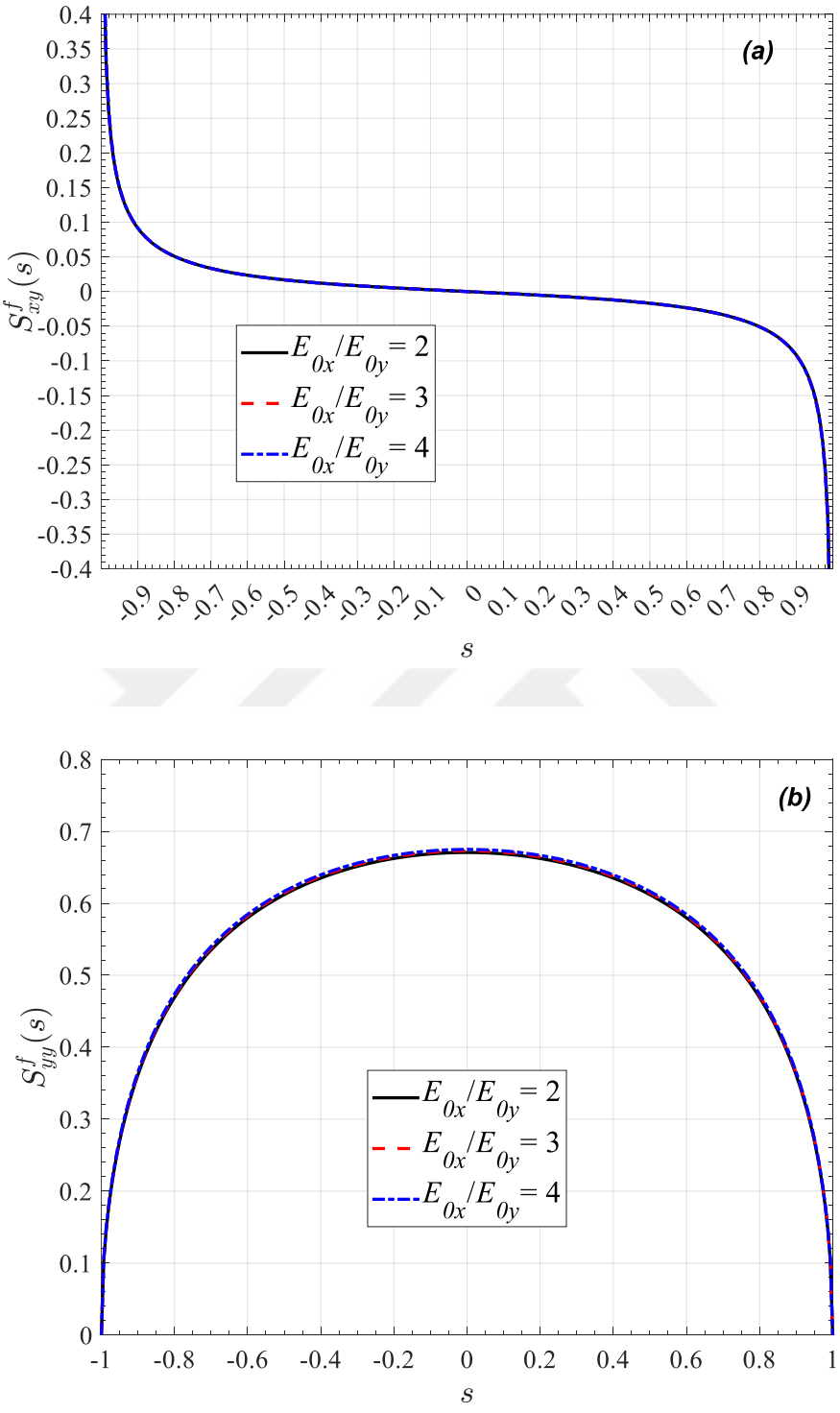

Figure 4-19. The computed shear stress ***(a)*** and the lateral stress ***(b)*** for the thin film and the lateral stress ***(c)*** for the uppermost layer by assuming a linearly graded coating with $\mu_f/\mu_0 = 5, \mu^s/\mu_0 = 7, 2h^c/b - a = 20, E^s/E_{0y} = \mathbf{7}, b - a/h_f = 32$.

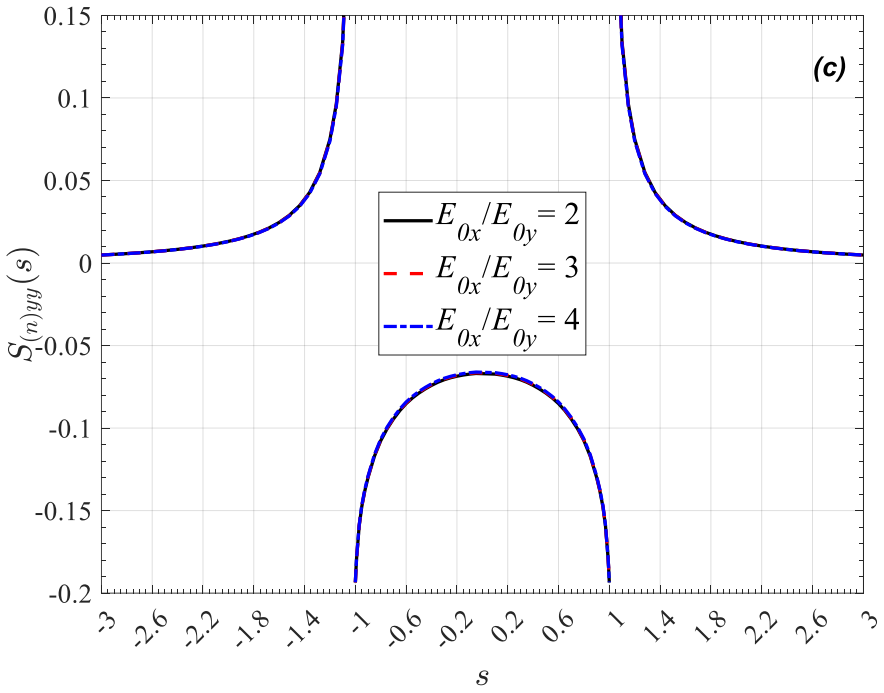

Figure 4-19. (continued)

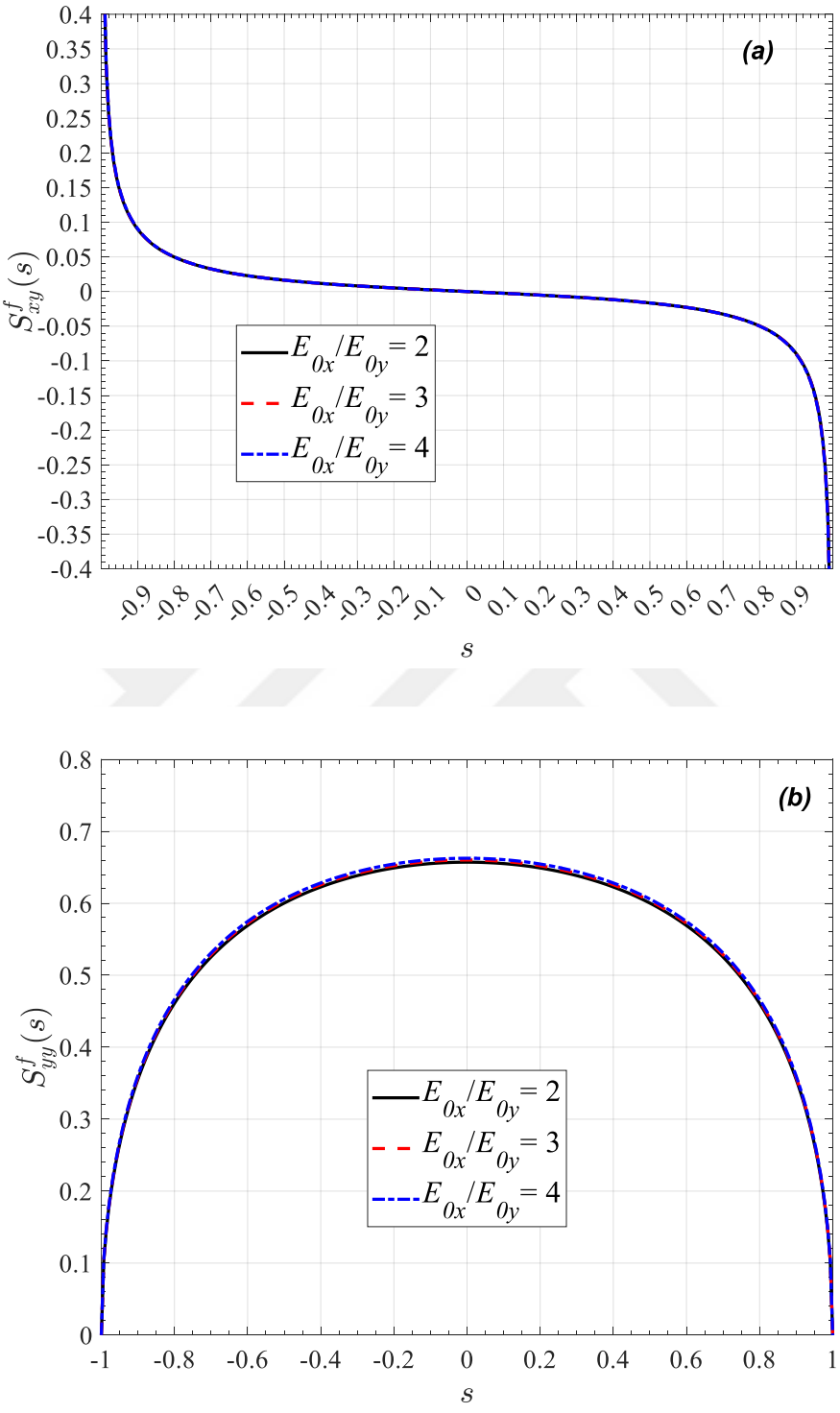

Figure 4-20. The computed shear stress ***(a)*** and the lateral stress ***(b)*** for the thin film and the lateral stress ***(c)*** for the uppermost layer by assuming an exponentially graded coating with $\mu_f/\mu_0 = 5, \mu^s/\mu_0 = 7, 2h^c/b - a = 20, E^s/E_{0y} = \mathbf{7}, b - a/h_f = 32$.

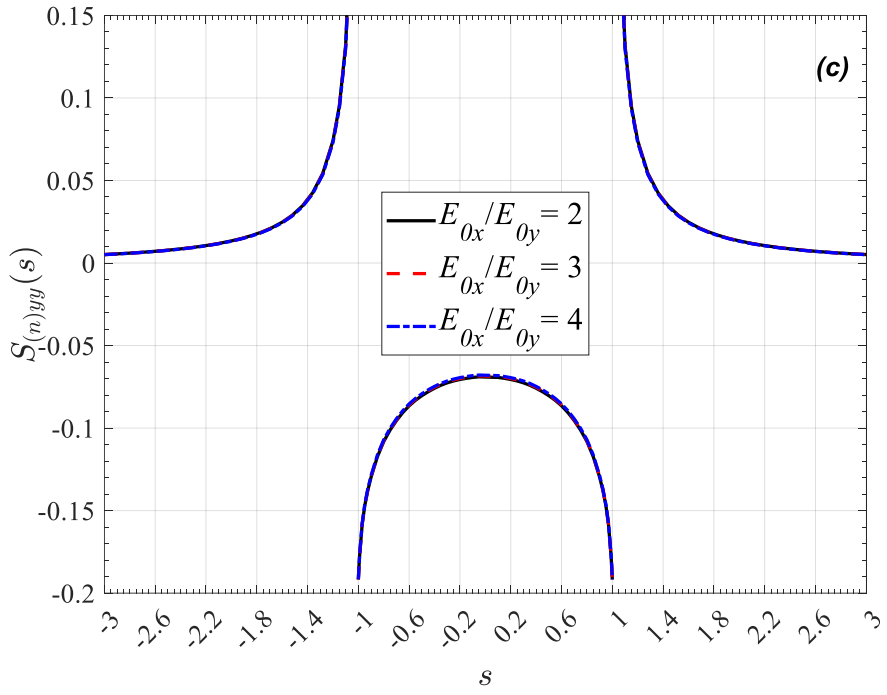

Figure 4-20. (continued)

The final study is conducted on the model for an ultrasonic transducer construction, as developed by Muralt et al. [28]. The material properties are delineated in **Table 4-12** using values derived from extant literature. The thickness of the Pt and SiO_2 are given as $\boldsymbol{h_{Pt}} = 0.1$ μm and $\boldsymbol{h_{SiO_2}} = 1.2$ μm in this study, respectively. The total thickness of the coating system is declared as $\boldsymbol{h^c} = \boldsymbol{h_{Pt}} + \boldsymbol{h_{SiO_2}}$. Both Pt and SiO_2 structures are modeled as multi-layers in the present study as illustrated in **Table 4-13** for different thickness ratios. The edge and far-field loadings are also assumed zero for this study and the normalization constant h_2 for the thin film is declared in this analysis as follows since it is piezoelectric.

$$h_2 = \left(\frac{c_{12}^f e_{11}^f}{c_{11}^f} - e_{12}^f\right) E_x^f. \tag{4.33}$$

The shear, lateral stresses and the stress intensity factors for the thin film are declared as follows with the following expressions.

$$S_{xy}^{f}(s) = \sigma_{xy}^{f}\left(0, \frac{b-a}{2}s + \frac{b+a}{2}\right)\frac{1}{h_2}, \tag{4.34}$$

$$S_{yy}^{f}(s) = \sigma_{yy}^{f}\left(0, \frac{b-a}{2}s + \frac{b+a}{2}\right)\frac{1}{h_2}, \tag{4.35}$$

$$S_{(n)yy}(s) = \sigma_{(n)yy}\left(0, \frac{b-a}{2}s + \frac{b+a}{2}\right)\frac{1}{h_2}, \tag{4.36}$$

$$K_{II,a} = \frac{k_{II,a}}{\sqrt{\frac{b-a}{2}}}\frac{1}{h_2}, \tag{4.37}$$

$$K_{II,b} = \frac{k_{II,b}}{\sqrt{\frac{b-a}{2}}}\frac{1}{h_2}. \tag{4.38}$$

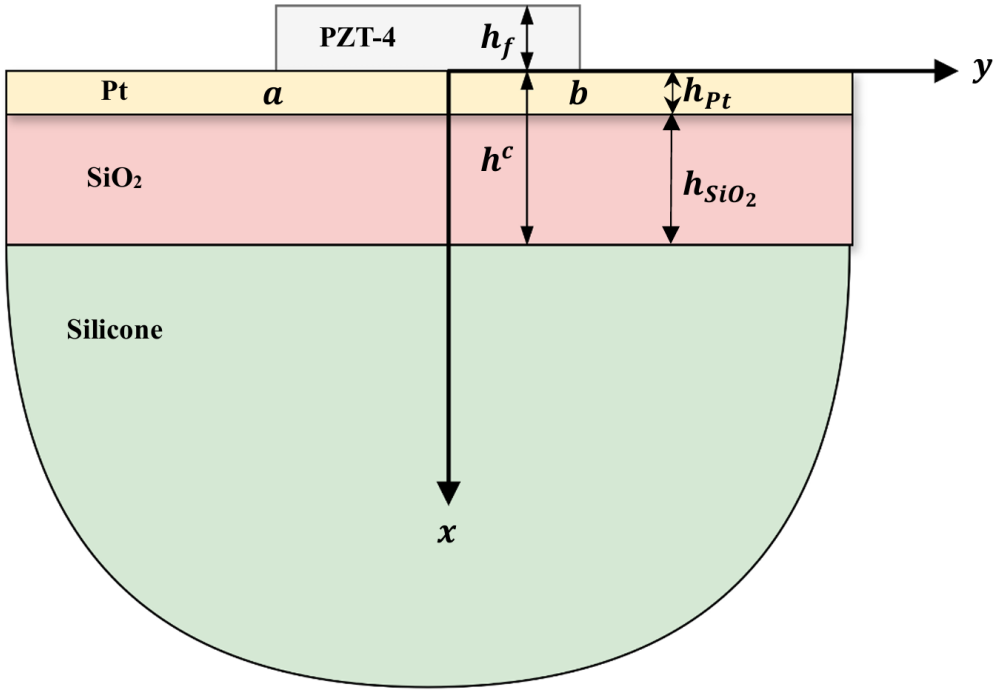

Figure 4-21. Geometry of the ultrasonic transducer

Table 4-12. The material properties for the system [28],[48],[49]

	Si	***SiO₂***	***Pt***	***PZT-4***
C_{11}[GPa]	-	76	339.1	132
C_{12}[GPa]	-	25.5	216.0	73
C_{22}[GPa]	-	76	339.1	115
C_{55}[GPa]	-	25.0	61.1	30
e_{11}[C/m^2]	-	-	-	14.1
e_{12}[C/m^2]	-	-	-	-13.1
υ	0.278	-	-	-
E[GPa]	130.6	-	-	-

Table 4-13. The number of layers for different thickness ratios.

The Number of Layers	**Pt**	**SiO_2**
8%Pt-92%SiO_2	2	23
20%Pt-80%SiO_2	5	20
40%Pt-60%SiO_2	10	15
50%Pt-50%SiO_2	13	13

The results obtained by using different parameters for the normalized stress intensity factors are reported in **Tables 4-14** to **4-18**. **Table 4-14** reveals the effect of the ratio of the width of the thin film to the thickness of it ($b - a/h_f$) on the normalized SIF for $2h^c/b - a = 2$. It has been demonstrated that the use of thinner films results in a smaller SIF value. **Table 4-15** and **Table 4-16** illustrate the relation of the ratio of the total thickness of the coating to the width of the thin film to the normalized SIF

for $b-a/h_f=4$ and $b-a/h_f=1/2$, respectively. The increase in this ratio has been indicated to increase the value of the SIFs for both conditions. **Table 4-17** and **Table 4-18** give information on the effect of the Pt / SiO_2 volumetric on the normalized SIF for $b-a/h_f=4$ and $b-a/h_f=1/2$, respectively. The increase in the volumetric fraction of Pt in the total coating results in elevated SIF values. The augmentation in the volumetric proportion of Pt within the total coating material results in elevated SIF values.

Table 4-14. The normalized stress intensity factors computed for the ultrasonic transducer problem with $2h^c/b-a=2$.

$\frac{b-a}{h_f}$	1/2	1	2	4	8
$K_{II,a}$	0.9113	0.8256	0.7055	0.5653	0.4288
$K_{II,b}$	-0.9113	-0.8256	-0.7055	-0.5653	-0.4288

Table 4-15. The normalized stress intensity factors computed for the ultrasonic transducer problem with $b-a/h_f=4$.

$\frac{2h^c}{b-a}$	1	2	4
$K_{II,a}$	0.5584	0.5653	0.5775
$K_{II,b}$	-0.5584	-0.5653	-0.5775

Table 4-16. The normalized stress intensity factors computed for the ultrasonic transducer problem with $b-a/h_f=1/2$**.**

$\frac{2h^c}{b-a}$	**2**	**4**	**8**
$K_{II,a}$	0.9113	0.9711	1.0245
$K_{II,b}$	-0.9113	-0.9711	-1.0245

Table 4-17. The normalized stress intensity factors computed for the ultrasonic transducer problem with $b-a/h_f=4, 2h^c/b-a=2$.

	8%Pt, 92%SiO_2	**20%Pt, 80%SiO_2**	**40%Pt, 60%SiO_2**	**50%Pt, 50%SiO_2**
$K_{II,a}$	0.5653	0.5856	0.5955	0.5974
$K_{II,b}$	-0.5653	-0.5856	-0.5955	-0.5974

Table 4-18. The normalized stress intensity factors computed for the ultrasonic transducer problem with $b-a/h_f=1/2, 2h^c/b-a=2$.

	8%Pt, 92%SiO_2	**20%Pt, 80%SiO_2**	**40%Pt, 60%SiO_2**	**50%Pt, 50%SiO_2**
$K_{II,a}$	0.9113	1.0066	1.0568	1.0689
$K_{II,b}$	-0.9113	-1.0066	-1.0568	-1.0689

The stresses for the thin film and uppermost layer are illustrated in **Figures 4-22** to **4-26**. **Figure 4-22** presents the effect of the ratio of the width of the thin film to its

thickness ($b - a/h_f$) on the stresses for $2h^c/b - a = 2$. It has been indicated that the use of thinner films leads to increased lateral stress for thin films, reduced shear and lateral stress values for the uppermost layer. **Figure 4-23** shows the influence of the ratio of the total thickness of the coating to the width of the thin film ($2h^c/b - a$) on the stresses for $b - a/h_f = 4$. The increase in this ratio results in larger lateral and shear stress for thin film and smaller lateral stress value for the uppermost layer. **Figure 4-24** gives information on the relation of the Pt / SiO_2 volumetric fraction with the stresses for $b - a/h_f = 4$. It has been demonstrated that an increase in the amount of platinum (Pt) in the coating results in greater lateral and shear stress for the thin film, and a reduced lateral stress value for the uppermost layer. **Figure 4-25** indicates the influence of the ratio of the total thickness of the coating to the width of the thin film ($2h^c/b - a$) on the stresses for $b - a/h_f = 1/2$. **Figure 4-26** illustrates the effect of the Pt / SiO_2 volumetric on the stresses for $b - a/h_f = 1/2$. As demonstrated in **Figure 4-25** and **Figure 4-26** the observed stress behaviors are analogous to those previously documented in **Figure 4-23** and **Figure 4-24**.

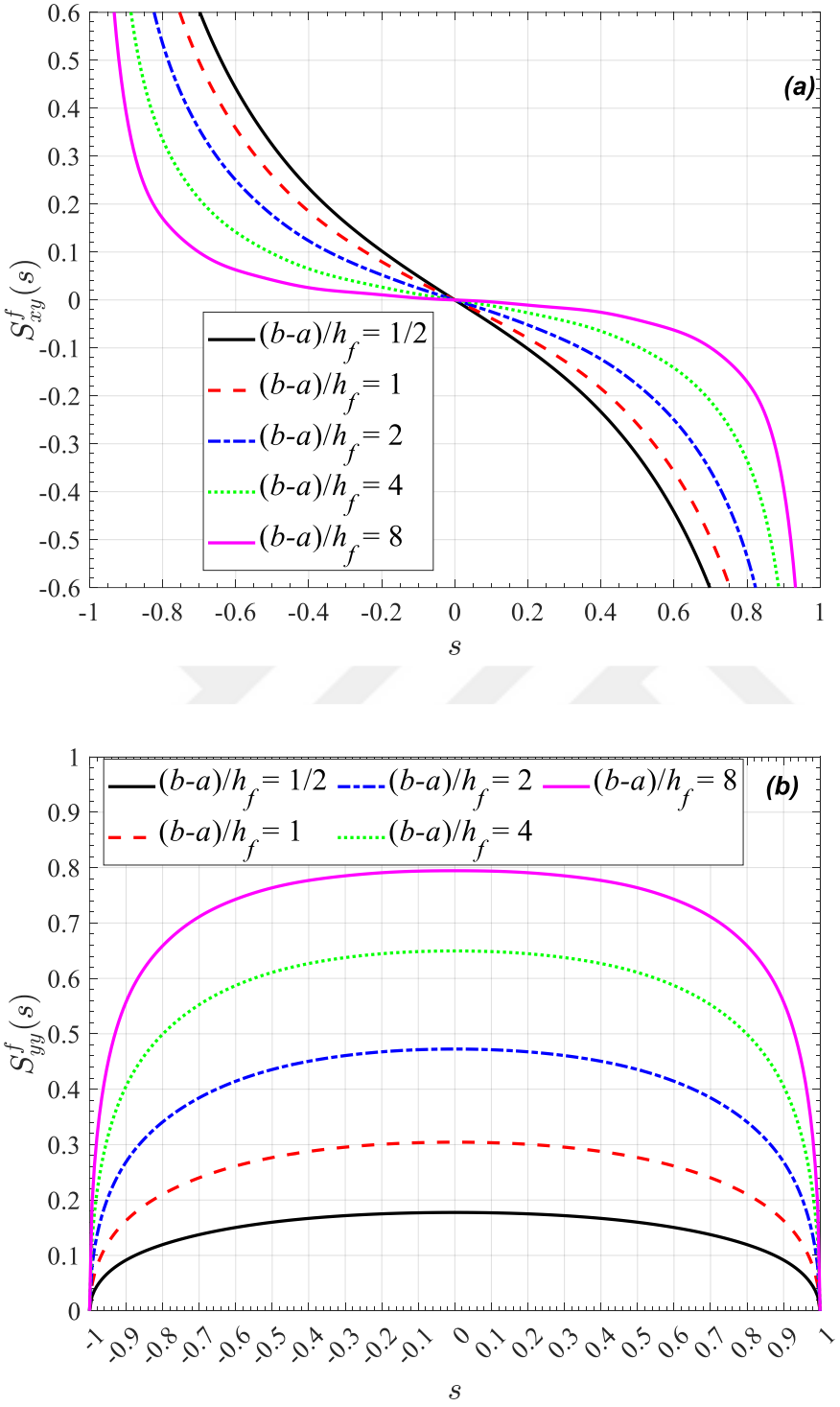

Figure 4-22. The computed shear stress ***(a)*** and the lateral stress ***(b)*** for the thin film and the lateral stress ***(c)*** for the uppermost layer by assuming $2h^c/b - a = 2$.

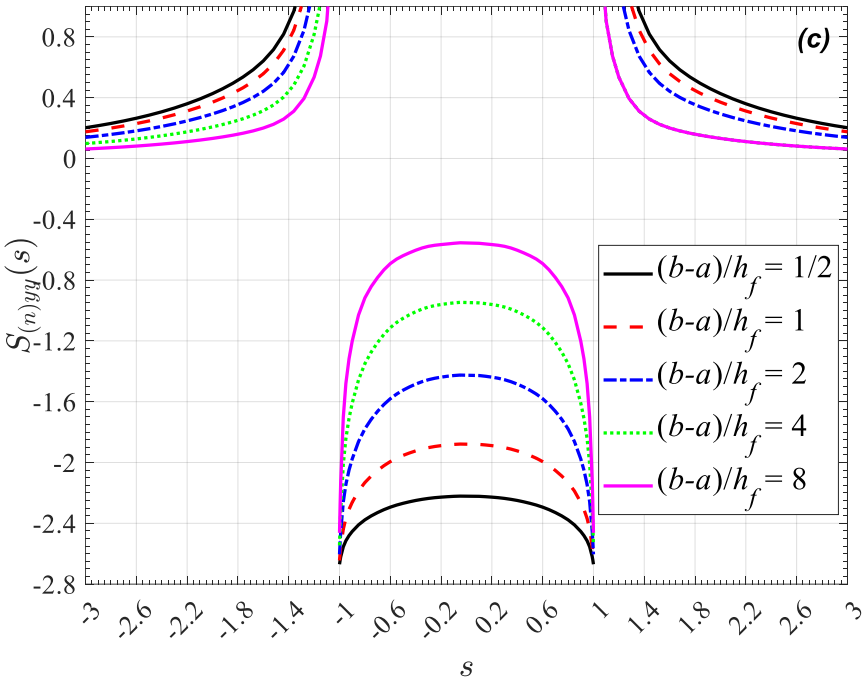

Figure 4-22. (continued)

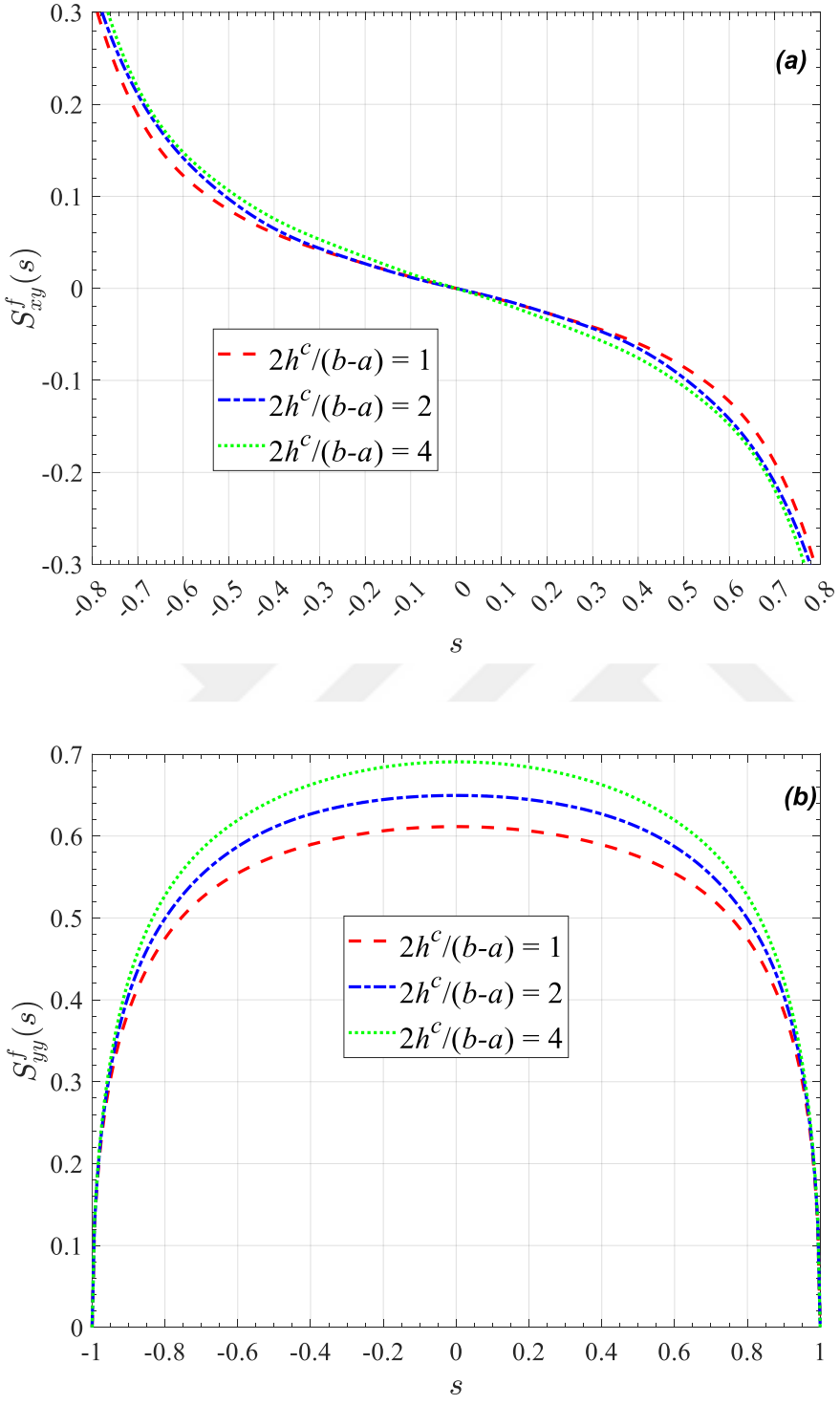

Figure 4-23. The computed shear stress ***(a)*** and the lateral stress ***(b)*** for the thin film and the lateral stress ***(c)*** for the uppermost layer by assuming $b - a/h_f = 4$.

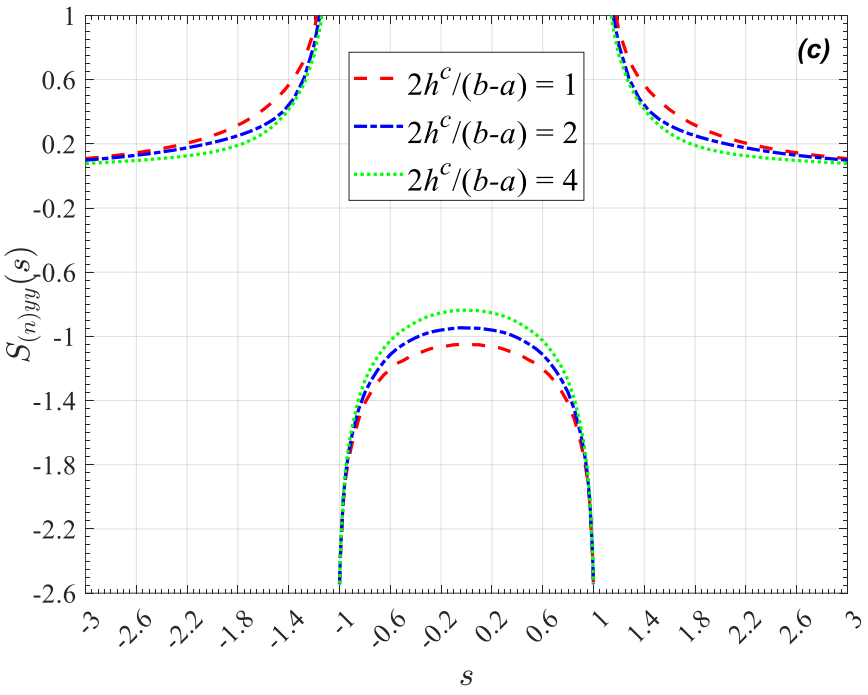

Figure 4-23. (continued)

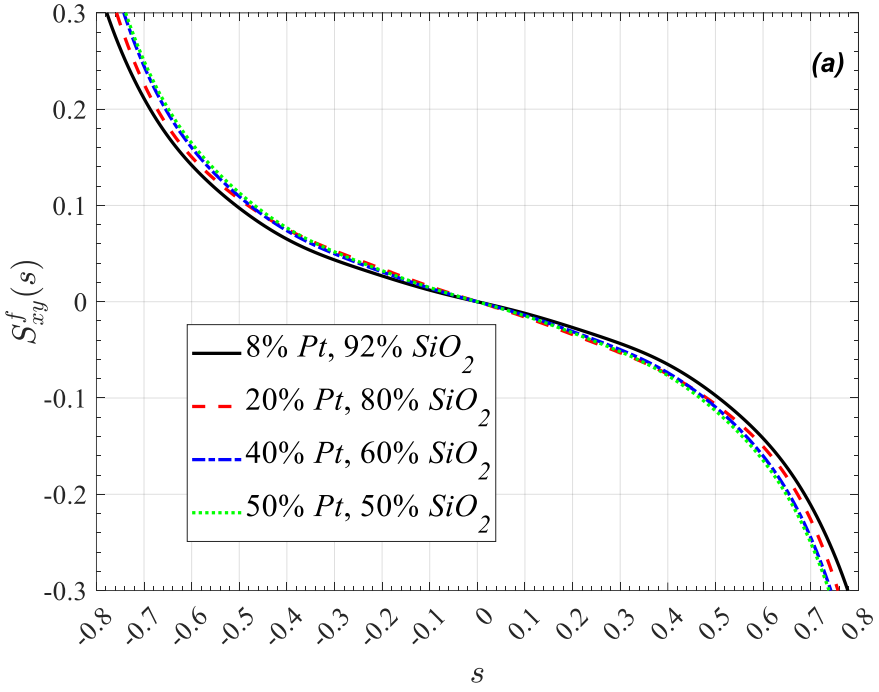

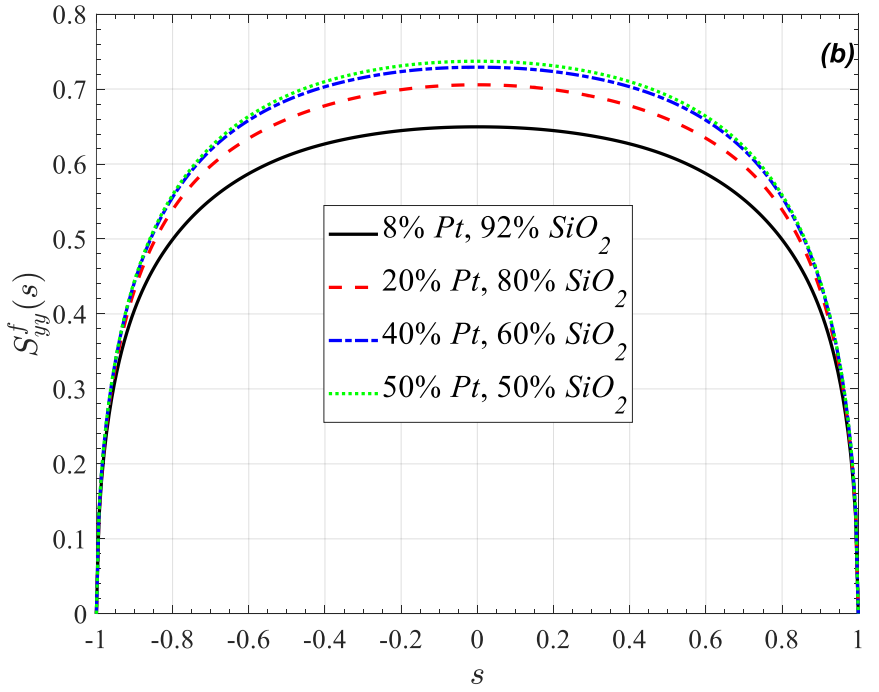

Figure 4-24. The computed shear stress ***(a)*** and the lateral stress ***(b)*** for the thin film and the lateral stress ***(c)*** for the uppermost layer by assuming $b - a/h_f = 4$ and $2h^c/b - a = 2$.

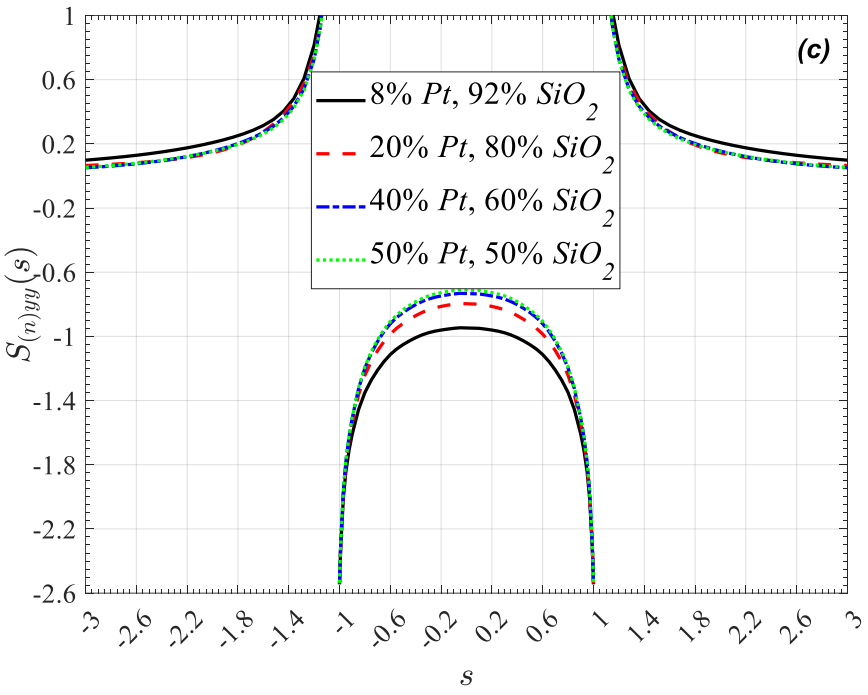

Figure 4-24. (continued)

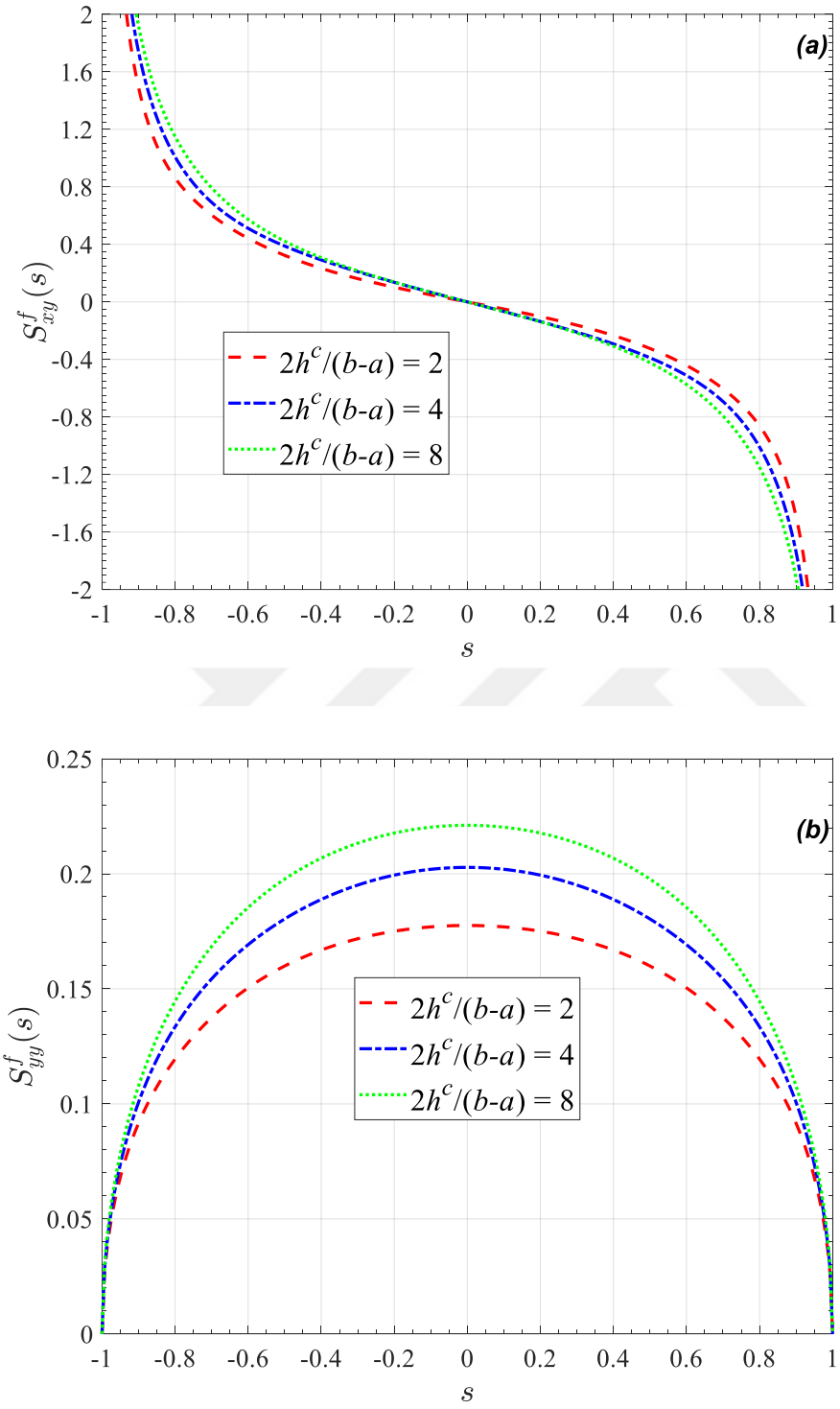

Figure 4-25. The computed shear stress ***(a)*** and the lateral stress ***(b)*** for the thin film and the lateral stress ***(c)*** for the uppermost layer by assuming $b - a/h_f = 1/2$.

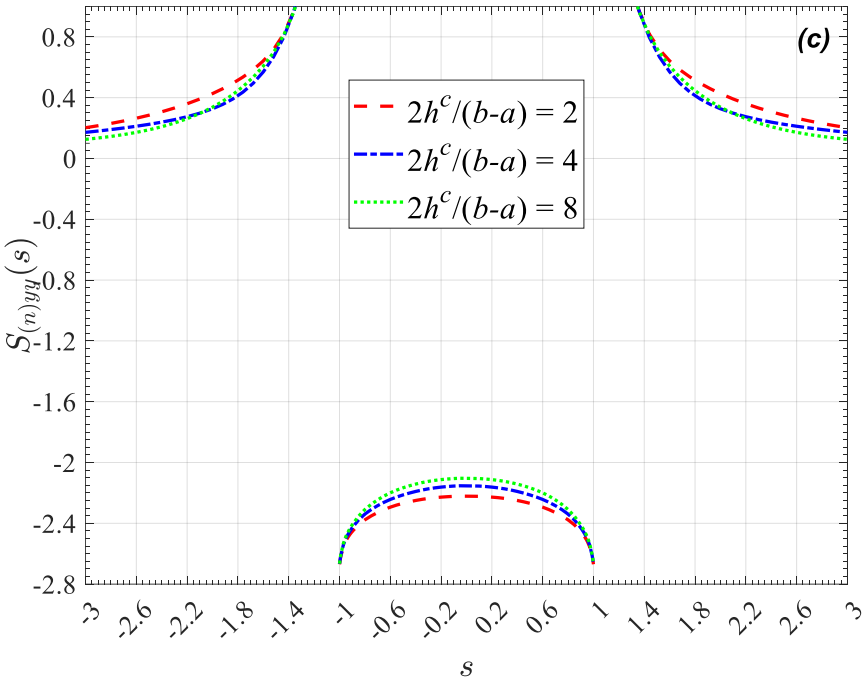

Figure 4-25. (continued)

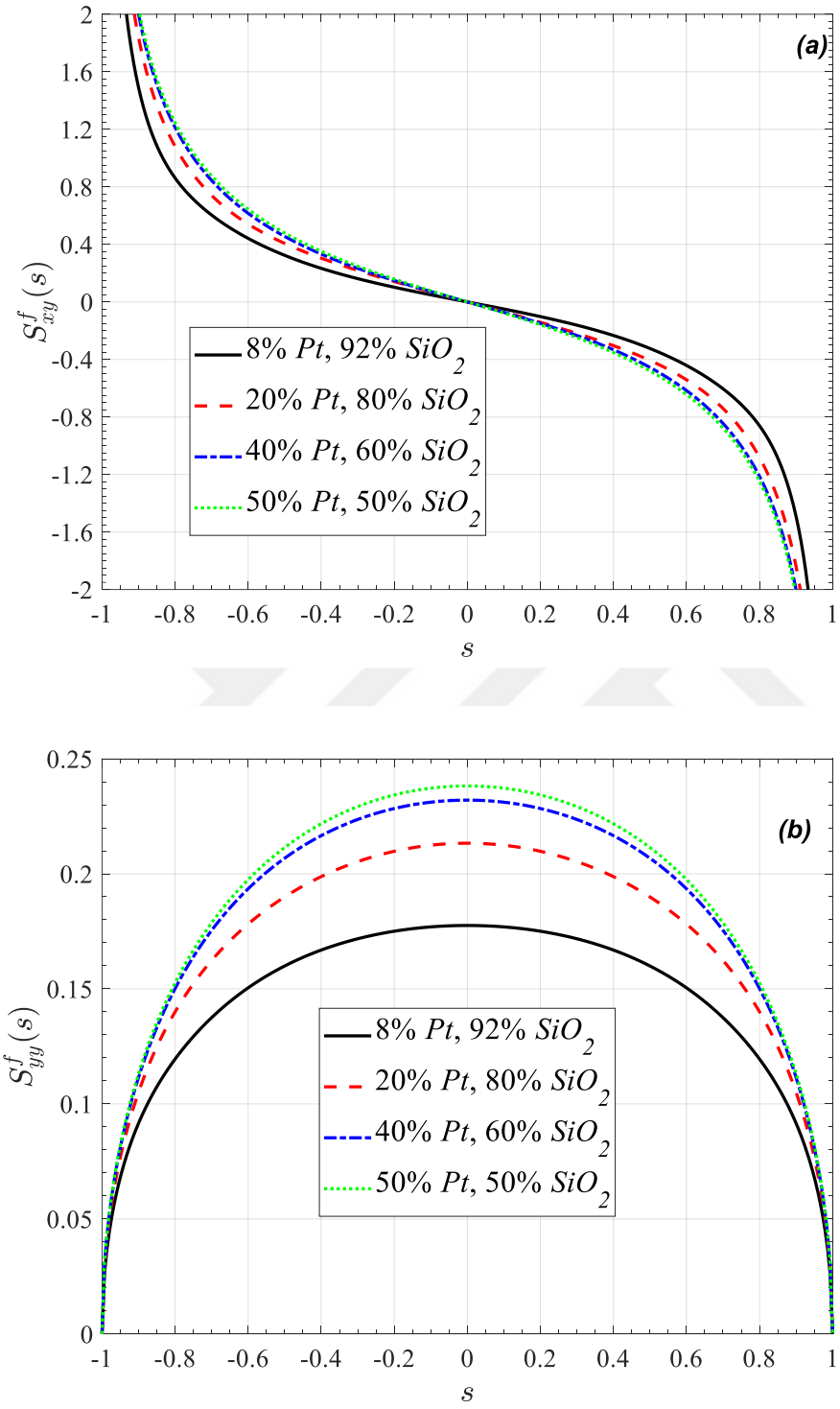

Figure 4-26. The computed shear stress ***(a)*** and the lateral stress ***(b)*** for the thin film and the lateral stress ***(c)*** for the uppermost layer by assuming $b - a/h_f = 1/2$ and $2h^c/b - a = 2$.

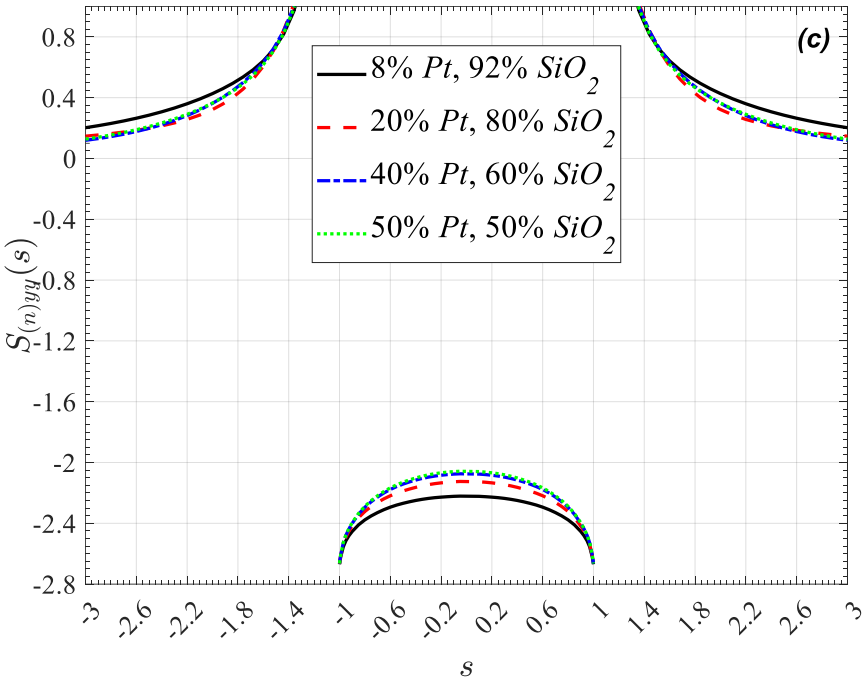

Figure 4-26. (continued)

CHAPTER 5

CONCLUSIONS AND FUTURE WORKS

5.1 Conclusions

This study offers an analytical investigation into the problem for a single layer multiferroic thin film on a transversely isotropic multilayer coating system that is bonded to an isotropic homogeneous substrate. The investigation is based on the assumptions of plane elasticity and perfect bonding between the layers. The study is performed for both edge-loading in the thin film and uniform strain conditions in the rest of the system. The analytical solution procedure is predicated on the derivation of a SIE. To derive the final equation, the expansion is initiated using the Chebyshev polynomials. Subsequently, a search is undertaken for the coefficients of the resulting expansion in order to identify the solution. Computer program codes have been developed using the MAPLE 2024 software for the execution of all numerical procedures outlined in Chapter 2 and Chapter 3. A comparison of the analytical solutions with those found in the extant literature is made for far-field loading of both an isotropic thin film on FGM multilayer coatings bonded to an isotropic substrate and a piezoelectric thin film on FGM substrate without any coating. As demonstrated in Chapter 4, the tabulated data and numerical values are consistent with the extant literature for both problems, exhibiting a high degree of accuracy. This finding serves as a testament to the validity of the present study. These results also demonstrate that the solution model under consideration has a high level of efficacy in generating solutions for a wide range of material models. The subject of parametric analyses in Section 4 pertains to multiferroic and piezoelectric thin films without edge and far-field loading. The present study investigates the effect of both

electrical and magnetic loading on a multiferroic film, while only electrical loading can be examined for the piezoelectric one due to its inherent nature. The findings of this parametric study are summarized in the following bullet points.

- The ratio of the width of the thin film to its thickness ($b-a/h_f$) is the most effective parameter for stress. Using **thinner films (increasing this ratio)** reduces the SIF, shear and lateral stress values of the top layer, while increasing the lateral stress values of the thin film. The maximum and minimum values are obtained by using **the metal-rich coating ($\boldsymbol{\eta = 0.4}$)** compared to the other grading functions.
- The ratio of the thickness of the coating to the width of the thin film ($2h^c/b-a$) results in different behavior depending on the relative hardness of the substrate to the coating. For **hard substrate-soft coating** condition **($\boldsymbol{\mu^s/\mu_0 = 7}$)** the increase in this ratio; decreases the SIF, the shear and lateral stress values of the thin film, while increases lateral stress values for the top layer. In the case of a **soft substrate and a hard coating condition ($\boldsymbol{\mu^s/\mu_0 = 1/7}$)**, the behavior is diametrically opposed. The lateral and shear stress values for the thin film with linearly graded coating are higher than those with the exponential one, while the lateral stress values for the top layer are lower.
- The influence of the ratio of the shear modulus of the substrate to the coating (μ^s/μ_0) and the elastic modulus ratio (E^s/E_{0y}) are examined concurrently. The **harder substrate (increasing this ratio**) causes higher lateral and shear stress values for the thin film and lower lateral stress for the uppermost layer. **The metal-rich coating ($\boldsymbol{\eta = 0.4}$)** on the harder substrate results in higher lateral stress values for the thin film compared to other grading functions.
- The increase in the amount of hard coating in a multi-layer coating results in greater lateral and shear stress for the thin film and reduces lateral stress value for the uppermost layer.
- The elastic modulus ratio E_{0x}/E_{0y} has no significant effect on stress.

- For **hard substrate-soft coating** condition **($\mu^s/\mu_0 = 7$)** the increase of the exponent η decreases the SIF, the shear and lateral stress values of the thin film, while increases lateral stress values for the top layer. For the **soft substrate and a hard coating condition ($\mu^s/\mu_0 = 1/7$)**, the behavior becomes opposite.

5.2 Future Works

The present study provides information regarding a multilayer coating system on a substrate in one stack. However, it is important to note that multiple structures can be employed in general for smart structure applications. Consequently, this problem can be expanded to encompass multiple thin film-multilayer coating systems on a substrate as future work.

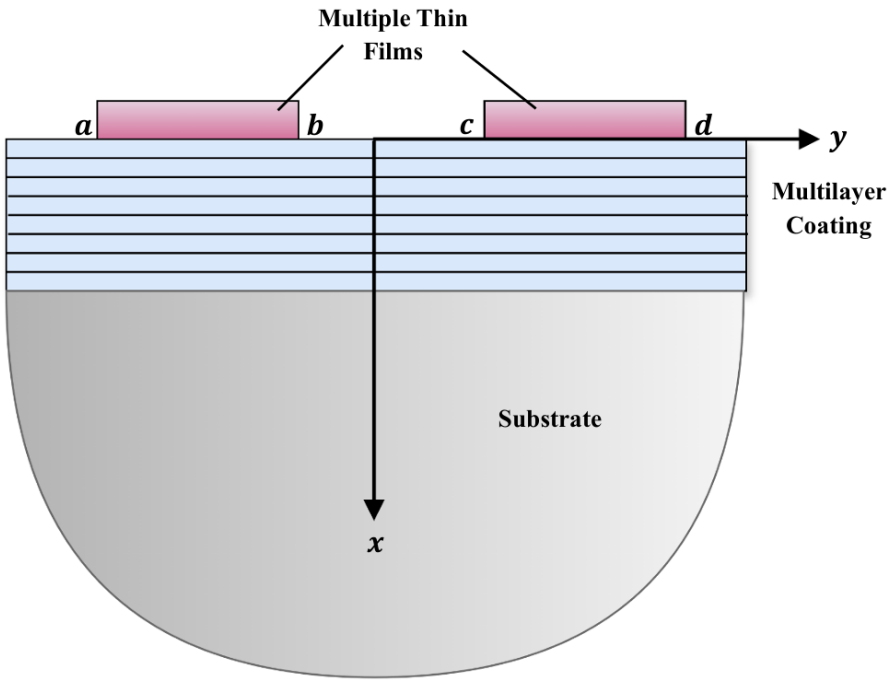

Figure 5-1. The problem with multiple thin film-multilayer coating system

The bonding process during the fabrication of such structures is a pivotal parameter. As a result, the bonding layers can also be modeled in the system to investigate the effect on stress. This extended problem can be solved in future work.

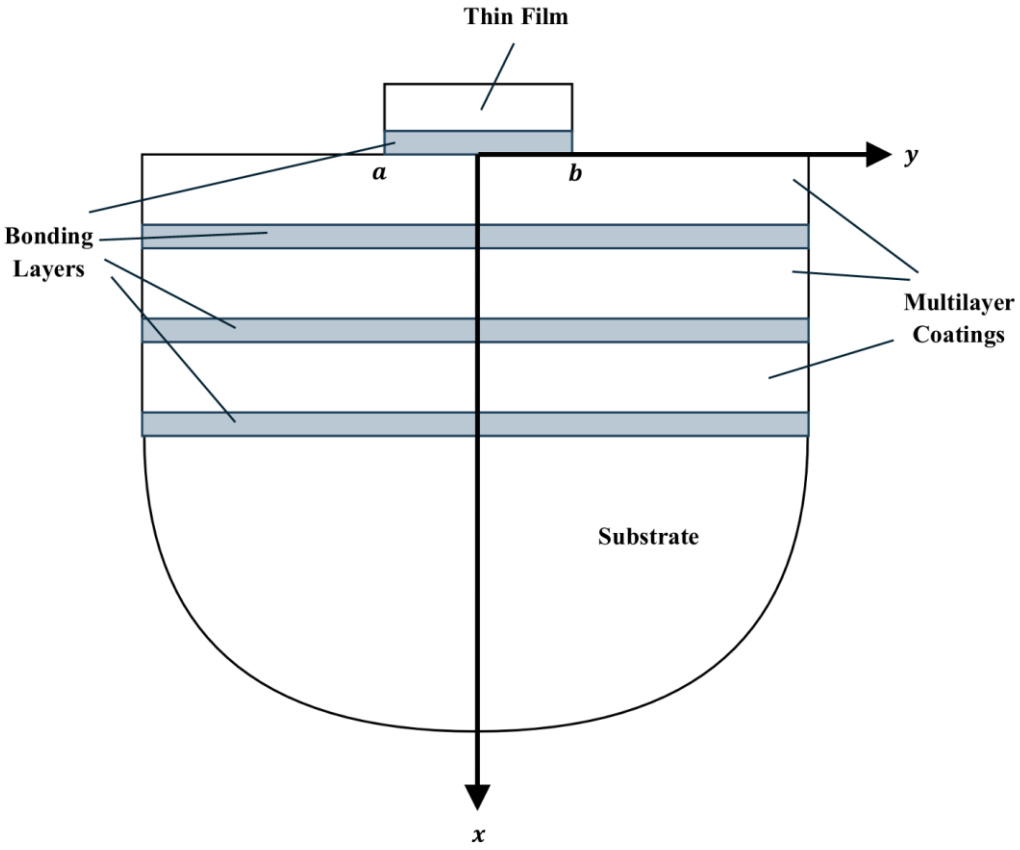

Figure 5-2. The problem with a thin film-multilayer coating system with bonding layers

REFERENCES

[1] Ramesh, R., and Spaldin, N. A. (2007). Multiferroics: progress and prospects in thin films. Nature materials, 6(1), 21-29.

[2] Aizu, K. (1970). Possible species of ferromagnetic, ferroelectric, and ferroelastic crystals. *Physical Review B*, *2*(3), 754.

[3] Schmid, H. (1994). Multi-ferroic magnetoelectrics. *Ferroelectrics*, *162*(1), 317-338.

[4] Fiebig, M., Lottermoser, T., Meier, D., and Trassin, M. (2016). The evolution of multiferroics. *Nature Reviews Materials*, *1*(8), 1-14.

[5] Khomskii, D. (2009). Classifying multiferroics: Mechanisms and effects. *Physics*, *2*, 20.

[6] Singh, A., Bhatia, P. G., Radha, S., and Mukherjee, S. Multiferroics: Novel Materials for Future.

[7] Vopson, M. M. (2015). Fundamentals of multiferroic materials and their possible applications. *Critical Reviews in Solid State and Materials Sciences*, *40*(4), 223-250.

[8] McGuire, T. R., Scott, E. J., and Grannis, F. H. (1956). Antiferromagnetism in a Cr_2O_3 crystal. *Physical Review*, *102*(4), 1000.

[9] Wang, J. B. N. J., Neaton, J. B., Zheng, H., Nagarajan, V., Ogale, S. B., Liu, B., and Ramesh, R. (2003). Epitaxial $BiFeO_3$ multiferroic thin film heterostructures. *science*, *299*(5613), 1719-1722.

[10] Palkar, V. R., and Malik, S. K. (2005). Observation of magnetoelectric behavior at room temperature in Pb (Fe_xTi_{1-x}) O_3. *Solid State Communications*, *134*(11), 783-786.

[11] Krichevtsov, B. B., Pavlov, V. V., and Pisarev, R. V. (1989). Giant linear magnetoelectric effect in garnet ferrite films. *Jetp Lett*, *49*(8), 535.

[12] Hur, N., Park, S., Sharma, P. A., Ahn, J. S., Guha, S., and Cheong, S. W. (2004). Electric polarization reversal and memory in a multiferroic material induced by magnetic fields. *Nature*, *429*(6990), 392-395.

[13] Spaldin, N. A. (2020). Multiferroics beyond electric-field control of magnetism. *Proceedings of the Royal Society A*, *476*(2233), 20190542.

[14] Ma, J., Hu, J., Li, Z., and Nan, C. W. (2011). Recent progress in multiferroic magnetoelectric composites: from bulk to thin films. *Advanced materials*, *23*(9), 1062-1087.

[15] Gupta, R., and Kotnala, R. K. (2022). A review on current status and mechanisms of room-temperature magnetoelectric coupling in multiferroics for device applications. *Journal of Materials Science*, *57*(27), 12710-12737.

[16] Srinivasan, G., Rasmussen, E. T., Levin, B. J., and Hayes, R. (2002). Erratum: Magnetoelectric effects in bilayers and multilayers of magnetostrictive and piezoelectric perovskite oxides [Phys. Rev. B 65, 134402 (2002)]. *Physical Review B*, *66*(2), 029901.

[17] Ma, J., Lin, Y., and Nan, C. W. (2009). Anomalous electric field-induced switching of local magnetization vector in a simple FeBSiC-on-Pb (Zr, Ti) O3 multiferroic bilayer. *Journal of Physics D: Applied Physics*, *43*(1), 012001.

[18] Jahns, R., Piorra, A., Lage, E., Kirchhof, C., Meyners, D., Gugat, J. L., and Quandt, E. (2013). Giant magnetoelectric effect in thin-film composites. *Journal of the American Ceramic Society*, *96*(6), 1673-1681.

[19] Pradhan, D. K., Kumari, S., and Rack, P. D. (2020). Magnetoelectric composites: applications, coupling mechanisms, and future directions. *Nanomaterials*, *10*(10), 2072.

[20] Spaldin, N. A., and Ramesh, R. (2019). Advances in magnetoelectric multiferroics. *Nature materials*, *18*(3), 203-212.

[21] Fetisov, Y. K., and Srinivasan, G. (2006). Electric field tuning characteristics of a ferrite-piezoelectric microwave resonator. *Applied physics letters*, *88*(14).

[22] Barman, R., and Kaur, D. (2016). Multiferroic tunnel junction of $Ni_{50.3}Mn_{36.9}Sb_{12.8}/BiFeO_3/Ni_{50.3}Mn_{36.9}Sb_{12.8}$ for magneto-electric random access memory devices. *Applied Physics Letters*, *108*(9).

[23] Ryu, J., Kang, J. E., Zhou, Y., Choi, S. Y., Yoon, W. H., Park, D. S., ... and Jeong, D. Y. (2015). Ubiquitous magneto-mechano-electric generator. *Energy and Environmental Science*, *8*(8), 2402-2408.

[24] Zhuang, X., Leung, C. M., Sreenivasulu, G., Gao, M., Zhang, J., Srinivasan, G., ... and Viehland, D. (2017). Upper limit for power conversion in magnetoelectric gyrators. *Applied Physics Letters*, *111*(16).

[25] Yarar, E., Salzer, S., Hrkac, V., Piorra, A., Höft, M., Knöchel, R., ... and Quandt, E. (2016). Inverse bilayer magnetoelectric thin film sensor. *Applied Physics Letters*, *109*(2).

[26] Naifar, S., Bradai, S., Viehweger, C., and Kanoun, O. (2017). Survey of electromagnetic and magnetoelectric vibration energy harvesters for low frequency excitation. *Measurement*, *106*, 251-263.

[27] Corso, C. D., Dickherber, A., and Hunt, W. D. (2007). Lateral field excitation of thickness shear mode waves in a thin film ZnO solidly mounted resonator. *Journal of Applied Physics*, *101*(5).

[28] Muralt, P., Ledermann, N., Paborowski, J., Barzegar, A., Gentil, S., Belgacem, B., ... and Setter, N. (2005). Piezoelectric micromachined ultrasonic transducers based on PZT thin films. *IEEE transactions on ultrasonics, ferroelectrics, and frequency control*, *52*(12), 2276-2288.

[29] Ortmann, J. E., Nookala, N., He, Q., Gao, L., Lin, C., Posadas, A. B., ... and Demkov, A. A. (2018). Quantum confinement in oxide heterostructures: Room-temperature intersubband absorption in $SrTiO_3/LaAlO_3$ multiple quantum wells. ACS nano, 12(8), 7682-7689.

[30] Chang, S. J., Chung, M. H., Kao, M. Y., Lee, S. F., Yu, Y. H., Kaun, C. C., ... and Tseng, Y. C. (2019). GdFe0. 8Ni0. 2O3: a multiferroic material for low-power spintronic devices with high storage capacity. *ACS applied materials and interfaces*, *11*(34), 31562-31572.

[31] Nikitin, A. O., Petrov, R. V., Khavanova, M. A., Tatarenko, A. S., and Bichurin, M. I. (2019, June). Modeling of magnetoelectric effect in multiferroic antenna. In *2019 PhotonIcs and Electromagnetics Research Symposium-Spring (PIERS-Spring)* (pp. 953-956). IEEE.

[32] Ribeiro, P., Khan, M. A., Alfadhel, A., Kosel, J., Franco, F., Cardoso, S., ... and Jamone, L. (2017). A miniaturized force sensor based on hair-like flexible magnetized cylinders deposited over a giant magnetoresistive sensor. *IEEE Transactions on Magnetics*, *53*(11), 1-5.

[33] Rupp, T., Truong, B. D., Williams, S., and Roundy, S. (2019). Magnetoelectric transducer designs for use as wireless power receivers in wearable and implantable applications. *Materials*, *12*(3), 512.

[34] Bhuktare, S., Bose, A., Singh, H., and Tulapurkar, A. A. (2017). Gyrator based on magneto-elastic coupling at a ferromagnetic/piezoelectric interface. *Scientific reports*, *7*(1), 840.

[35] Hertz, H. (1881). The contact of elastic solids. *J Reine Angew, Math*, *92*, 156-171.

[36] Dag, S. (2001) ‘Crack and Contact Problems in Graded Materials’, Ph.D. dissertation, Lehigh University

[37] Balci, M. N. (2018) ‘Dynamic Frictional Contact Problems Involving Functionally Graded Materials’, Ph.D. dissertation, Middle East Technical University.

[38] Toktaş, S. E. (2024). ‘Multi-layer models for moving contact problems of graded materials and multiferroics’, Ph.D. dissertation, Middle East Technical University.

[39] Muskhelishvili, N. I. (1953). *Some basic problems of the mathematical theory of elasticity* (Vol. 15). Groningen: Noordhoff.

[40] Erdogan, F., and Gupta, G. D. (1971). The problem of an elastic stiffener bonded to a half plane.

[41] Erdogan, F., and Joseph, P. F. (1990). Mechanical modeling of multilayered films on an elastic substrate—part I: analysis.

[42] Erdogan, F., and Joseph, P. F. (1990). Mechanical modeling of multilayered films on an elastic substrate—Part II: Results and discussion.

[43] Guler, M. A., Erdogan, F., and Dag, S. (2008, February). Modeling of thin films and cover plates bonded to graded substrates. In *AIP Conference Proceedings* (Vol. 973, No. 1, pp. 790-795). American Institute of Physics.

[44] Gulver, Y. F. (2009) ‘İşlevsel Derecelendirilmiş Kaplamalara Bağlı İnce Filmlerin Mekanik Modellenmesi’, M.S. Thesis, TOBB University.

[45] Chen, P., Peng, J., Liu, H., Gao, F., and Guo, W. (2018). The electromechanical behavior of a piezoelectric actuator bonded to a graded substrate including an adhesive layer. *Mechanics of Materials*, *123*, 77-87.

[46] Chen, P., Chen, S., and Peng, J. (2016). Interface behavior of a thin-film bonded to a graded layer coated elastic half-plane. *International Journal of Mechanical Sciences*, *115*, 489-500.

[47] Abramowitz, M. and Stegun, I. A. (1964) Handbook of Mathematical Functions with Formulas, Garphs and Mathematical Tables, National Bureu of Standards, Applied Mathematics Series.

[48] Carlotti, G., Doucet, L., & Dupeux, M. (1997). Elastic properties of silicon dioxide films deposited by chemical vapour deposition from tetraethylorthosilicate. *Thin Solid Films*, *296*(1-2), 102-105.

[49] Alinia, Y., & Güler, M. A. (2022). On the problem of an axisymmetric thin film bonded to a transversely isotropic substrate. *International Journal of Solids and Structures*, *248*, 111636.

[50] Chen, P., Peng, J., Liu, H., Gao, F., & Guo, W. (2018). The electromechanical behavior of a piezoelectric actuator bonded to a graded substrate including an adhesive layer. *Mechanics of Materials*, *123*, 77-87.

[51] Nakamura, T., Wang, T., & Sampath, S. (2000). Determination of properties of graded materials by inverse analysis and instrumented indentation. *Acta materialia*, *48*(17), 4293-4306.

[52] Shen, H. S. (2016). Functionally graded materials: nonlinear analysis of plates and shells. CRC press.

[53] Suresh, S., & Mortensen, A. (1998). Fundamentals of functionally graded materials: processing and thermomechanical behaviour of graded metals and metal-ceramic composites. Cambridge University Press.

[54] Naik, A. K., Pillari, L. K., Lessoway, K., Bichler, L., Laha, T., & Roy, S. (2024). A comparative assessment of thermal conductivity of functionally graded and equivalent non-graded ZrB2–B4C–SiC–LaB6 ultra-high-temperature ceramic composites. *Open Ceramics*, *19*, 100653.

[55] Aebi, L., Schwank, L., Vollmann, J., Bryner, J., Wenke, I., & Dual, J. (2010). High resolution measurement of FGM thin films using picosecond ultrasonics. *Physics Procedia*, *3*(1), 727-733.

APPENDIX A

THE PROPERTIES OF CHEBYSHEV POLYNOMIALS

The Chebyshev polynomials of the first kind T_n in trigonometric form are given by the following relation.

$$T_n(\cos(\theta)) = \cos(n\theta) \tag{A.1}$$

The Chebyshev polynomials of the second kind U_n in trigonometric form are defined by the following relation.

$$U_n(\cos(\theta)) = \frac{\sin((n+1)\theta)}{\sin(n\theta)} \tag{A.2}$$

The Chebyshev polynomials of the first kind are derived by the following recurrence relation.

$$T_0(x) = 1, \tag{A.3}$$

$$T_1(x) = x, \tag{A.4}$$

$$T_{n+1}(x) = 2xT_n(x) - T_{n-1}(x). \tag{A.5}$$

The Chebyshev polynomials of the second kind are derived by the recurrence relation.

$$U_0(x) = 1, \tag{A.6}$$

$$U_1(x) = 2x, \tag{A.7}$$

$$U_{n+1}(x) = 2xU_n(x) - U_{n-1}(x). \tag{A.8}$$